Institutional Repository - Research Portal
Dépôt Institutionnel - Portail de la Recherche
researchportal.unamur.be
University of Namur

THESIS / THÈSE

DOCTOR OF SCIENCES

Study of the putative role of MPV17 in cancer cell proliferation

Canonne, Morgane

Award date:
2020

Awarding institution:
University of Namur

Link to publication

General rights
Copyright and moral rights for the publications made accessible in the public portal are retained by the authors and/or other copyright owners and it is a condition of accessing publications that users recognise and abide by the legal requirements associated with these rights.

- Users may download and print one copy of any publication from the public portal for the purpose of private study or research.
- You may not further distribute the material or use it for any profit-making activity or commercial gain
- You may freely distribute the URL identifying the publication in the public portal ?

Take down policy
If you believe that this document breaches copyright please contact us providing details, and we will remove access to the work immediately and investigate your claim.

Download date: 03. Jul. 2025

Study of the putative role of MPV17 in cancer cell proliferation

Dissertation submitted by

Morgane Canonne

In fulfilment for the award of the degree of

Doctor of Sciences in Biology

On the 27th of August, 2020

Supervising board :

Prof. Patricia Renard (Université de Namur, supervisor)

Prof. Thierry Arnould (Université de Namur, co-supervisor)

Examining board :

Dr. Frédérique Coppée (Université de Mons)

Prof. Jean-Pierre Gillet (Université de Namur)

Prof. Benoît Muylkens (Université de Namur)

Dr. Mustapha Najimi (Université Catholique de Louvain)

CONTENT

ACKNOWLEDGEMENTS

Je remercie Patsy Renard, ma promotrice, pour m'avoir accueillie au sein de son équipe et pour m'avoir fait confiance dans la gestion du projet. Un projet émotionnellement frustrant et aux tournants inattendus mais un projet qui reste productif et qui, à sa manière, a contribué à faire évoluer la recherche, mais pas que. Je te remercie pour m'avoir fait grandir scientifiquement et m'avoir aidée à l'élaboration d'un joli papier. Je retiendrai ton intelligence scientifique à la fois théorique, pratique et manuscrite, ton accessibilité, ton soutien et ta dédication à l'URBC. Je te souhaite que les années à venir t'apportent de belles choses.

Je remercie également Thierry Arnould, mon co-promoteur, pour sa confiance et son implication qui ont aussi participé à l'élaboration du papier. Je vous en souhaite bien d'autres. Je retiendrai votre passion et pertinence scientifiques ainsi que vos pointes d'humour. Je vous souhaite également beaucoup d'épanouissement pour la suite.

Je remercie Frédérique Coppée, Benoît Muylkens, Jean-Pierre Gillet et Mustapha Najimi, membres du jury, pour leur temps consacré à la lecture et l'amélioration du manuscrit. Merci à tous pour votre présence, implication, et input scientifique pertinent. Particulièrement, un grand merci à Benoît Muylkens et Damien Coupeau pour leur accueil en URVI, le partage de leurs compétences et connaissances qui m'ont permis de développer mes capacités en biologie moléculaire. De manière générale, merci aux membres de l'URVI qui abrite des personnalités remarquables.

Je remercie Emilie Bauwens, mon amie, ma collègue de bureau et d'assistanat. Je suis reconnaissante que tu aies été avec moi du premier jour jusqu'au dernier. Tu es une personne très intelligente, tant scientifiquement qu'au niveau du cœur. Merci pour tous ces moments où tu as été présente et à l'écoute. Je te remercie d'avoir partagé rires et larmes avec moi. Merci à mon ami Benjamin Le Calvé. Merci de m'avoir enseignée, guidée, conseillée. Merci pour ces rires et ton grand cœur. Merci à vous deux d'avoir rempli de rires mes journées. Vous allez me manquer.

Merci à Martine Raes de m'avoir fait confiance et offert un soutien sans faille pendant l'assistanat. Merci d'avoir toujours pris le temps de savoir comment j'allais et d'être à l'écoute.

Merci à ma magnifique Team TP, Mélanie Gastellier, Marie-Laurence Hubin et Bénédicte Noël. Je n'aurais jamais pu mieux tomber qu'avec vous les filles. Merci de votre accueil, de vos enseignements, de nos rires et de notre efficacité. Merci d'avoir toujours été là pour moi. Vous allez me manquer.

Je remercie mes amies Fofie (Sophie Ayama) et GéGé (Géraldine Génard), mes inséparables, pour leur présence, écoute, pour leurs belles âmes et nos rires ; Je remercie mon amie Kathleen Schmit pour ces années partagées avec moi, de m'avoir écoutée et conseillée. Je vous remercie les filles pour votre amitié tout simplement.

Merci à mes deux mémorants Alexis Khelfi et An Thuy N'Guyen d'avoir partagé un bout de chemin avec moi. Merci pour votre soutien et talent.

Merci à Maude Fransolet et Antoine Fattaccioli pour avoir été là chaque fois que j'en avais besoin, et pas seulement professionnellement. Merci à Noëlle Ninane, Catherine Demazy, Martine Van Steenbrugge et Marc Dieu pour leur aide également et leur gentillesse. Merci à Guy Van Steenbrugge pour juste être lui !

Merci, sans les citer, aux membres de l'équipe DYSO, présents et passés. Vous m'avez chacun fait grandir à votre manière. Il en va de même pour tous les autres membres de l'URBC. Merci tout spécialement à Sébastien Meurant, que j'ai connu étudiant et qui est ensuite venu égayer davantage notre bureau. Merci pour ton écoute et ton aide, professionnelle et personnelle.

Merci à Nina, ma talentueuse tatoueuse qui est devenue mon âme sœur amicale.

Merci à Mathieu Van Loo pour tous ces rires. Merci pour notre amitié. Merci également à Mathieu Limauge et Charline Dorn, pour ces agréables moments et discussions.

Merci à ma jolie Maman, qui, malgrè ses expériences difficiles, est toujours restée remplie d'amour. S'il est vrai que nous choisissons nos parents alors je ne suis pas étonnée d'avoir eu la meilleure. Merci aussi à mon Papa, unique en son genre et à Alexia, ma grande sœur adorée. Merci à vous trois pour votre éternelle protection, amour et soutien. Merci de me montrer ma valeur.

Srdane, hvala ti za sve. Nitko zapravo nikada nece znati koliko si izvanredan. Zivot nam je bio tezak ali mi smo jedna izuzetna ekipa i pobijedit cemo sve od sada pa nadalje. Volim te.

Enfin, merci moi-même. Merci d'avoir tant évoluée ces dernières années et de me permettre de vivre la trentaine éclairée.

ABSTRACT

MPV17 is described as a mitochondrial inner membrane channel. Although its biological function remains elusive, mutations in the *MPV17* gene result in hepatocerebral Mitochondrial DNA Depletion Syndrome (MDDS) in humans.

In the first part of this study, we show that *MPV17* silencing does not induce depletion in mitochondrial DNA content in cancer cells. We also show that MPV17 does not control cancer cell proliferation despite the fact that we initially observed a reduced proliferation rate in five *MPV17*-silenced cancer cell lines. ShRNA-mediated *MPV17* knockdown performed in this work provided misguiding results regarding the resulting proliferation phenotype and only a rescue experiment was able to shed definitive light on the non-implication of MPV17 in cancer cell proliferation. Our results therefore emphasize the caution that is required when scientific conclusions are drawn from a work based on lentiviral vector-mediated gene silencing and clearly demonstrate the need to systematically perform a rescue experiment in order to ascertain the specific nature of the experimental results.

In the second part of this study, we investigated the putative existence of circular RNAs (ciRNAs) derived from the *MPV17* gene. CiRNAs are covalently closed RNA loop structures that have become rising stars in disease research. In this work, we identified many putative *MPV17* ciRNAs, in need of further validation. Among them, one turned out to be common to Huh7 and HepG2 (hepatocellular carcinomas) and T98G (glioblastoma) cell lines, evocative of the hepatocerebral form of MPV17-related MDDS. We therefore hypothesize that ciRNAs might, at least partly, be accountable for the organ-specificity of the pathogenic phenotype seen in patients.

PREFACE

This research work was originally focused on exploring the role of MPV17, an enigmatic protein located in the inner membrane of mitochondria, in cancer cell proliferation. Results relative to this aspect constitute the first part of this thesis. Indeed, while MPV17 is commonly investigated regarding its role in a rare hepatocerebral syndrome characterized by mtDNA depletion in patients who display mutations in this gene, we were serendipitously led to consider a relevant role of this protein in the context of cancer, notably in term of cell proliferation. The exploration of this hypothesis initially led us to suspect a functional connection between MPV17 and Activating Transcription Factor 4 (ATF4), a critical player driving several biosynthetic pathways indispensable for cell proliferation such as nucleotide synthesis and amino acid metabolism. Later on, our research uncovered unexpected and baffling results, emphasizing the care that needs to be taken regarding result interpretation when working with shRNA-mediated knockdown. While this first part revealed valuable technical and biological messages leading to a recently accepted publication in PLOS One (Canonne *et al.*, 2020), it also incited us to look upon the importance of non-coding RNA classes in establishing/modulating cellular and molecular phenotypes. Thus, in the second part of this work, the aim was to precisely describe and characterize the potential *MPV17* circular RNA (ciRNA) population in various cell lines. Beyond providing, for the first time, a proof of existence of such putative *MPV17* ciRNAs, it also aimed at bringing more light on the disturbing results obtained in the first part of this work as well as on the crucial factors contributing to the tissue-specificity observed in MPV17-related disease. At the time of writing this document, results presented in the second part of this thesis, while inspirational, are still preliminary and are in need of further validations/investigations.

LIST OF ABBREVIATIONS

ADAR	Adenosine Deaminase Acting on RNA
ASNS	ASparagiNe Synthetase
ATF4	Activating Transcription Factor 4
ATP	Adenosine TriPhosphate
BME	β-mercaptoethanol
CiAmotl1	ciAngiomotin-like 1
ciANRIL	ciAntisense Non-coding RNA in the Inhibitor of cyclin-dependent kinase 4 Locus
ciFBXW7	ciF-BoX/WD repeat-containing protein 7
ciRHOT1	ciRas HOmolog family member bT1
CiRNA	Circular RNA
ciRS-7	circular RNA Sponge for miR-7
ciZNF609	ciZiNc Finger protein 609
CREB	ATF/Cyclic AMP Response Element Binding
dAdo	deoxyAdenosine
dCtd	deoxyCytidine
dGK	deoxyGuanosine Kinase
dGTP	deoxyGuanosine TriPhosphate
dGuo	deoxyGuanosine
DMEM	Dulbecco's Modified Eagle's Medium
DOCK6	Dedicator Of CytoKinesis 6
dThd	deoxyThymidine
dTMP	deoxyThymidine MonoPhosphate

dUTP	deoxyUridine TriPhosphate
EciRNA	Exonic circular RNA
EIciRNA	Exon-Intron containing circular RNA
eIF2α	eukaryotic Initiation Factor 2α
EMT	Epithelial to Mesenchymal Transition
ER	Endoplasmic Reticulum
FBS	Foetal Bovine Serum
fMet-tRNA	N-formylMethionine-tRNA
FOXO3	Forkhead bOX O3
GCN2	General Control Nonderepressible 2
GFP	Green Fluorescent Protein
GSK3ß	Glycogen Synthase Kinase 3ß
GTEx	Genotype-Tissue Expression
HCC	HepatoCellular Carcinoma
HRI	Heme-Regulated eukaryotic Initiation Factor 2α kinase
IciRNA	Intronic circular RNA
Int ciRNA	Interior circular RNA
IPTG	IsoPropyl β-D-1-ThioGalactopyranoside
IRES	Internal Ribosome Entry Site
ISR	Integrated Stress Response
KDM4C	histone lysine DeMethylase 4C
KIF	KInesin Family
KO	KnockOut
LB	Luria Bertoni
Mbl	Muscleblind

MDA	MalonDiAldehyde
MDDS	Mitochondrial DNA Depletion Syndrome
MMP-2	Matrix MetalloProteinase 2
MSP	Mitochondrial deoxynucleotide Salvage Pathway
mtDNA	mitochondrial DNA
MTHFD1	MethyleneTetraHydroFolate Dehydrogenase 1
MTHFD1L	MethyleneTetraHydroFolate Dehydrogenase 1 Like
MTHFD2	MethyleneTetraHydroFolate Dehydrogenase/cyclohydrolase 2
mTORC1	mammalian Target Of Rapamycin Complex 1
NAC	N-AcetylCysteine
ND2	NADH Dehydrogenase 2
NEAA	Non Essential Amino Acid
NGS	Normal Goat Serum
NH4OH	ammonium hydroxide
OA	Orotic Acid
OBB	Odyssey Blocking Buffer
ODC1	2-OxoDicarboxylate Carrier 1
PBS	Phosphate Buffered Saline
PERK	PKR-like Endoplasmic Reticulum Kinase
PHGDH	PHosphoGlycerate DesHydrogenase
PKR	RNA-dependent Protein Kinase
PNC1/PNC2	Pyrimidine Nucleotide Carrier 1/2
Pol II	RNA Polymerase II
PPARα	Peroxisome Proliferator-Activated Receptor α
PSAT1	PhosphoSerine AminoTransferase 1

PSPH	PhosphoSerine Phosphatase
QKI	QuaKIng
rAMP	riboAdenosine MonoPhosphate
RBL1/2	RetinoBlastoma Like 1/2
RBP	RNA Binding Protein
rGMP	riboGuanosine MonoPhosphate
ROS	Reactive Oxygen Species
RT-qPCR	Reverse Transcription quantitative Polymerase Chain Reaction
SAM	S-Adenosyl-Methionine
SEM	Standard Error of the Mean
SHMT2	Serine HydroxyMethylTransferase 2
SHS	Short Homologous Sequence
Sry	Sex-determining region Y
SYM1	Stress-inducible Yeast Mpv17
T	Tween 20
TGCA	The Genome Cancer Atlas
THF	TetraHydroFolate
Tra	Transparent
uORF	upstream Open Reading Frame
USP28	Ubiquitin Specific Peptidase 28
UTR	UnTranslated Region

FIGURES CONTENT

TABLES CONTENT

PART I: STUDY OF THE ROLE OF MPV17 IN CANCER CELL PROLIFERATION

INTRODUCTION

1. MPV17

MPV17 is a functionally elusive protein located on chromosome 2p23.3. It encodes a 176-residue protein predicted to have four transmembrane domains (Weiher *et al.*, 1990) (Karasawa *et al.*, 1993) (Wong *et al.*, 2007) (El-Hattab *et al.*, 2009) (Fig 1). Originally thought to be in peroxisomes (Zwacka *et al.*, 1994), MPV17 was then localized in the inner membrane of mitochondria (Spinazzola *et al.*, 2006) (Trott and Morano, 2004) (Krauss *et al.*, 2013). While mitochondrial DNA (mtDNA) defects/depletion and mitochondria ultrastructure alterations are unavoidable features of MPV17-related diseases, the resulting phenotypes present species-specificities, despite a proven functional conservation between the different orthologs (see below).

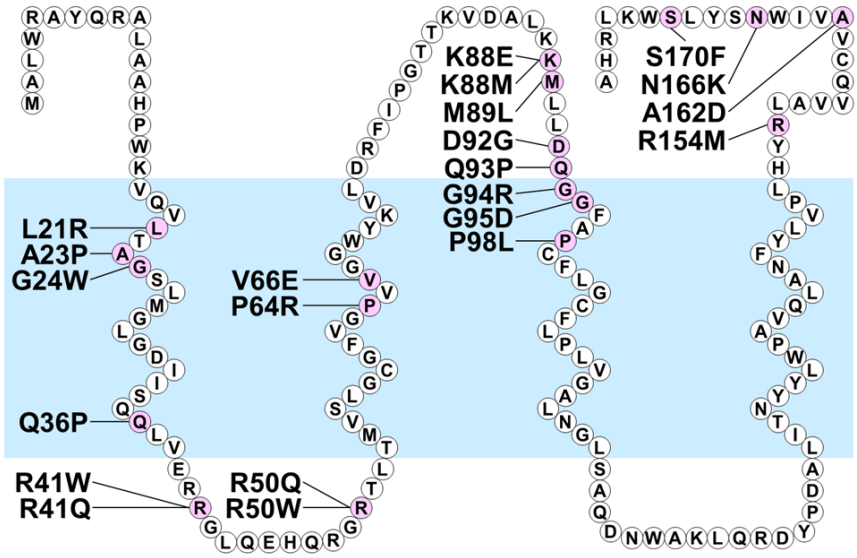

Figure 1 : Representation of MPV17 protein and localization of the missense pathogenic mutations.
MPV17 is a protein located in the inner membrane of mitochondria. MPV17 molecular modeling predicts four transmembrane domains. Both C- and N-terminal residues are localized in the mitochondrial intermembrane space. The known missense pathogenic mutations in humans are indicated in pink. (El-Hattab *et al.*, 2018)

In the following section, we will go through the current scientific literature regarding MPV17 in order to apprehend its evasive function, going from its discovery and first characterization in mice to the most recent insight regarding its physio-pathological role.

1.1. MPV17: from mouse to human.

The group of Weiher was the first to shed light on the *Mpv17* gene while generating transgenic mouse lines using retrovirus-based random insertional mutagenesis (Weiher *et al.*, 1990). The homozygous *Mpv17* mutant embryos (lacking MPV17 expression in all tissues, both at the mRNA and protein levels) develop normally but, as adults, suffer from nephrotic syndrome characterized by age-onset glomerulosclerosis and eventually die from kidney failure from 2-month of age (Weiher *et al.*, 1990). The ubiquitous expression of *Mpv17* contrasts with this tissue-specific phenotype. Nonetheless, Schenkel and collaborators successfully rescued the renal *Mpv17*$^{-/-}$ mice phenotype by transgenesis with the human *MPV17* ortholog, definitively proving the causal relationship between MPV17 loss-of-function and the kidney phenotype in mice (Schenkel *et al.*, 1995). Doing so, they also enlightened a functional conservation between the human and murine MPV17 proteins that share 92 % homology (Karasawa *et al.*, 1993) (Zwacka *et al.*, 1994).

Gottesberge and collaborators later offered a complement to the phenotype observed in *Mpv17*$^{-/-}$ mice by characterizing substantial abnormalities and degeneration in the mice inner ear (leading to hearing loss), more particularly in the *stria vascularis*, but also in the spiral ligament, and the organ of Corti (zum Gottesberge Meyer, Reuter and Weiher, 1996). The association of these two phenotypes may first seem singular, but the kidney and inner ear share some analogies. For example, some drugs present both nephrotoxic and ototoxic side effects (Begg and Barclay, 1995). Also, type IV collagen is a major component of both cochlea and glomerular basement membranes and mutations in any of the three cysteine-rich chain isoforms

of type IV collagen are responsible for Alport's syndrome, characterized by deafness and alterations in the glomerular basement membrane, which is therefore reminiscent of the overall phenotype observed in *Mpv17*$^{-/-}$ mice (zum Gottesberge Meyer, Reuter and Weiher, 1996). However, no particular loss of type IV collagen was detected in the kidney and inner ear of *Mpv17*$^{-/-}$ mice (Reuter *et al.*, 1998; unpublished data). In their search for a common mediator potentially responsible for the *Mpv17*$^{-/-}$ mice phenotype and based on the observation that both glomerular and cochlear basement membranes present alterations/thickening in these animals, Reuter and collaborators later linked Matrix MetalloProteinase-2 (MMP-2) to these pathological observations (Reuter *et al.*, 1998). Indeed, the authors showed an inverse causal relationship between MPV17 and MMP-2 expressions in the kidney and inner ear of *Mpv17*$^{-/-}$ mice but also in *Mpv17*-negative fibroblasts (derived from *Mpv17*$^{-/-}$ mice skin) artificially overexpressing *Mpv17*, placing MMP-2 somewhere in the mediation process of the mechanism underlying the renal and ear phenotypes in mice (Reuter *et al.*, 1998).

Further studies conferred contradictory roles to MPV17 in Reactive Oxygen Species (ROS) metabolism. Zwacka and collaborators showed that skin fibroblasts from *Mpv17*$^{-/-}$ mice seem defective in ROS production (Zwacka *et al.*, 1994). Contrariwise, the team later showed an excessive production of ROS in isolated glomeruli of *Mpv17*$^{-/-}$ mice (Binder *et al.*, 1999). Beyond the fact that these studies were performed on different materials in terms of organ type and scale (cell culture of skin fibroblasts versus isolated glomeruli structures), the ROS detection methods were also different (fluorescent versus chemiluminescent dye), possibly generating compound-dependent bias. Nonetheless, the observation that MPV17 depletion leads to an excess of ROS in mice isolated glomeruli is compatible with the causal relationship usually described between the damaging effect of ROS and glomerulosclerosis (Wardie, 1994) (Johnson *et al.*, 1994). Moreover, Binder and collaborators demonstrated that glomerular damage in *Mpv17*$^{-/-}$ mice can be prevented by interventional therapy with the ROS scavenger

drug dimethylthiourea, definitely incriminating ROS in the settlement of the renal phenotype. In addition, the authors noticed higher levels of lipid peroxydation products in the isolated glomeruli of *Mpv17*$^{-/-}$ mice compared to wild type littermates. Lipid peroxydation is the process during which polyunsaturated fatty acids are attacked by free oxygen radicals leading to the second generation of reactive aldehyde end-products such as MalonDiAldehyde (MDA) and 4-HydroxyNonEnal (4-HNE). Those compounds are highly diffusible and form damaging (mutagenic/toxic) adducts with biomolecules such as DNA and proteins (Ayala, Muñoz and Argüelles, 2014). Accordingly, Binder and colleagues were able to prevent the settlement of the disease with a systemic treatment with probucol, a hypolipidemic agent also displaying powerful lipophilic antioxidant properties (Binder *et al.*, 1999).

However, the precise origin and role of ROS in the development of the disease are still unclear. Noteworthy, MMP-2 expression has been shown to be proportionately influenced by ROS content (Kawaguchi *et al.*, 1996). Interestingly, *Mpv17*$^{-/-}$ mice progressively turn gray from 5-month of age, which does not constitute a normal ageing sign for them. Viscomi and collaborators then suggested that ROS induction could account for this phenotype by damaging melanocytes (Viscomi *et al.*, 2009).

Of note, researchers were confronted to the disappearance of the kidney phenotype in *Mpv17*$^{-/-}$ mice after few generations (Spinazzola *et al.*, 2006). Viscomi and collaborators were however able to witness it again, when noticing a time-shift onset of the disease. Indeed, while the first generations exhibited the phenotype from 2-month of age, the later ones only developed the disease from 18-month of age, concomitantly with a marked decrease in mtDNA content in glomerular tufts (Viscomi *et al.*, 2009).

Altogether, in light of the present literature, it could be suggested that in *Mpv17*$^{-/-}$ mice kidneys, mtDNA depletion (notably in podocytes), concomitantly with a decrease in respiratory complexes proficiency, leads to an excess of ROS modifying cellular components and damaging the glomerular basement membrane. Also, a putatively ROS-induced MMP-2 expression could further contribute to the basement membrane deterioration (Johnson *et al.*, 1992) (Knowlden *et al.*, 1995), ultimately leading to its degeneration (Viscomi *et al.*, 2009) (Reuter *et al.*, 1998) (Binder *et al.*, 1999) (Löllgen and Weiher, 2015) (Fig 2).

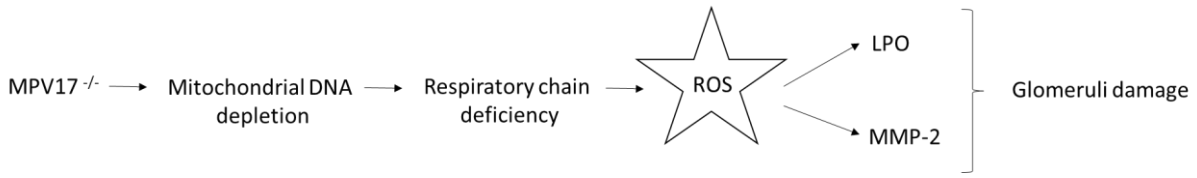

Figure 2 : Representation of the putative mechanism mediating the nephropathic phenotype in *MPV17*$^{-/-}$ mice.
The production of Reactive Oxygen Species (ROS) has a central involvement in the MPV17-dependent glomerulopathy in mice. The ROS-mediated generation of Lipid PerOxidation (LPO) adducts but also the suspected ROS-induced expression of Matrix MetalloProteinase 2 (MMP-2) would both contribute to the loss of glomeruli integrity.

It was more than 15 years after the discovery and characterization of the mouse *Mpv17* gene, that its human ortholog was pointed out as a causative agent of a rare autosomal recessive mitochondrial disorder called Mitochondrial DNA Depletion Syndrome (MDDS) marked by a highly reduced mtDNA copy number in affected tissues (El-Hattab *et al.*, 2018). There are three clinical presentations of MDDS: hepatocerebral, myopathic and encephalomyopathic. The genes responsible for the disease have been identified in only 20 % of the cases and, when determined, their function is implicated either directly or indirectly in mtDNA maintenance (Löllgen and Weiher, 2015). For example, mutations in the gene coding for the catalytic subunit of polymerase γ, responsible for mtDNA replication, causes hepatocerebral MDDS (Ferrari *et al.*, 2005).

To date, they are 100 known individuals affected by at least one of the 48 described *MPV17* pathogenic variants (46 % missense mutations (Fig 1), 12.5 % nonsense mutations, 12.5 % frameshift mutations, 17 % splice site mutations, 8 % inframe deletions and 4 % large deletions) (El-Hattab *et al.*, 2018). The vast majority of these patients (96 %) suffers from the hepatocerebral form of MDDS and exhibits a severe mtDNA depletion in the liver (60-99 % reduction). This is correlated with a decreased activity of respiratory chain complexes, with a higher incidence for the complexes containing subunits encoded by the mitochondrial genome. The onset of the disease takes place early in life (neonatal period/infancy) and condemns the affected individual to a premature death due to liver dysfunction progressing into liver failure (El-Hattab *et al.*, 2018). The remaining 4 % of the patients suffer from a late-onset neuromyopathic disease with, interestingly, mild or no liver involvement. This rarer phenotype is particularly associated with the p.R41Q mutation as half of the affected individuals are homozygous for this misense mutation. Another individual displays heterozygosity for three mutations in the *MPV17* gene (misense mutations p.K88M and p.M89L and nonsense mutation p.L143*). The last individual is homozygous for the misense mutation p.P98L, and contrary to the other aforementioned ones, this particular mutation is also described in a homozygous patient part of the majoritary group presenting a hepatic phenotype. Interestingly however, this latter patient presents a better survival than the other patients also afflicted with liver manifestations as she was still alive at 25 years old, which strongly contrasts with the individuals' deaths usually occuring in infancies/early childhood (El-Hattab *et al.*, 2018). There is currently no treatment for MPV17-dependent MDDS, and liver transplantation does not constitute a sustainable alternative as 60 % of the attempts led to the death of the patients (El-Hattab *et al.*, 2018).

1.2. MPV17: from homeostasis to stress

The species-specific phenotype of *MPV17* mutants between human and mice seems intriguing at first sight, especially knowing that, similarly to humans, the mtDNA depletion is the most severe in the liver of mutant mice (up to 95 % reduction). Despite that fact, *Mpv17*$^{-/-}$ mice do not display a clinical hepatic phenotype (Dalla Rosa *et al.*, 2016) (Spinazzola *et al.*, 2006) (Viscomi *et al.*, 2009). Moreover, hepatic mitochondria of *Mpv17*$^{-/-}$ mice clearly present substantial ultrastructure alterations (mitochondria ballooning surrounded by membranous structures, disappearance of the cristae and accumulation of amorphous material in the matrix) (Viscomi *et al.*, 2009). Strikingly, mtDNA-dependent respiratory chain complexes in *Mpv17*$^{-/-}$ mice liver are able to maintain around 40 % of remaining respiratory activity compared to control littermates, which appears remarkable despite the strong reduction in mtDNA content (up to 95 % reduction) (Viscomi *et al.*, 2009). This suggests the existence of an impressive compensatory mechanism enabling the *Mpv17*$^{-/-}$ mice to be extremely resistant to the settlement of a liver phenotype. The latter seems to take place at the transcriptional level, as the authors evidenced a higher mtDNA transcription efficiency in the liver of *Mpv17*$^{-/-}$ mice (Viscomi *et al.*, 2009).

Alhough *Mpv17*$^{-/-}$ mice die from kidney failure and not from liver damage, Bottani and collaborators evidenced an altered liver phenotype under specific stressful conditions. Indeed, they showed that *Mpv17*$^{-/-}$ mice displayed liver cirrhosis and failure when fed with a ketogenic diet (Bottani *et al.*, 2014). The authors suggest that the respiratory defective mice would then be unable to consume the excess of NADH derived from fat metabolism. Of interest, virus-mediated hepatic expression of the human *MPV17* cDNA was able to prevent this diet-dependent liver phenotype and to reverse the hepatic molecular alterations (restoration of mtDNA copy number and of respiratory complexes activity) (Bottani *et al.*, 2014), confirming

the previous data showing an MPV17 functional equivalence between mouse and human (Schenkel *et al.*, 1995).

The observation that *Mpv17*$^{-/-}$ genotype is reflected in the phenotype only under stressful conditions correlates with the results obtained by Trott and collaborators while studying Stress-inducible Yeast Mpv17 (Sym1), the yeast functional ortholog of MPV17 (Trott and Morano, 2004). The authors showed that Sym1 is required for yeast growth on ethanol at elevated temperature, two known detrimental factors for viability. Indeed, *SYM1* mutants fail to grow on ethanol at 37 °C, while growth is normal at 30 °C. This observation seems specific to ethanol as glycerol, another nonfermentable carbon source, did not lead to growth inhibition at 37 °C (Trott and Morano, 2004). Interestingly, both ethanol-based growth and elevated temperature independently induce an increased expression of Sym1 but only the synergetic effect of their combination leads to a growth defect in the mutants. More particularly, *SYM1* mutants seem to undergo a temperature-dependent metabolic defect in the utilization of acetaldehyde, a metabolic intermediate in ethanol catabolism, whose accumulation would eventually become toxic and subsequently impair growth (Trott and Morano, 2004). Of interest, the yeast growth phenotype was partially rescued following complementation with human MPV17, proving an interspecies functional conservation between these two orthologs sharing 48 % homology (Trott and Morano, 2004) (Spinazzola *et al.*, 2006).

Dallabona and collaborators, contrary to Trott and colleagues, noticed an impaired *SYM1* mutant growth at 37 °C in all tested aerobic carbon sources (glycerol, ethanol, lactate, acetate), suggesting a general respiratory impairment (Dallabona *et al.*, 2010). The technical differences between the two studies include the strain ploïdy, the culture medium used and the yeast genotype. While the first paramater does not seem to bear much influence regarding the

phenotypical divergence, the growth medium nutrient composition could hypothetically mask some mutant phenotypes. However, because of their different types of supplementations, the relative richness of these two media is not easy to determine (the growth medium used by Trott and collaborators is the Synthetic Complete medium composed of 0.67 % bacto-yeast nitrogen base (without amino acids) with amino acids supplementation and the one used by Dallabona and colleagues is the Yeast Peptone medium composed of 1% bacto-yeast extract and 2% bacto-peptone). Finally, the haploïd yeast strain used in the study of Dallabona and colleagues is auxotrophic for methionine. The fact that this amino acid is provided in the experiment appears to render this feature irrelevant. However, one could hypthesize that the methionine synthesis pathway occuring in the strain used in the study of Trott and colleagues somehow alleviates the general impaired oxidative growth phenotype through the metabolic intermediates/co-factors it may provide.

Dallabona and colleagues also went further into the characterization of the yeast *SYM1* mutant phenotype and detected mtDNA instability leading to the observation of "petite" colonies, concomitant with profound alterations in mitochondria (organelle ballooning, cristae flattening). Notably, they were able to partially rescue the oxidative growth defect following supplementation with specific Non-Essential Amino Acids (NEAA), namely asparagine, glutamine, aspartate or glutamate (Dallabona *et al.*, 2010). As these amino acids allow the production of common Krebs cycle intermediates (α-ketoglutarate, oxaloacetate), this observation suggests a putative role of Sym1 in anaplerotic mitochondrial pathways (Fig 3). Further strengthening this hypothesis, the independent overexpression of genes encoding two mitochondrial transporters, 2-OxoDicarboxylate Carrier 1 (*ODC1*) and Yeast Mitochondrial Carrier 1 (*YMC1),* was able to suppress the defective respiratory growth phenotype (Dallabona *et al.*, 2010). Odc1 is involved in the transport of α-ketoglutarate, α-ketoadipate and citrate between the cytosol and the mitochondria. The substrates of Ymc1 are unclear, but α-

ketoglutarate is suspected to be one of them and Ymc1 has been shown to be of importance for glutamate metabolism (Trotter *et al.*, 2005). Interestingly, while both *ODC1* and *YMC1* overexpressions were able to rescue the metabolic impairment caused by *SYM1* deficiency, only Ymc1 was able to completely rescue the mtDNA instability (Dallabona *et al.*, 2010). These authors then suggest that the defective oxidative growth and the mtDNA instability occur independently in *SYM1* mutants. Also, they propose an implication of Sym1 in mitochondria morphology maintenance as structural alterations actually might precede mtDNA instability in mutants (Dallabona *et al.*, 2010). This idea is reinforced with the results obtained in the zebrafish *Danio rerio* with spontaneous mutations in the *MPV17* ortholog *transparent* (*tra*) gene (Martorano *et al.*, 2019). Indeed, these authors observed an impairment of mitochondria ultrastructure (ballooning and cristae disappearance) and respiratory complexes (reduced abundance of OXPHOS subunits and lower basal respiration level in mutants) before mtDNA depletion. MtDNA-containing nucleoids being physically connected to the mitochondrial inner membrane, it is likely that a disorganisation of its ultrastructure could engender mtDNA defects.

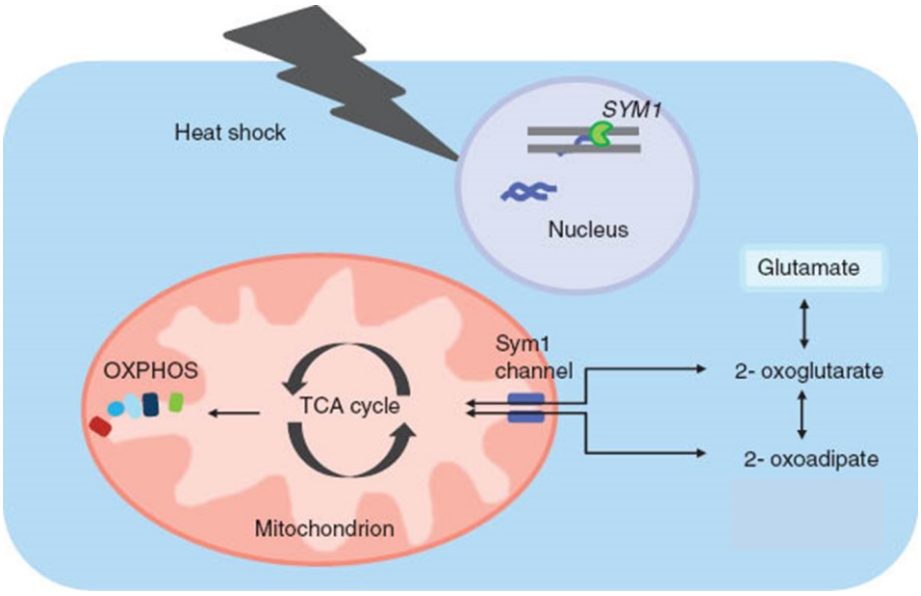

Figure 3 : Representation of the putative role of Sym1 as a bidirectional transporter of metabolic intermediates in yeast.

Sym1 is speculated to be a channel transporting TriCarboxylic Acid (TCA) cycle derivatives between the cytosol and the mitochondrion in non-permissive conditions (i.e. high temperature). Particularly, its substrate could

include α-ketoglutarate (2-oxoglutarate) and α-ketoadipate (2-oxoadipate) (involved in glutamate metabolism). Adapted from (Löllgen and Weiher, 2015).

Of interest, the defective ethanol-based growth phenotype of *SYM1* mutants is complemented by the expression of both *AtMPV17* and *PyMPV17*, the plant *Arabidopsis thaliana* and red algae *Pyropia yezoensis MPV17* orthologs, respectively (Wi, Na, *et al.*, 2020) (Wi, Park, *et al.*, 2020). Both AtMPV17 and PyMPV17, located in mitochondria, contribute to osmotic stress tolerance. More specifically, while the germination and seedling growth of *AtMPV17* mutants are comparable to wild type plants in stressless conditions, they are delayed during mannitol-induced osmotic stress (Wi, Na, *et al.*, 2020). ROS are known to increase in response to abiotic stresses (Choudhury *et al.*, 2017). Interestingly, under osmotic stress, *Chlamydomonas* cells overexpressing *PyMPV17* displayed a lower MDA content than wild type cells (Wi, Park, *et al.*, 2020). Altogether, these studies reflect a protective role of MPV17 against oxidative damages occurring during osmotic stress/desiccation. The ROS implication in the settlement of the *MPV17* mutant phenotype in plants/algae is reminiscent of what is observed in the mice mutant model.

Altogether, these studies imply a role of MPV17 in cell/mitochondria (metabolic) homeostasis and stress coping. This correlates with data obtained from a synthetic model composed of purified MPV17/Sym1 into lipid bilayers, suggesting that MPV17 behaves as a channel with stress-dependent gating properties affected by membrane potential, oxidative and pH stress (Antonenkov *et al.*, 2015) (Reinhold *et al.*, 2012). MPV17 seems to be a weakly cation-selective channel with a size exclusion limit of 1.8 nm, suggesting that almost all mitochondrial solutes could potentially flux through it (Antonenkov *et al.*, 2015). The channel would however be able to adopt an intermediate conformation, allowing a more selective transfer of reduced-size solutes like inorganic ions (maximum 0.8 nm), over larger metabolites (Antonenkov *et al.*,

2015). Nonetheless, as the channel electrophysiological analyses have been performed from a reconstitution of the purified protein into lipid bilayers, these data have to be treated with caution considering the absence of Sym1/MPV17 interacting partners. Indeed, it has been shown that Sym1/MPV17 belong to a 600 kDa complex of yet unidentified composition (Bottani *et al.*, 2014) (Dallabona *et al.*, 2010). This absence of native environment could notably affect the ion selectivity of the channel.

In a nutshell, MPV17 is thought to be a channel prone to open in conditions that are deleterious for the mitochondria in order to reinstate homeostasis. It then begs the question of the identity of the solute(s) transported through MPV17. While it is reasonable to wonder whether MPV17 is a transporter of metabolic intermediates or not based on Dallabona and colleagues' work (Dallabona *et al.*, 2010), other studies tend to closely link MPV17 and deoxynucleotides.

1.3. MPV17: from purine to pyrimidine

Exploring the functional relevance of MPV17, the group of Dalla Rosa enlightened a role for the protein in the Mitochondrial deoxynucleotide Salvage Pathway (MSP) (Dalla Rosa *et al.*, 2016). Indeed, they first noticed that MPV17 expression was increased in quiescent human fibroblasts compared to proliferating ones. In addition, *MPV17*-deficient fibroblasts only exhibited mtDNA depletion (40 % reduction) in a state of quiescence. This resting state implies that the cells mostly rely on the MSP to provide deoxynucleotides for mtDNA replication. Indeed, nuclear DNA replication is suspended in non-proliferating cells and, as a consequence, cytosolic deoxynucleotide *de novo* synthesis is considerably reduced (Fig 4). Specifically, *MPV17*-deficient fibroblasts showed a decrease in some enzymes involved in the purine branch of the MSP (adenylate kinase 3 and deoxyGuanosine Kinase (dGK)). The mtDNA depletion in quiescent *MPV17*-deficient fibroblasts was concomitant with a dearth in mitochondrial

deoxynucleotides, also observed in *Mpv17*$^{-/-}$ mice liver, but not in other organs unaffected by mtDNA depletion. Importantly, a deoxynucleoside supplementation was able to rescue the mtDNA depletion in *MPV17*-deficient fibroblasts (the best results were obtained with a cocktail of deoxyguanosine, deoxyadenosine and deoxycytidine) (Dalla Rosa *et al.*, 2016). Since the MSP is repressed in those cells, it is probable that the exogenous deoxynucleosides are first processed into deoxynucleotides in the cytosol and then imported into the mitochondrion through transporters implicated in the deoxynucleotide *de novo* synthesis, as suggested by the compensatory overexpression of Pyrimidine Nucleotide Carrier 2 (PNC2) in *MPV17*-deficient fibroblasts and *Mpv17*$^{-/-}$ mice liver, a key cytosol-to-mitochondria deoxynucleotide transporter normally repressed in resting cells. The authors therefore proposed the shortage of deoxynucleotides as the underlying cause of mtDNA depletion in MPV17 deficiencies.

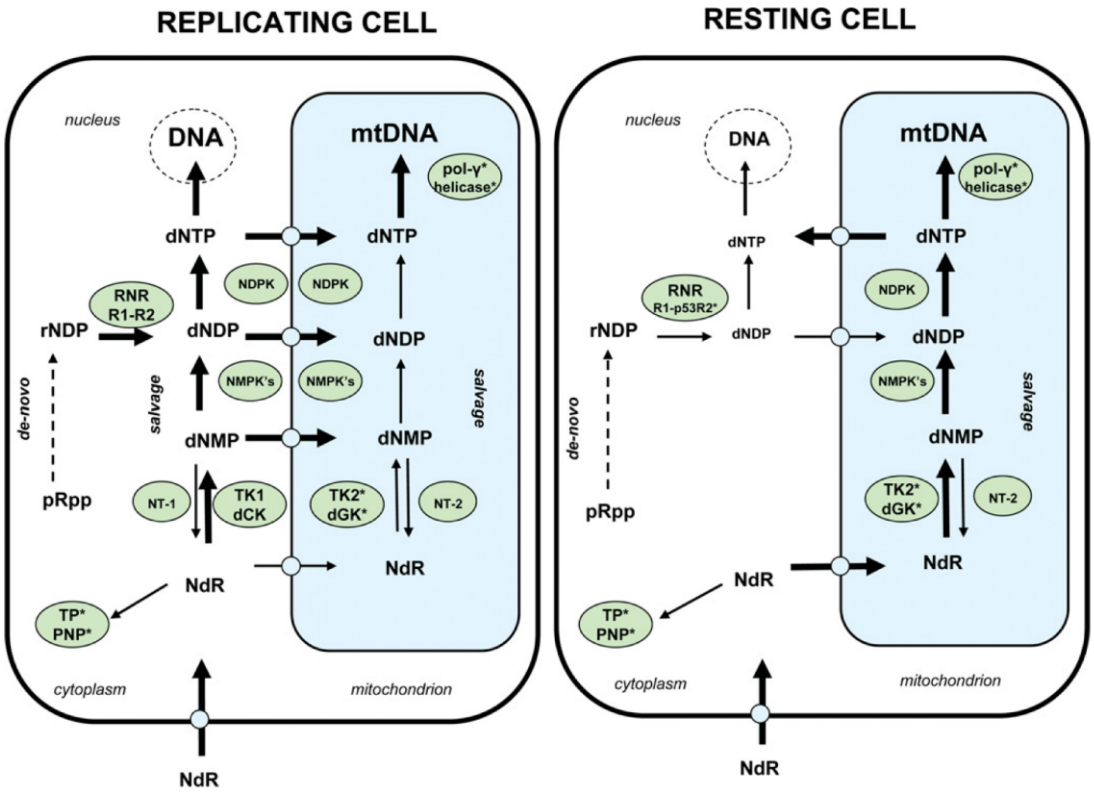

Figure 4 : Cytosolic and mitochondrial deoxynucleotide supply from the *de novo* and salvage pathways in proliferating and quiescent cells.

In replicating cells, the cytosolic and mitochondrial deoxynucleotide pools are mostly sustained by the cytosolic *de novo* synthesis. To a lesser extent, the mitochondrion also relies on its own salvage pathway. In resting cells where nuclear DNA replication is suspended, the cytosolic deoxynucleotide *de novo* synthesis is strongly reduced

and the cytosolic salvage pathway is inexistent. MtDNA replication is still ongoing in quiescent cells, which then rely on the mitochondrial salvage pathway to provide, not only for their own DNA replication, but also for nucleus DNA repair. pRpp: phosphoRibosyl pyrophosphate; rNDP: riboNucleoside DiPhosphate; RNR: RiboNucleotide Reductase; NdR: deoxyRiboNucleoside; dNMP: deoxyriboNucleoside MonoPhosphate; dNDP: deoxyriboNucleoside DiPhosphate; dTDP: deoxyriboNucleoside TriPhosphate; TK1 (cytosolic) and TK2 (mitochondrial): Thymidine Kinases; dGK: deoxyGuanosine Kinase; dCK: deoxyCytidineKinase; NMPK: deoxyriboNucleoside MonoPhosphate Kinase ; NDPK: deoxyriboNucleoside DiPhosphate Kinase. NT1 (cytosolic) and NT2 (mitochondrial): deoxyNucleoTidases; PNP: Purine Nucleoside Phosphorylase; TP: Thymidine Phosphorylase. Asterisks refer to enzymes implicated in human diseases. (Saada, 2009)

Mounting evidence intimately links MPV17 and purines. Besides the former observation that *MPV17* deficiency particularly seems to affect the purine branch of the MSP, deoxyGuanosine TriPhosphate (dGTP) is the most depleted deoxynucleotide in *Mpv17*$^{-/-}$ mice liver (Dalla Rosa *et al.*, 2016). In addition, the dGK loss of function in humans also leads to a similar hepatocerebral MDDS (Mandel *et al.*, 2001). Moreover, in the zebrafish *Danio rerio*, the *MPV17* ortholog *tra* gene seems to be responsible for the maintenance of specific guanine crystal-filled cells (Krauss *et al.*, 2013). Indeed, while *tra* mutants display mtDNA depletion, disruption of mitochondrial ultrastructure and defective respiratory complexes in liver similarly to the other vertebrate species (Martorano *et al.*, 2019), they specifically exhibit a decreased pigmentation in iridophores, normally accounting for their silver/golden reflection due to the presence of large amounts of guanine crystals in specific organelles called iridosomes. The loss of iridophores leads to a reduction in melanophores (responsible for the dark stripes), eventually making the fish transparent. In iridophores, since iridosomes are highly demanding in guanine, the mitochondrial supply in guanine precursors may be limiting in physiological conditions as the reaction would be strongly shifted towards the production of guanine directed to iridosomes (Fig 5). The absence of Tra, providing that it allows directly or indirectly the transport of guanine precursors in the mitochondria, would disrupt the particular guanine-related equilibrium required in this particular cell type, leading to apoptosis (Krauss *et al.*, 2013) (Löllgen and Weiher, 2015) (Fig 5). Noteworthy, the injection of human *MPV17* mRNA was

able to increase *in vivo* the number of iridophores in zebrafish mutant larvae (Martorano *et al.*, 2019).

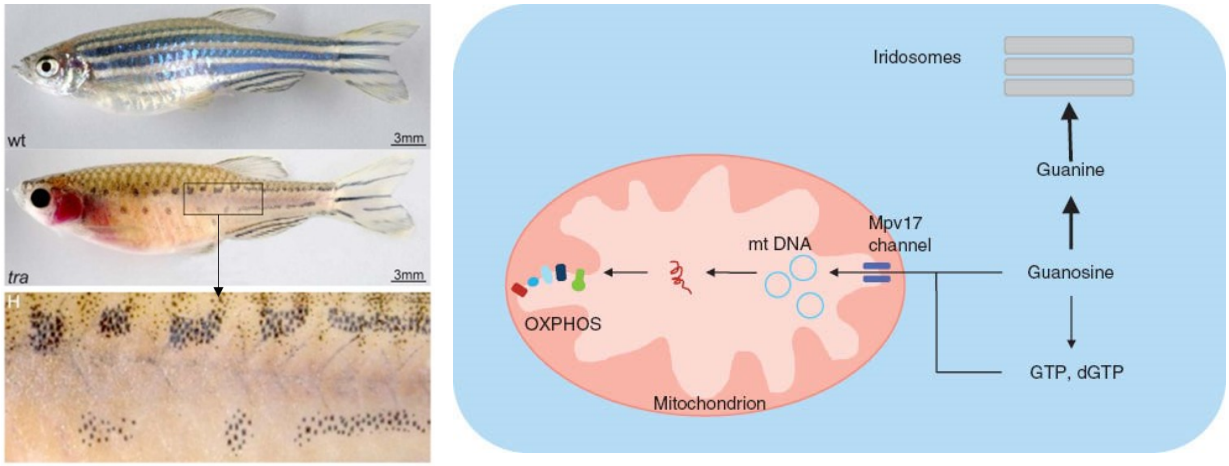

Figure 5 : Representation of the putative mechanism underlying the transparent phenotype in *MPV17* mutant zebrafish.

In zebrafish, mutations in the *MPV17* ortholog transparent (*tra*) gene renders the fish transparent following the loss of a specific cell type named iridophores normally responsible for the golden/silver reflection in wild type (wt) animals (left). The particularity of these cells is to accumulate large amounts of guanine-based crystals in iridosomes, generating a physiological limiting supply of guanine precursors for the mitochondrion as they are substantially used for the generation of guanine appointed to iridosomes. Tra is thought to be involved in the transport of guanine precursors in mitochondria and in its absence, subsequent mtDNA depletion and mitochondrial dysfunction leads to the cell apoptosis (right). (Löllgen and Weiher, 2015)

Finally, Moss and collaborators showed that, while riboAdenosine MonoPhosphate (rAMP) is the predominant ribonucleotide to be misincorporated in mtDNA of healthy mice liver, it is replaced by riboGuanosine MonoPhosphate (rGMP) in *Mpv17*$^{-/-}$ mice (Moss *et al.*, 2017). This switch in ribosubstitution could be explained by the switch in the deoxynucleotide pool size. Indeed, while healthy mitochondria harbour a high amount of Adenosine TriPhosphate (ATP), predicting rAMP misincorporation, *Mpv17*$^{-/-}$ mice hepatic mitochondria display a higher rGTP/dGTP ratio due to dGTP shortage. However, this higher incorporation of rGMP was also occuring in tissues not affected by neither mtDNA depletion nor deoxynucleotide shortage, for example in mitochondria of *Mpv*17$^{-/-}$ mice brain. This tissue was however affected by mtDNA

deletions (Moss *et al.*, 2017). Based on these findings, Moss and collaborators suggest a particular mechanism underlying MPV17-related MDDS. They propose that *MPV17* deficiency would somehow lead to an inevitable increased misincorporation of rGMP in mtDNA. When this incorporation passes a certain threshold (that would be both time and tissue-dependent), mtDNA replication is hindered, causing stalling and deletions, further worsening into replication arrest and mtDNA depletion. Ultimately, the reduction in deoxynucleotides would reflect a cell attempt to readjust deoxynucleotide pools and slow down mtDNA replication in order to preserve fidelity (Moss *et al.*, 2017) (Fig 6).

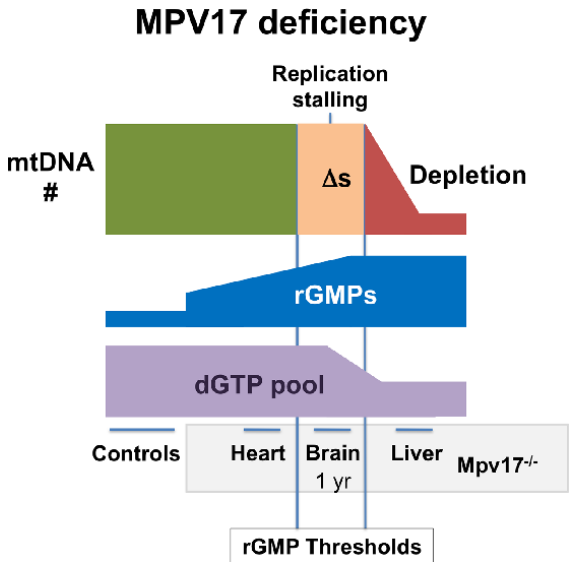

Figure 6 : Model proposed by the group of Moss regarding the underlying mechanism of mtDNA depletion in MPV17-related disease.

MPV17 deficiency leads to mitochondrial DNA (mtDNA) deletions (Δs) and mtDNA copy number (#) depletions. In *Mpv17*$^{-/-}$ mice, an aberrant incorporation of riboGuanosine MonoPhosphate (rGMP) into mtDNA has been observed in both liver and brain compared to wild-type littermates (controls). The proportion of embedded rGMP is thought to be tissue and time-dependent but whenever a certain threshold is passed, high embedded rGMP levels cause stalling of mtDNA replication resulting in deletions. As an adaptive response, dGTP pool would be reduced in an attempt to restore homeostasis and slow down mtDNA replication. (Moss *et al.*, 2017)

Other recent studies rather implicate MPV17 in the pyrimidine metabolism as deoxyUridine TriPhosphate (dUTP) supplementation was the most effective in increasing iridophore number in *tra*$^{-/-}$ zebrafish embryos, compared to purine or complete deoxynucleotide supplementation.

Dihydroorotate deshydrogenase, located in the inner membrane of mitochondria, is the only mitochondrial enzyme involved in the *de novo* pyrimidine synthesis and catalyses the conversion of dihydroorotic acid into Orotic Acid (OA). The authors noticed a reduced activity of this enzyme in the liver of *tra*$^{-/-}$ larvae, and a significant rescue of the iridophore phenotype after supplementation of *tra*$^{-/-}$ embryos with OA (Martorano *et al.*, 2019).

Also, Alonzo and colleagues showed a 3-fold increase in uracil incorporation in mtDNA of *MPV17*-deficient HeLa cells, despite an increase in deoxyThymidine MonoPhosphate (dTMP) *de novo* and salvage biosynthesis pathways. Thus, they postulated that the apparent dTMP pool disruption accounting for the uracil misincorporation was due to an impaired mitochondrial access to a third source of cytosolic dTMP. They therefore suggested that MPV17 is a dTMP carrier, as evidence supports the existence of such a specific transporter (Ferraro *et al.*, 2006) (Fig 7). However, there are some limitations entailed to this study. First, the authors are attempting to provide insight into the mechanisms underlying the deoxynucleotide disturbed supply and mtDNA depletion in MPV17 deficiencies using a cell background and context in which no mtDNA depletion is detected when MPV17 is downregulated. Moreover, it is difficult to extrapolate results obtained in a specific cancer cell background to a completely different patient context. Finally, the use of only one shRNA and clonal populations as well as the absence of rescue experiment put a reasonable doubt in terms of result specificity.

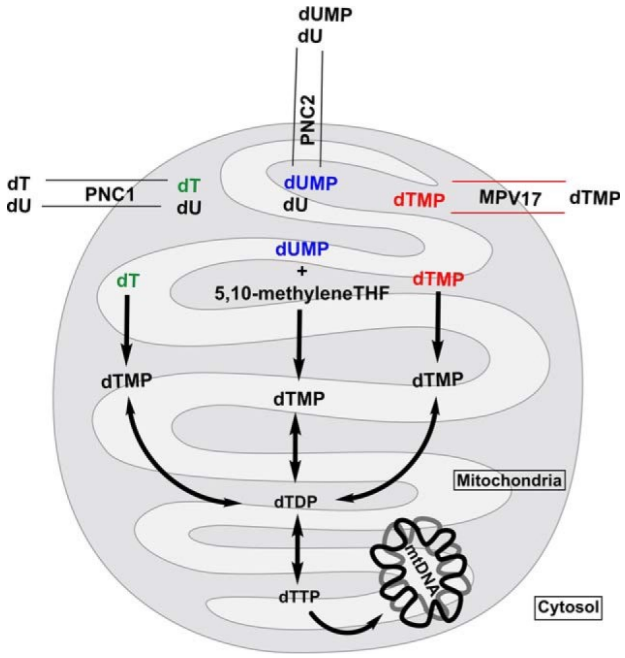

Figure 7 : Representation of the putative role of MPV17 as a deoxyThymidine MonoPhosphate (dTMP) transporter.

The mitochondrion can be supplied in dTMP via the *de novo* synthesis (in blue) from cytosolic deoxyUridine MonoPhosphate (dUMP) transported into the mitochondria through Pyrimidine Nucleotide Carrier 2 (PNC2) or via the mitochondrial salvage pathway which provides dT imported into the mitochondrion via PNC1. Alonzo and collaborators propose MPV17 as a third carrier supplying the mitochondrion with cytosolic dTMP (in red). (Alonzo *et al.*, 2018)

To sum up, MPV17 seems to be implicated in mitochondrial nucleotide homeostasis and while it is premature to attribute a function of nucleotide transporter to MPV17, this cannot be ruled out either.

The literature also puts into perspective the chronology of events and their interdependence in *MPV17* deficiencies. Indeed, does the shortage in deoxynucleotides account for the depletion in mtDNA (Dalla Rosa *et al.*, 2016) or is it the actual opposite? (Moss *et al.*, 2017). Likewise, is mtDNA depletion responsible for the respiratory complexes deficiency or are they both a (independent?) consequence of alterations in mitochondrial ultrastructure? (Martorano *et al.*, 2019) (Dallabona *et al.*, 2010).

During this work, the investigation of MPV17 biological functions in the context of cancer led us to consider a role of the protein in cell proliferation, possibly mediated by Activating Transcription Factor 4 (ATF4). Thus, in the following part, we will focus on this pleiotropic transcription factor, a master regulator of cellular pathways essential for cell proliferation.

2. ATF4

ATF4 is a central transcription factor belonging to the family of ATF/Cyclic AMP Response Element Binding protein (CREB) (Ameri and Harris, 2008) (Karpinski *et al.*, 1992) (Vallejo *et al.*, 1993). ATF4 can bind as a homodimer or a heterodimer to a specific promoter sequence on its target genes called C/EBP:ATF4 Response Element (CARE). As ATF4 regulates the expression of plethora of genes involved in diverse biological pathways, a wide spectrum of trancriptional interacting partners with which it forms a heterodimer has been described, thus enabling a tailored response to a specific cell demand (Pakos-Zebrucka *et al.*, 2016). ATF4 is frequently upregulated in malignant tissues (Ameri and Harris, 2008) and has been shown to drive angiogenesis (Chen *et al.*, 2017), cancer cell migration (Zeng *et al.*, 2019) and chemoresistance (Hu *et al.*, 2016). In a first part, we will specifically focus on the cellular pathways controlled by ATF4 that are critical for cell proliferation and thus exploited by cancer cells. In a second part, we will address the upstream regulators of ATF4. ATF4 is probably best known as the key effector of the Integrated Stress Response (ISR), an elaborate signaling network aiming at restoring cell homeostasis following a stress insult such as mitochondrial disturbance, nutrient deprivation, Endoplasmic Reticulum (ER) or oxidative stress. Cancer cells were shown to take advantage of the primarily pro-survival ISR in order to cope with the intrinsic challenges related to tumor growth (Wortel *et al.*, 2017).

2.1. ATF4-controlled metabolic pathways in proliferating cells

Because of their sustained proliferation rate, cancer cells are highly dependent on biosynthetic pathways such as the one-carbon metabolism, the serine biogenesis and the glutathione biosynthesis (Yang and Vousden, 2016) (Huggins *et al.*, 2016). All these pathways controlled by ATF4 are represented in Fig 8 and detailed hereafter.

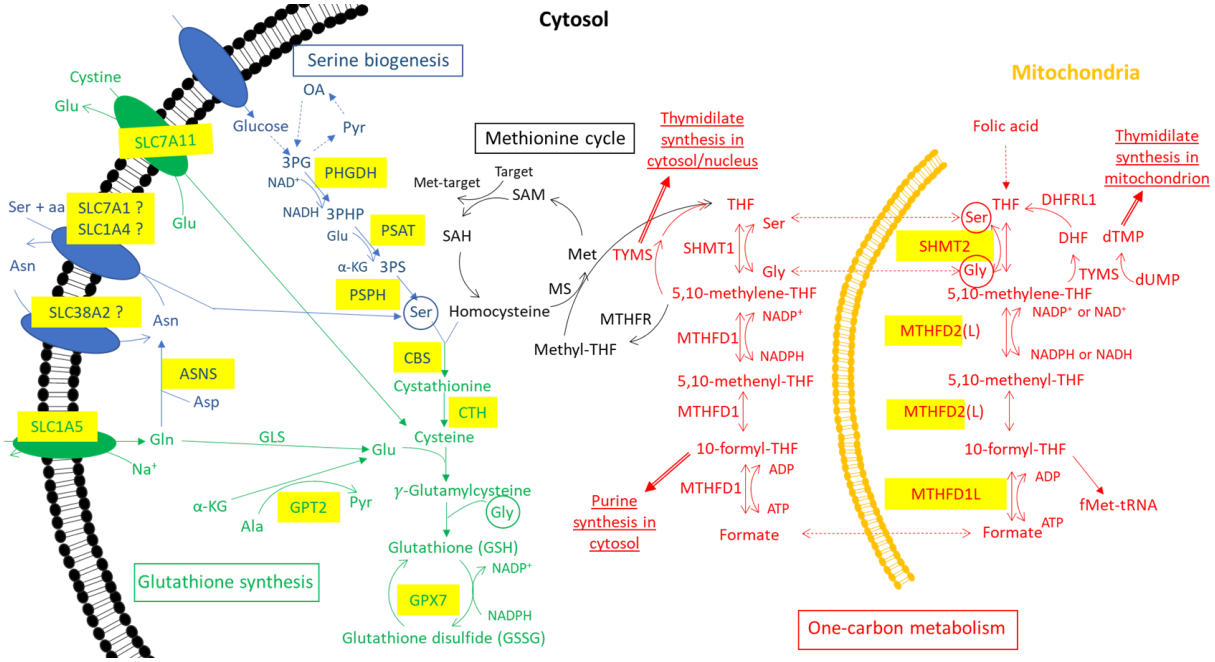

Figure 8: ATF4-controlled one-carbon metabolism, serine biogenesis and glutathione synthesis.

One-carbon metabolism (in red) is compartmentalized between the mitochondrion and the cytosol. In the mitochondrion, Serine HydroxyMethylTransferase 2 (SHMT2) catalyses the generation of Glycine (Gly) and 5,10-methylene-TetraHydroFolate (5,10-methylene-THF) from tetrahydrofolate (THF) and Serine (Ser). MethyleneTetraHydroFolate Dehydrogenase cyclohydrolase 2 (MTHFD2) or MTHFD2-Like (MTHFD2L) then catalyses the oxidation of 5,10-methylene-THF into 10-formyl-THF, which is necessary for the generation of N-formylMethionine-tRNA (fMet-tRNA), the mitochondrial translation initiator. MTHFD1L then catalyses the conversion of 10-formyl-THF into formate. Unlike the other one-carbon intermediates, formate can cross the mitochondrial membrane to the cytosol where it is used by MTHFD1 to produce 10-formyl-THF, which serves as a carbon donor for the purine synthesis, and to produce 5,10-methylene-THF which supports thymidylate synthesis and the Methionine (Met) cycle. Transport between mitochondrion and cytosol are indicated in dashed arrows. MTHFR: MethyleneTetraHydroFolate Reductase; TYMS: ThYMidilate Synthase; DHFRL1: DiHydroFolate Reductase Like 1; dUMP: deoxyUridine MonoPhosphate; dTMP: deoxyThymidine MonoPhosphate; SAM: S-Adenosyl-Methionine; SAH: S-Adenosyl-Homocysteine; MS: Methionine Synthase.

The serine synthesis pathway (in blue) uses 3-PhosphoGlycerate (3PG), originating from the glycolysis or the gluconeogenesis, in a three-step enzymatic cascade. PHosphoGlycerate DeHydrogenase (PHGDH) catalyses the oxidation of 3PG into 3-PhosphoHydroxyPyruvate (3PHP), which is then converted into 3-PhosphoSerine (3PS) by PhosphoSerine AminoTransferase 1 (PSAT1). PhosphoSerine PHosphatase (PSPH) then catalyses the hydrolysis of 3PS into Ser. OA: OxaloAcetate; α-KG: α-KetoGlutarate; Glu: Glutamate; Pyr: Pyruvate; Ala: Alanine; aa= amino acids. Ser can also be supplied from the extracellular environment, in which case Asparagine (Asn) plays an important role as an amino acid exchanger. The cell can be provided in Asn via import or synthesis mediated by ASparagiNe Synthetase (ASNS) from its substrates Aspartate (Asp) and Glutamine (Gln).
Glutathione is the most abundant antioxidant in the cell, and its synthesis (in green) from homocysteine, Ser, Glutamate (Glu) and Gly is essential for redox homeostasis. CTH: CystaTHionine lyase; SLC7A11: SoLute Carrier family 7, member 11; GPT2: Glutamate Pyruvate Transaminase; SLC1A5: SoLute Carrier family 1, member 5; GPX7, Glutathione PeroXidase 7; CBS: Cystathionine-Beta-Synthase; GLS: GlutaminaSe.
The enzymes/actors transcriptionally controlled by ATF4 are highlighted in yellow. Dashed arrows symbolize multi-step reactions. Personal illustration realized from combined information from the literature (Yang and Vousden, 2016) (Huggins *et al.*, 2016) (Krall *et al.*, 2016) (Shen *et al.*, 2020) (Andersona, Quintero and Stovera, 2011) (Woeller *et al.*, 2007).

Folate-mediated one-carbon metabolism is a prime pathway for cell proliferation as it is essential for nucleic acid supply (Stover and Field, 2011). Indeed, *de novo* purine synthesis and *de novo* thymidylate synthesis both rely on the folate cycle which provides formate-mediated one-carbon moieties (Fig 8). Folate cycle occurs in a parallel way in both cytosol and mitochondrion and each compartment possesses its own set of enzymes (Ducker and Rabinowitz, 2017). The cycle however fluxes from mitochondrion to cytosol. Mitochondria, that harbour around 40 % of the total cellular folate pool (Yoon Soon Shin *et al.*, 1976) (Lin, Huang and Shane, 1993), thus constitute the dominant branch in terms of formate synthesis. Indeed, this directionality of the cycle can be explained by a higher $NADPH/NADP^+$ ratio in the cytosol when compared to mitochondria, thereby supporting serine formation in the former compartment by driving MethyleneTetraHydroFolate Dehydrogenase 1 (MTHFD1) activity in the direction of folate intermediates reduction (Ducker and Rabinowitz, 2017).

Typically, in the mitochondrion, formate is generated from TetraHydroFolate (THF) and serine following a multi-step enzymatic cascade. In humans, THF supply requires vitamin B9 (folic acid) food intake. Formate is then exported to the cytosol where it is used to generate

intermediates, 10-formyl-THF and 5,10-methylene-THF, that feed purine synthesis and thymidylate synthesis, respectively (Ducker and Rabinowitz, 2017). Purine synthesis requires the bigger part of folate one-carbon units in proliferating cells, as 5,10-methylene-THF-dependent thymidylate synthesis is only required for DNA replication, whereas 10-formyl-THF-dependent purine synthesis is needed for both DNA and RNA synthesis. Besides providing the purine backbone with two carbon moieties, 10-formyl-THF, the most oxidized form of folate, also provides the cell with N-formylMethionine-tRNA (fMet-tRNA), the initiator tRNA required for the translation of proteins encoded by the mitochondria (Ducker and Rabinowitz, 2017). Of interest, the three mitochondrial enzymes supporting the folate cycle, namely Serine HydroxyMethylTransferase 2 (SHMT2), bifunctional MethyleneTetraHydroFolate Dehydrogenase/cyclohydrolase 2 (MTHFD2) and MTHFD1 Like (MTHFD1L) are regulated at the transcriptional level by ATF4 (Ben-Sahra *et al.*, 2016) (S. Wang *et al.*, 2015) (Fig 8).

A third cellular purpose of the folate cycle is feeding the methionine cycle. Indeed, formate-derived 5-methyl-THF, the most reduced form of formate, is destined to support the remethylation of homocysteine to methionine, thereby allowing the generation of S-Adenosyl-Methionine (SAM) (Fig 8). The metabolic importance of SAM in the cell can be compared to the one of ATP as it is a strong methyl group donor involved in plethora of cellular processes, especially in epigenetics (Ducker and Rabinowitz, 2017).

Consistently with their inherent rapid proliferation rate, cancer cells upregulate folate-mediated one-carbon metabolism (Ducker and Rabinowitz, 2017) (Yang and Vousden, 2016). In this context, MTHFD2 is of particular interest. MTHFD2 is normally expressed in embryogenic and undifferentiated tissues but absent in adult differentiated ones, where MTHFD2L ensures the enzymatic functions (Mejia and MacKenzie, 1985). However, MTHFD2 expression is reactivated and upregulated in proliferating malignant cells (Nilsson *et al.*, 2014). In these cells,

MTHFD2 has also been shown to localize in the nucleus where it is suspected to ensure an enzymatic-unrelated function driving cell proliferation, as the overexpression of *MTHFD2* lacking its dehydrogenase activity is still successful in increasing the proliferation of human colon cancer cells. The observation that MTHFD2 overexpression alone is sufficient to increase cell proliferation reflects a putative important role of upstream signaling regulator (Gustafsson Sheppard *et al.*, 2015).

Serine is an important precursor of the folate cycle (Fig 8). This is especially true regarding the purine synthesis. Indeed, not only does it allow the generation of 10-formyl-THF, a carbon donor for the purine backbone, but its catabolism into glycine also provides carbon and nitrogen moieties to the purine skeleton (Ben-Sahra *et al.*, 2016) (Fig 9). Catabolism of serine in the folate cycle constitutes a crucial source of glycine since CHO cells become auxotroph for glycine when their folate metabolism is disrupted (Taylor and Hanna, 1982) (McBurney and Whitmore, 1974).

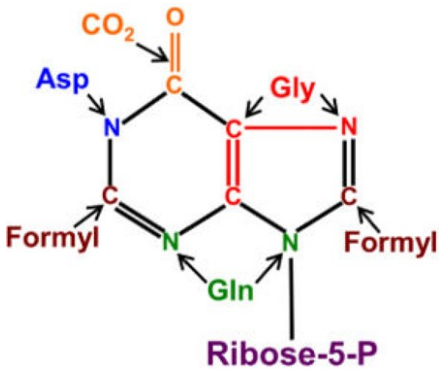

Figure 9 : Representation of a purine backbone.

During the *de novo* purine synthesis, several actors contribute to the formation of the purine backbone by providing carbon and/or nitrogen moieties: Gly: Glycine; Ribose-5-P: Ribose-5-Phosphate; Formyl: 10-formyl-THF; Glutamine: Gln; Aspartate: Asp. (Ben-Sahra *et al.*, 2016)

There are two possible sources of serine for the cell: either from the endogenous serine biosynthesis pathway and/or from an exogenous supply by serine uptake (Fig 8). The serine biogenesis initiates from 3-phosphoglycerate and is supported by three cytosolic enzymes, all

transcriptionally regulated by ATF4: PHosphoGlycerate DesHydrogensase (PHGDH), PhosphoSerine AminoTransferase 1 (PSAT1) and PhosphoSerine PHosphatase (PSPH) (Yang and Vousden, 2016) (Fig 8).

The control of serine exogenous supply is highly dependent on asparagine. Indeed, besides its basic but prime role as a building block provider, asparagine is also an amino acid exchange factor that allows import of several amino acids, especially serine, alongside its own export (Krall *et al.*, 2016). Asparagine is either directly imported from the extracellular environment or synthetized from glutamine and aspartate under the activity of the ASparagiNe Synthetase (ASNS), encoded by an ATF4-controlled gene (Krall *et al.*, 2016) (Fig 8).

In cancer cells, ATF4, as a regulator of amino acid homeostasis, is an actor of particular importance in this context of high bioenergetic demands (Mattaini, Sullivan and Vander Heiden, 2016). Thus, fibrosarcoma cancer cells silenced for ATF4 display a reduced proliferation rate, alleviated in the presence of NEAA (glycine, alanine, asparagine, aspartic acid, glutamic acid, proline and serine). More specifically, asparagine alone is able to rescue the survival of these cells that exhibit a severely reduced expression of ASNS, thus reflecting a defective ATF4-dependent asparagine biosynthesis (Ye *et al.*, 2010). This observation underlines the major importance of asparagine for cancer cells. The latter even seems to favour asparagine over glutamine for amino acid import (Krall *et al.*, 2016). The asparagine dependency of cancer cells is exploited therapeutically as the enzyme L-asparaginase that catalyses the degradation of asparagine is a common treatment for acute lymphoblastic leukaemia (Ertel *et al.*, 1979). However, the inherent adaptability of cancer cells leads to the upregulation of ASNS abundance and activity in order to compensate the loss of exogenous asparagine supply, leading to treatment resistance (Hutson *et al.*, 1997) (Aslanian, Fletcher and Kilberg, 2001).

Aside from their role in purine synthesis, serine and glycine are also essential for the cell redox homeostasis as they are important precursors for glutathione biosynthesis (Fig 8). Among other mechanisms, glutathione performs its antioxidant function as a substrate for glutathione peroxydases which are specific enzymes catalysing the reduction of hydrogen peroxyde and other peroxydes, a process that leaves glutathione in a disulfide oxidized state. In turn, oxidized glutathione will be further reduced by glutathione reductase, using NADPH coming from the pentose phosphate pathway (Lu, 2013). The synthesis of glutathione is composed of two major steps, the serine-dependent generation of γ-glutamylcysteine, and the subsequent glycine-dependent formation of glutathione (Lu, 2013). ATF4 regulates the transcription of many actors involved in glutathione synthesis in partnership with C/EBPγ (Huggins *et al.*, 2016) (Fig 8). Cancer cells are also highly dependent on ATF4 to maintain their oxidative homeostasis, challenged by higher ROS generation due to their accelerated metabolic activity. Thus, the silencing of ATF4 partner *C/EBP*γ in lung cancer cells A549 reduced their proliferation, restored in the presence of N-Acetyl Cysteine (NAC) (Huggins *et al.*, 2016).

Hence, ATF4 is a major regulator of amino acid metabolism/transport, nucleotide synthesis and oxidative stress, making it indispensable for a proper cell proliferation. *Atf4*$^{-/-}$ MEFs are thus unable to grow unless supplemented with NEAA, reflecting an ATF4-dependent defective amino acid synthesis (Harding *et al.*, 2003). Moreover, NEAA supplementation was necessary but not sufficient to completely restore the growth of *Atf4*$^{-/-}$ MEFs as they also require the presence of an antioxidant (glutathione, β-mercaptoethanol (BME) or NAC), suggesting an impaired redox homeostasis and particularly an impaired glutathione biosynthesis as cysteine supplementation, an intermediate in glutathione biosynthesis, also restores the growth phenotype (Harding *et al.*, 2003).

2.2. ATF4 upstream regulators

Histone lysine DeMethylase 4C (KDM4C) has been identified as an important transcriptional regulator of *ATF4* (Zhao *et al.*, 2016). KDM4C catalyses the demethylation of histone 3 at lysine 9, thereby removing the repressive transcription marks of certain genes. It has been shown that KDM4C upregulates the ATF4-dependent serine biogenesis and subsequently cancer cell proliferation (Zhao *et al.*, 2016).

The ATF4-dependent upregulation of serine biogenesis and one-carbon metabolism in response to growth signals or oncogenes is also mediated by mammalian Target Of Rapamycin Complex 1 (mTORC1), which increases *ATF4* mRNA stability and translation (Park *et al.*, 2017). mTORC1 is a major actor regulating cell growth and proliferation and its serine 2448 phosphorylation-mediated activation has been shown to be dependent on the availability of amino acids (Chiang and Abraham, 2005). More specifically, mTORC1 activation is notably sensitive to the presence of leucine and arginine. Indeed, the binding of these amino acids to specific mTORC1 inhibitors (Sestrin1 and Castor 2, respectively) triggers the activation of the signaling pathway (Wolfson and Sabatini, 2017).

Noteworthy, in a mouse model of mitochondrial myopathy carrying a mutation in the mitochondrial helicase Twinkle leading to mtDNA deletions, mTORC1 has been identified in muscle as the main executor of ATF4 activation, resulting in an ATF4-driven metabolic imbalance and aberration contributing to the disease progression (Khan *et al.*, 2017). Therefore, beyond integrating environmental cues for cell growth, mTORC1 also responds to mitochondrial dysfunction via ATF4. Along those lines, ATF4 is generally activated following mitochondrial disturbances (Fig 10) (Quirós *et al.*, 2017) (Kasai *et al.*, 2019).

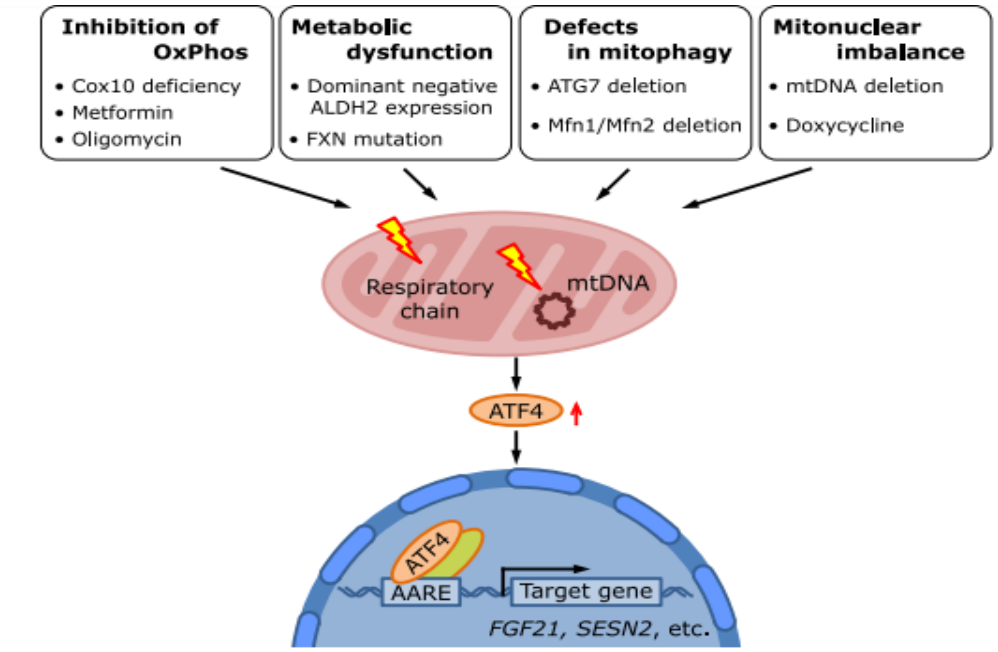

Figure 10 : ATF4 is activated in response to mitochondrial disturbances.

Various stresses affecting mitochondrial function can activate ATF4 (Kasai *et al.*, 2019), leading to the expression of specific target genes (SEStriN2 (SESN2), Fibroblast Growth Factor 21 (FGF21), …) through binding to the consensus sequence Amino Acid Responsive Element (AARE). Thus, an inhibition of the oxidative phosphorylation caused by either genetic mutations (*Cytochrome c assembly factor 10* (*Cox10*)-deficient mice) (Tyynismaa *et al.*, 2010) (Fujita *et al.*, 2007) or by treatment with a chemical compound like metformin (complex I inhibitor) (Kim, Jeong, Kim, *et al.*, 2013) and oligomycin (complex V inhibitor) (Garaeva *et al.*, 2016) has been shown to increase ATF4 expression. ATF4 is also activated in the context of metabolic dysfunction resulting for example from mutations in the gene coding for FrataXiN (FXN), a mitochondrial matrix protein necessary for the biosynthesis of iron-sulfur clusters (Huang *et al.*, 2013). Metabolic dysfunction and subsequent ATF4 activation can also occur during mitochondrial aldehyde stress as shown in *Aldehyde dehydrogenase 2* (*Aldh2*) mutant mice (Endo *et al.*, 2009). The actifvation of ATF4 has also been seen in a muscle-specific *Autophagy-related 7* (*Atg7*) KO mouse model in which the mitophagy is defective (Kim, Jeong, Oh, *et al.*, 2013). The impairment of mitochondrial dynamic, notably via deletion of mitochondrial fusion actors Mitofusin (Mfn) 1 and 2, also leads to ATF4 activation (Kim, Jeong, Oh, *et al.*, 2013). Finally, ATF4 also responds to an imbalance between proteins coded by the mitochondria and proteins coded by the nucleus following mtDNA depletion (Bao *et al.*, 2016) or doxycycline (inhibitor of mitochondrial translation) treatment (Michel *et al.*, 2015).

The ATF4 activation following mitochondrial impairment has often been shown to be driven by the ISR (S. F. Wang *et al.*, 2016) (Michel *et al.*, 2015) (Silva *et al.*, 2009). The ISR is an intricate signaling pathway activated in response to various cellular stresses in order to restore homeostasis (Pakos-Zebrucka *et al.*, 2016) (Fig 11, left). Upstream the pathway, four kinases

can be activated in response to distinct stresses. Double-stranded RNA-dependent Protein Kinase (PKR) is activated in response to viral infection, Heme-Regulated eukaryotic Initiation Factor 2α (eIF2α) kinase (HRI) in response to heme deprivation (occurring mainly in the erythroid lineage), PKR-like Endoplasmic Reticulum Kinase (PERK) in response to endoplasmic reticulum (ER) stress and General Control Nonderepressible 2 (GCN2) is activated in response to amino acid deprivation (more specifically to uncharged tRNAs). The latter is of particular importance for cancer cells since nutrient supply at the core of the tumor is often limited due to the scarcity of blood vessels. Moreover, the activation of the PERK-mediated axis of the ISR in cancer cells has been shown to be an adaptative response to hypoxic stress (Fels *et al.*, 2005). Noteworthy, these four kinases can have overlapping actions and compensate for each other. For example, they are all activated following oxidative stress (Pakos-Zebrucka *et al.*, 2016). Specifically, GCN2 can also be activated in response to the inhibition of mitochondrial protein translation. Indeed, Michel and collaborators showed that HeLa cells treated with doxycycline display an activation of the GCN2-mediated axis of the ISR (Michel *et al.*, 2015).

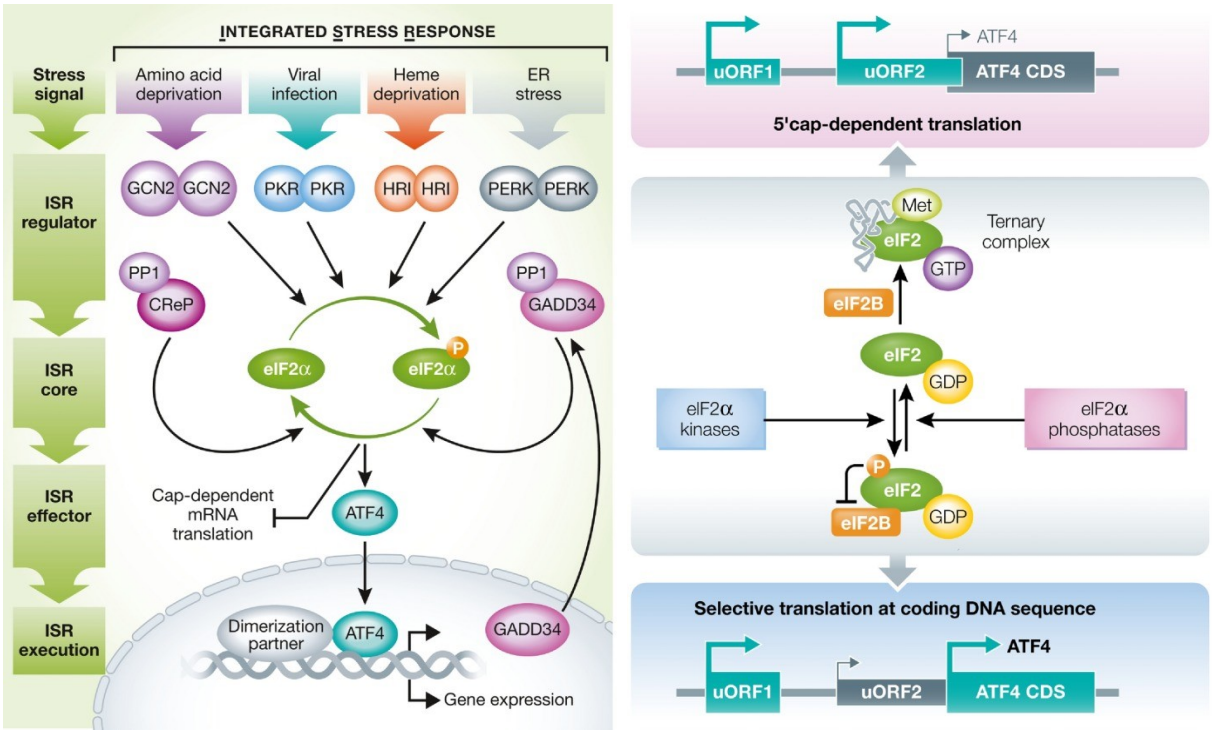

Figure 11 : The Integrated Stress Response (ISR) (left) and the translational control of Activating Transcription Factor 4 (ATF4) (right).

(Left) The ISR is activated by four major kinases, responding to specific cell stresses, namely General Control Nonderepressible 2 (GCN2), double-stranded RNA-dependent Protein Kinase (PKR), Heme-Regulated eukaryotic Initiation Factor 2α (eIF2α) kinase (HRI) and PKR-like Endoplasmic Reticulum Kinase (PERK). They all converge towards the activation of eukaryotic Initiation Factor 2α (eIF2α) kinase which, in turn, leads to an increase in *ATF4* translation. The latter then regulates the expression of target genes aiming at restoring cell homeostasis. The ISR is terminated under the action of Protein Phosphatase 1 (PP1) which catalyzes the dephosphorylation of eIF2α by recruiting either the constitutively expressed Constitutive Repressor of eIF2α Phosphorylation (CReP) or the ISR-induced Growth Arrest and DNA Damage-inducible protein 34 (GADD34). (Pakos-Zebrucka *et al.*, 2016)

(Right) The translation preinitiation complex composed of eukaryotic Initiation Factor 2α (eIF2α), Met-tRNA^{Met}, 40S ribosomal subunit and GTP is involved in mRNA translation as it recognizes the start codon of transcripts. The complex formation is dependent on eIF2B as it catalyses the reconversion of inactive eIF2α-GDP to active eIF2α-GTP. Under physiological conditions, ribosomes scanning starts at upstream Open Reading Frame 1 (uORF1) and promptly re-initiates at uORF2 which overlaps with *ATF4* CDS, thereby preventing its expression. In the presence of a cellular stress, the phosphorylation of eIF2α impairs eIF2B activity. This favours the translation of *ATF4* as a shortage of active complex eIF2α-GTP delays ribosome scanning which thus re-initiates at *ATF4* CDS instead of uORF2. (Pakos-Zebrucka *et al.*, 2016)

The ISR activation leads to the phosphorylation of eIF2α at serine 51 (Fig 11, left). Under physiological conditions, eIF2α plays a major role in global mRNA translation and constitutes the 43S preinitiation complex together with Met-tRNA^{Met}, 40S ribosomal subunit and GTP. This complex allows the recognition of the start codon upon which eIF2α catalyses the hydrolysis of GTP, thus inducing eIF2α-GDP dissociation from the complex and allowing the formation of the complete 80S initiation complex with the binding of the 60S ribosomal subunit. eIF2B then promotes the formation of a new complex by catalysing the reconversion of inactive eIF2α-GDP to active eIF2α-GTP (Rzymski *et al.*, 2009). Under cellular stress, the phosphorylation of eIF2α (PeIF2α) increases the stability of the PeIF2α-GDP-eIF2B complex and therefore prevents the formation of the active eIF2α-GTP complex. This leads to a general decrease in mRNA 5'-cap-dependent translation and simultaneously to a preferential translation of a subset of mRNAs, including *ATF4* whose 5'UnTranslated Region (5'UTR) is characterized by the presence of two upstream Open Reading Frames (uORFs). uORF1 acts positively towards *ATF4* translation by facilitating ribosome re-initiation at *ATF4* coding sequence. uORF2 acts negatively towards *ATF4* translation as it overlaps with *ATF4* coding sequence. Under physiological conditions, ribosomes tend to re-initiate at uORF2, therefore leading to low levels of ATF4 protein. Under cellular stress however, a dearth of the active complex eIF2α-GTP delays ribosome re-initiation, leading them to scan downstream uORF2 and re-initiate translation at *ATF4* ORF (Rzymski *et al.*, 2009) (Fig 11, right). The ATF4 protein then proceeds to a fine regulation of adaptive genes in order to alleviate the cellular stress or brings upon cell death if the stress insult is too severe (Pakos-Zebrucka *et al.*, 2016).

OBJECTIVES

In a previous work conducted in URBC and aiming at characterizing the mitochondrial biogenesis in stem cell plasticity, an increased expression of *MPV17* was noticed during mesenchymal stem cell differentiation towards hepatocytic lineage (Wanet *et al.*, 2017) (data deposited in NCBI's Gene Expression Omnibus through GEO Series accession number GSE75184). Unexpectedly, *MPV17* silencing had no impact on hepatogenic differentiation and mitochondrial DNA, while it significantly reduced the proliferation of culture-expanding Bone Marrow Mesenchymal Stem Cells (BM-MSC) and Umbilical Cord-MSC (UC-MSC) from different donors (Wanet A, personal communication). This observation is in accordance with the work of Choi and colleagues who showed that *MPV17* knockdown reduces the proliferation of NSC34 cells, a mouse motor neuronal cell line (Choi *et al.*, 2015). As MPV17 has been implicated in stress responses (Dallabona *et al.*, 2010) (Bottani *et al.*, 2014) and has been described as a channel with stress-dependent gating properties (oxidative and pH stress, etc) (Antonenkov *et al.*, 2015), we then wondered if MPV17 could have a role in the proliferation of human cancer cells, as they inherently experience oxidative and metabolic stress. Moreover, according to Protein Atlas, *MPV17* expression is associated with an unfavourable prognostic in liver cancer patients (www.proteinatlas.org/ENSG00000115204-MPV17/pathology) further suggesting a role of the protein in the process of oncogenicity.

In order to explore the putative role of MPV17 in the control of cancer cell proliferation, we will use a loss-of-function approach and silence *MPV17* expression in different cancer cell lines by lentivirus-mediated delivery of shRNAs.

MATERIALS AND METHODS

Cell culture

Human hepatoma cell lines Huh7 and HepG2 cells were grown in Dulbecco's Modified Eagle's Medium (DMEM) 1g/L glucose (Life technologies, #31885). Human renal embryonic cell line HEK293T was cultured in DMEM 4.5g/L glucose (Life technologies, #41965), human pulmonary adenocarcinoma cell line A549 and human squamous cell carcinoma cell line SQD9 in MEM GlutaMAX-1 (Life technologies, #42360), and human hepatoma cell line Hep3B in Roswell Park Memorial Institute medium 1640 (Life technologies, #21875). All those media were supplemented with 10 % Foetal Bovine Serum (FBS) (Life technologies, #10270) and used in a 5% CO_2 humid atmosphere at 37 °C. Huh7 cells (JCRB0403) were kindly provided by Prof. Sven Diederichs (DKFZ, Heidelberg, Germany). HepG2 (ATCC, HB-8065) were kindly provided by Prof. Luc Bertrand (UCL, Woluwe, Belgium). A549 cells (ATCC, CCL-185) were kindly provided by Dr Jacques Piette (ULg, Liege, Belgium). SQD9 cells were obtained from UCL (Vanessa Bol, Woluwe, Belgium). HEK293T (CRL-11268) and Hep3B (HB-8064) were purchased from ATCC. All these cell lines were used within 20 passages.

Plasmid amplification

Escherichia coli Stbl3 or *CcdB* survival strain was transformed with the plasmid to amplify by heat shock. Precisely, a mix of 1 µL of plasmid and 100 µL of bacteria was gently vortexed, placed 30 min on ice, 1 min on a 42 °C heat block and immediately put back on ice for 2 min. A volume of 250 µL of Luria Bertani broth (LB) (Carl Roth, X964) was added to the transformed bacteria and the tube was incubated 1 h under 225 rpm agitation. A volume of 100 µL of transformed bacteria was then spread on petri dish (Greiner bio-one, 664160) with 1.5 % agar (VWR, 84609) LB containing ampicillin (Sigma Aldrich, 10835242001) at 50 µg/mL and

grown overnight at 37 °C. The next day, one colony was picked and amplified in mini culture for 8 h and in maxi culture overnight. Plasmids were then extracted and purified using HiPure Plasmid Filter Maxiprep Kit (Invitrogen, K210017) according to the manufacturer's recommendations.

Lentivirus production

HEK293T were seeded at $4x10^6$ cells in 75 cm^2 culture flask (Corning, #430641U). The next day, the DNA mixture and the lipofectamine solution were prepared separately. The DNA mixture was composed of 0.4 µg of the envelope-encoding vector pCMV-VSVG (Addgene, #8454), 3.6 µg of the packaging vector psPAX2 (Addgene, #12260) and 4 µg of the expressing plasmid (Table 1), in 240 µL of 5 % opti-MEM (Invitrogen, #31985). The lipofectamine solution was composed of 16 µL of lipofectamine 2000 (Invitrogen, #11669) in 240 µL of 5 % opti-MEM. Both preparations were incubated for 5 min at room temperature, combined, incubated for 30 min at room temperature and added in the flask. After 18 h, the medium was renewed and at 48 h and 72 h post-transfection, the medium was collected and filtered on 0.45 µm steriflip (Millipore, SE1M003M00). Lentiviruses were titrated by Reverse Transcription quantitative Polymerase Chain Reaction (RT-qPCR) according to manufacturer's recommendations (Lentivirus qPCR Titer Kit, Applied Biological Materials, LV900).

MPV17 silencing

Sub-confluent cells were transduced with the adequate lentiviruses in the presence of 60 µg/mL protamine sulphate (Sigma-Aldrich, P4020), a positively-charged molecule favouring the binding of lentiviral particles to the cell membrane by reducing repulsion forces. Briefly, for the constitutive silencing of *MPV17*, cells were transduced with different shRNA-encoding vectors (pLKO.1-puro shNT, sh127649, sh128669, sh129921, sh131201, sh131038), selected

for 6 days with puromycin (Sigma-Aldrich, P8833) at 2.5 µg/mL and let to recover for 2 days without puromycin. They were then seeded and allowed to grow for 4 days before assessing the proliferation (Fig 12a).

For the inducible silencing of *MPV17*, cells were transduced or not with pLKO-puro-IPTG-3xLacO encoding sh129921, selected for 6 days with puromycin (Sigma-Aldrich, P8833) at 2.5 µg/mL and let to recover for 2 days. *MPV17* silencing was then obtained by incubation of the transduced cells with 0.1 mM of IsoPropyl ß-D-1-ThioGalactopyranoside (IPTG) (Sigma-Aldrich, I6758), renewed daily for 5 days unless stated otherwise. Cells were then seeded and allowed to grow for 4 days in presence of IPTG renewed daily (unless stated otherwise) before assessing the proliferation (Fig 12b).

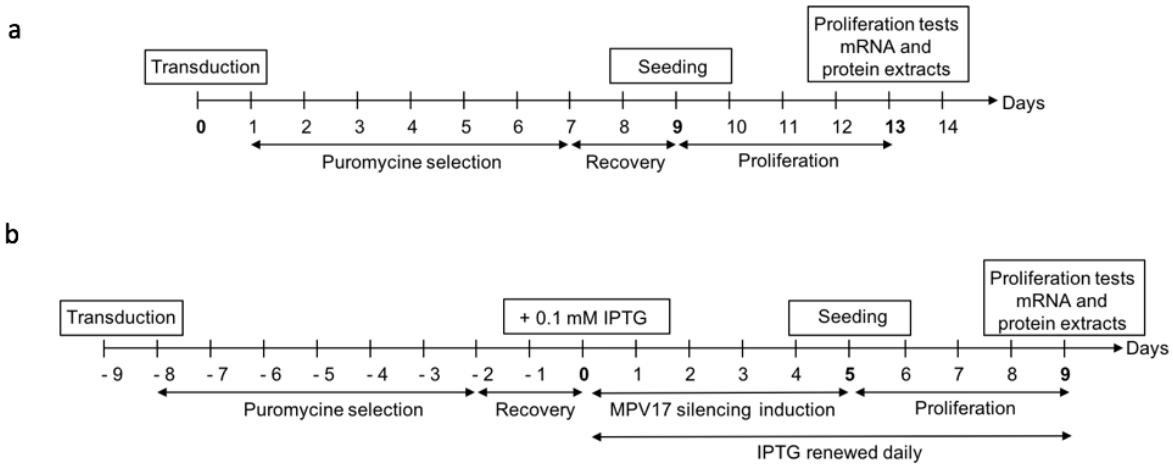

Figure 12 : Experimental timelines of *MPV17* silencing in the constitutive and inducible expression models.
Cells were transduced and puromycin-selected with a vector allowing a constitutive (a) or an inducible (b) *MPV17* silencing. After 2 days of recovery, cells were either seeded and allowed to grow for 4 days before assessment of proliferation (a) or treated with 0.1 mM of IsoPropyl ß-D-1-ThioGalactopyranoside (IPTG) for 5 days to induce *MPV17* silencing prior to the seeding. The proliferation was then assessed after 4 days of growth in the presence of IPTG renewed daily (b).

Proliferation assessment

- Cell counting

Cells were seeded in 25 cm^2 culture flask (Corning, #430639) and grown for 4 days. Cells were rinsed with Phosphate Buffered Saline (PBS) pH 7.4, detached using 0.05 % trypsin-EDTA (ThermoFisher, 25300) and centrifuged for 5 min at 200 g. The pellet was resuspended in culture medium and cell suspension density was counted in a Neubauer chamber. Doubling time was calculated as follow: time*ln(2) / (ln(number of cells at the end of the experiment) - ln(number of seeded cells)).

- MTT assay

This colorimetric assay, based on the enzymatic reduction (mainly catalysed by mitochondrial succinate dehydrogenase) of a tetrazolium dye to water insoluble formazan, is used as an indicator of cell proliferation (Mosmann, 1983). Cells were seeded in 24-well culture plates as indicated (Corning, #3524), grown for 4 days and incubated for 1 h with 500 µL of 3-(4,5-diMethylThiazol-2-yl)-2,5-diphenyl-2H-Tetrazolium bromide (MTT) (Sigma-Aldrich, M2128) (2.5 µg/mL in PBS) at 37 °C. Cells were then lysed for 1 h in lysis buffer (9 % sodium dodecyl sulphate, 60 % N, N-dimethylformamide, pH 4.7), and absorbance was measured with a spectrophotometer (xMark, Bio-Rad) at 570 nm.

- Protein content: Folin protein assay

This colorimetric method is based on the reaction of peptide bonds with copper ions under alkaline conditions followed by the reduction of phosphomolybdic-phosphotungstic acid by aromatic amino acids which generates a blue end product (heteropolymolybdenum blue). Cells were seeded in 24-well culture plates as indicated (Corning, #3524), grown for 4 days and rinsed twice with PBS. The bovine serum albumin (VWR, 0332) protein standards and samples were incubated 30 min in the presence of 200 µL of 0.5 M sodium hydroxide, then 10 min with

750 µL of a solution A (1.96 % sodium carbonate, 0.02 % sodium and potassium tartrate and 0.01 % copper sulphate) and finally 30 min with 75 µL of Folin and Ciocalteu's phenol reagent (Sigma-Aldrich, F9252) diluted twice in distilled water. Absorbance was measured with a spectrophotometer (xMark, Bio-Rad) at 740 nm (LOWRY *et al.*, 1951).

- Cyquant cell proliferation assay

This commercial assay allows the quantification of DNA following the binding of a fluorescent dye. Cells were seeded in 24-well culture plates (Corning, #3524) and grown for 4 days. DNA content was then measured using Cyquant cell proliferation assay (ThermoFisher, C7026) according to the manufacturer's recommendations.

Cell lysates and Pierce protein assay

Cells were seeded in 75 cm^2 culture flask as indicated (Corning, #430641U), rinsed once with PBS and lysed with radioimmunoprecipitation assay buffer (20 mM tris hydroxymethyl, 150 mM sodium chloride, 1 mM EDTA, 1 mM EGTA, 1 % sodium deoxycholate, 10 % glycerol, 1 % NP40, pH 7.6) supplemented with protease inhibitor cocktail (Sigma-Aldrich, 11697498001) and phosphatase inhibitor buffer (25 mM sodium orthovanadate, 250 mM 4-nitrophenylphosphate, 250 mM ß-glycerophosphate, 125 mM sodium fluoride). Lysates were sonicated 3 x 10 sec (amplitude 50) and centrifuged (10 min, 15000 g). Cleared cell lysates were assessed for protein content with Pierce 660 Protein Assay Reagent (ThermoFisher, 22660) according to the manufacturer's recommendations.

Western blotting analysis

Amounts of 20 µg of protein samples were prepared in loading buffer (0.03 M Tris-hydrochloride acid; pH 6.8, 0.04 M sodium dodecyl sulphate, 0.4 M BME, 5 % glycerol, 0.15

mM bromophenol blue), boiled for 5 min, resolved on polyacrylamide gel and transferred on a nitrocellulose membrane (Bio-Rad). Membrane was blocked for 1 h at room temperature in Odyssey Blocking Buffer (OBB) (LI-COR, P/N 927) diluted twice in PBS and incubated overnight at 4 °C with the primary antibody diluted in OBB with 0.1 % Tween-20 (OBB-T). For the particular detection of MPV17, the membrane was treated prior to blocking step with Super Signal Western Blot Enhancer (ThermoFisher, 46640) according to the manufacturer's recommendations. The next day, membrane was rinsed 3 x 5 min in PBS with 0.1 % Tween-20 (PBS-T), incubated with secondary antibody diluted in OBB-T 0.1 % for 1 h at room temperature, rinsed 3 times in PBS-T 0.1 %, dried and scanned with the Odyssey Infrared Imager (LI-COR, 9120). For the description of the antibodies used in this study, see Table 2.

Construct for MPV17 overexpression

MPV17 mRNA was reverse transcribed (Transcriptor First Strand cDNA kit, Roche, 04379012001) using a specific primer (5'-AGGTGGAAACGATGGAGTGA-3'). A PCR was then performed using a forward primer containing a restriction site for BamH1 (F: 5'-AGGATCCAGGAAGCATGGCA-3') and a reverse primer containing a restriction site for Sal1 (R: 5'-AGTCGACGGCAGGCTTAGA-3'). PCR products were purified using Wizard SV Gel and PCR Clean-Up System (Promega, A9281). An amount of 1 µg of PCR product and pLenti PGK Green Fluorescent Protein (GFP) Puro (Addgene, #19070) (Fig 13) was digested with BamH1, purified, restricted with Sal1, purified and finally ligated with T4 DNA ligase (Biolabs, M0202S) to construct the pLenti PGK MPV17 Puro plasmid. Lentiviruses were produced as described above.

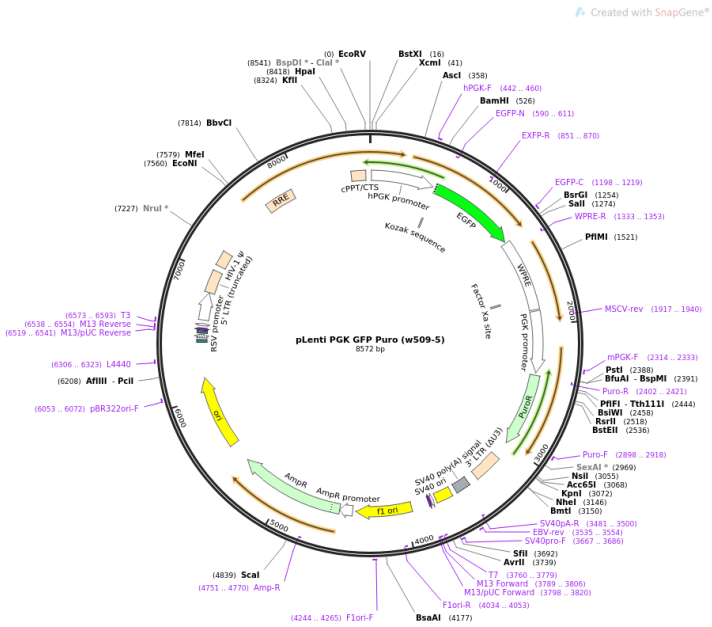

Figure 13 : Map of the plasmid used for the generation of *MPV17* overexpressing plasmid.

The map of pLenti PGK Green Fluorescent Protein (GFP) Puro plasmid (Addgene, #19070) used for the generation of MPV17 overexpressing plasmid is detailed here.

Rescue experiment

HepG2 cells were transduced with pLenti PGK GFP puro or pLenti PGK MPV17 puro-containing lentiviruses and selected for 6 days with puromycin (2.5 µg/mL). Cells were then transduced with PLKO.1-puro vector constitutively encoding sh129921 or shNT (Table 1). Cells were then allowed to recover and generate *MPV17*-targeting shRNA for 5 days, seeded and allowed to grow for 4 days. Cell proliferation was assessed by MTT assay at day 1 and day 4. To overexpress MPV17, we used *MPV17*-silencing and *MPV17*-overexpression vectors that were both bearing the resistance to puromycin. This obviously constitutes an obstacle in the selection of the cells that are double transduced. However, we decided to proceed further based on the knowledge that the sh129921-encoding vector robustly led to a very efficient transduction rate (nearly 100 %), therefore allowing to bypass the need for an ensuing antibiotic selection.

mtDNA content determination

DNA was extracted with the Wizard Genomic DNA Purification Kit (Promega, A1120) according to the manufacturer's recommendations. qPCR for mtDNA amplification was performed on the gene encoding NADH Dehydrogenase 2 (ND2) using the forward primer 5'-TGTTGGTTATACCCTTCCCGTACTA-3' and the reverse primer 5'-CCTGCAAAGATGGTAGAGTAGATGA-3'. For the normalization with nuclear DNA, the gene encoding Beclin was amplified with the forward primer 5'-CCCTCATCACAGGGCTCTCTCCA-3' and the reverse primer 5'-GGGACTGTAGGCTGGGAACTATGC-3'. Real time PCR was performed with SYBR Select Master Mix (ThermoFisher, 4472908). mtDNA copy number was calculated according to the following formula: $2*2^{\wedge-\Delta Ct}$ (where $\Delta Ct = Ctmean_{ND2} - Ctmean_{Beclin}$).

RNA extraction and RT-qPCR

RNA was extracted with RNeasy Mini kit (Qiagen, 74104) according to manufacturer's recommendations and QIAcube (Qiagen). RT was performed with GoScript™ Reverse Transcription Mix (Promega, A2791) according to the manufacturer's recommendations. qPCR was performed with SYBR Select Master Mix (ThermoFisher, 4472908). We used the $2^{-\Delta\Delta Ct}$ method to assess the relative mRNA expression. For the description of the primers (IDT) used in this study, see Table 3.

Supplementations with formate, deoxynucleosides, asparagine, NAC, NEAA and/or BME.

Cells were seeded at 8×10^3 cells/cm^2 and grown for 4 days in the presence/absence of 1, 5 or 10 mM of formate (Sigma-Aldrich, 71539) in DMEM with 0.1% FBS or in the

presence/absence of 0.7 mM asparagine (Sigma-Aldrich, A4284) or in the presence/absence of 50 μM of Thymidine (dThd) (Sigma-Aldrich, T1895), deoxyCytidine (dCtd) (Sigma-Aldrich, D3897) deoxyAdenosisne (dAdo) (Sigma-Aldrich, D8668) and deoxyGuanosine (dGuo) (Sigma-Aldrich, D0901) or 50 μM of dCtd, dAdo, dGuo or in the presence/absence of 0.1, 0.5, 5, 10 μM of NAC (Sigma-Aldrich, A7250) or in the presence/absence of 100 μM of NEAA (Gibco, 11140035) and/or 25, 50 or 100 μM of BME (Sigma-Aldrich, 63690).

While dAdo, dCtd, and dThd were diluted in distilled water, dGuo was diluted in ammonium hydroxyde (NH_4OH) 1M (Sigma-Aldrich, 338818) and heated 3 min at 105°C in order to achieve dissolution. When necessary, pH was readjusted.

RNA sequencing

Huh7 cells were transduced with shRNA non-target lentiviral vector (shNT) or vector targeting *MPV17* expression (sh129921). RNA quality was analysed with the Bioanalyzer 2100 (Agilent). RNA samples (n=4) were sent to Genomic Core Leuven (Belgium) for RNA sequencing and data were analysed with Ingenuity Pathway Analysis (QIAGEN Inc., https://www.qiagenbioinformatics.com/products/ingenuitypathway-analysis).

Immunohistochemistry

Liver paraffin embedded slices of 5 μm thickness (kindly provided by Professors Mustapha Najimi and Etienne Sokal, UCL) were incubated 2 x 5 min in xylene (ThermoFisher, X/0200/21), 2 x 3 min in isopropanol (VWR, 20842.330) and 10 min in 1% H_2O_2 (VWR, 23.613.446) / methanol prepared extemporaneously. They were then washed 3 min in tap water, 3 min in demineralized water, incubated 30 min in the 98°C water bath with the "Target Retrieval Solution 1x" pH 6.1 (Dako, S169984-2) and let to cool down for 15 min at room temperature. Slices were then washed 5 min in tap water, 2 x 3 min in PBS and incubated 1 h

at room temperature with a solution of PBS-2 % Normal Goat Serum (NGS) (ThermoFisher, 16210064). They were then incubated with the primary antibody anti-MPV17 (Table 2) diluted 1/100 in a solution of PBS-0.5 % NGS overnight at 4°C and, the next day, they were washed 3 x 3 min in PBS-T 0.05 % baths and 3 min in PBS. Slices were then incubated 30 min at room temperature with the secondary antibody EnVision-HRP anti-rabbit (Dako, K400311) before 3 washes of 3 min in PBS-T 0.05 % and one additional 3-min wash in PBS. They were then incubated 4 min at room temperature in the DAB solution (Dako, K346811), washed 5 min in running tap water, incubated 5 min in Mayer Hematoxyline and washed 5 min in running tap water. Finally, slices were incubated 3x 3 min in isopropanol, 3x 3 min in xylene and mounted on coverslip with Entellan glue (Merck Millipore, 107960).

Statistical analyses

Data are expressed as the mean ± Standard Error of the Mean (S.E.M). Figure plotting was performed with Prism software. Statistical analysis was performed using a one-tailed Mann-Whitney Test or a two-tailed Wilcoxon signed rank Test ($\alpha = 5$ %; *: $p<0.05$; **: $p<0.01$; ***: $p<0.001$; ****: $p<0.0001$).

Vector	**Supplier and reference**
pLKO.1-puro sh131201	Sigma-Aldrich SHCLND-NM_002437 TRCN0000131201
pLKO.1-puro sh128669	Sigma-Aldrich SHCLND-NM_002437 TRCN0000128669
pLKO.1-puro sh127649	Sigma-Aldrich SHCLND-NM_002437 TRCN0000127649
pLKO.1-puro sh129921	Sigma -Aldrich SHCLND-NM_002437 TRCN0000129921
pLKO.1-puro sh131038	Sigma-Aldrich SHCLND-NM_002437 TRCN0000131038
pLKO.1-puro shNT	Sigma-Aldrich SHC016-1EA
pLKO-puro-IPTG-3xLacO sh129921	Sigma-Aldrich 09301606MN TRCN0000129921

Table 1 : List of the plasmids used for *MPV17* silencing.

The vectors backbone and encoding shRNA are specified along with their references.

Antibody	**Supplier and reference**	**Dilution**
Anti -Actin	Sigma-Aldrich A5441	1/10000
Anti-ASNS	Proteintech 14681-1-AP	1/2000
Anti-ATF4	Santa Cruz Sc-390063	1/1000
Anti-ATF4	Cell Signaling #11815 lot 3	1/1000
Anti-eIF2α	Santa Cruz Sc-133132	1/1000
Anti-GAPDH	Abcam 128915	1/10000
Anti-mouse IgG IRDye 680RD Goat	LI-COR 926-68070	1/10000
Anti-mouse IgG IRDye 800CW Goat	LI-COR 926-32210	1/10000
Anti-MPV17	Proteintech 10310-1-AP	1/1000
Anti-MTHFD2	Proteintech 12270-1-AP	1/500
Anti-mTORC1	Cell Signaling #2972	1/1000
Anti-PeIF2α (ser51)	Cell Signaling #9721	1/1000
Anti-PmTORC1 (ser2448)	Cell Signaling #2971	1/1000
Anti-rabbit IgG IRDye 800CW Goat	LI-COR 926-32211	1/10000
Anti-rabbit IgG IRDye 680RD Goat	LI-COR 926-68071	1/10000
Anti-TFIID (TBP)	Santa Cruz Sc-204	1/500
Anti-Tubulin	Sigma-Aldrich T5168	1/10000

Table 2 : List of antibodies and their working dilutions used for western blotting.

The antibodies used for western blot analysis are specified with their reference and working dilutions.

Target gene	Forward primer (5'→3')	Reverse primer (5'→3')	Company
ATF4	GCCAAGCACTTCAAACCTCA	GCATCCTCCTTGCTGTTGTT	IDT
KDM4C	CCGATGACTCTTGTGAAGCAGC	GACTTCGTCTGCCAAAGGTGGA	IDT
MPV17	GCTCAGGAAGCATGGCACTCT	AATGTCACCCAGGCCCATCA	IDT
MTHFD1L	TGCTCTACAATGCCTGTTCC	AAGGGGAATCTCTTCTGGCT	IDT
MTHFD2	TGGCTGCGACTTCTCTAATG	CCTTCCAGAAATGACAACAGC	IDT
PHGDH	GCGGAAAGTGCTCATCAGT	GCAGAGCGAACAATAAGGC	IDT
PSAT1	CGTTCACCCTAAACTTGGGA	AGTCAAACTCCACACCATGC	IDT
PSPH	GACTCATAGCAGAGCAACCC	CCTGAACATTTCGCTCCTGT	IDT
SHMT2	GCATGAGAGAGGTGTGTGAT	TGAGTAGTGGTGGTGACGAT	IDT

Table 3 : List of primers used for qPCR.

The target genes and their associated primers as well as the provenance of the primers are specified.

RESULTS

MPV17 is overexpressed in several tumours.

Taking advantage of The Genome Cancer Atlas (TGCA) database, we showed that the abundance of *MPV17* transcript is significantly higher in tumours of 10 different tissues, including liver, bile duct, and colon (Fig 14a). This was confirmed at the protein level by immunohistochemistry staining performed on liver tumour biopsies from patients with adenocarcinoma (Fig 14b).

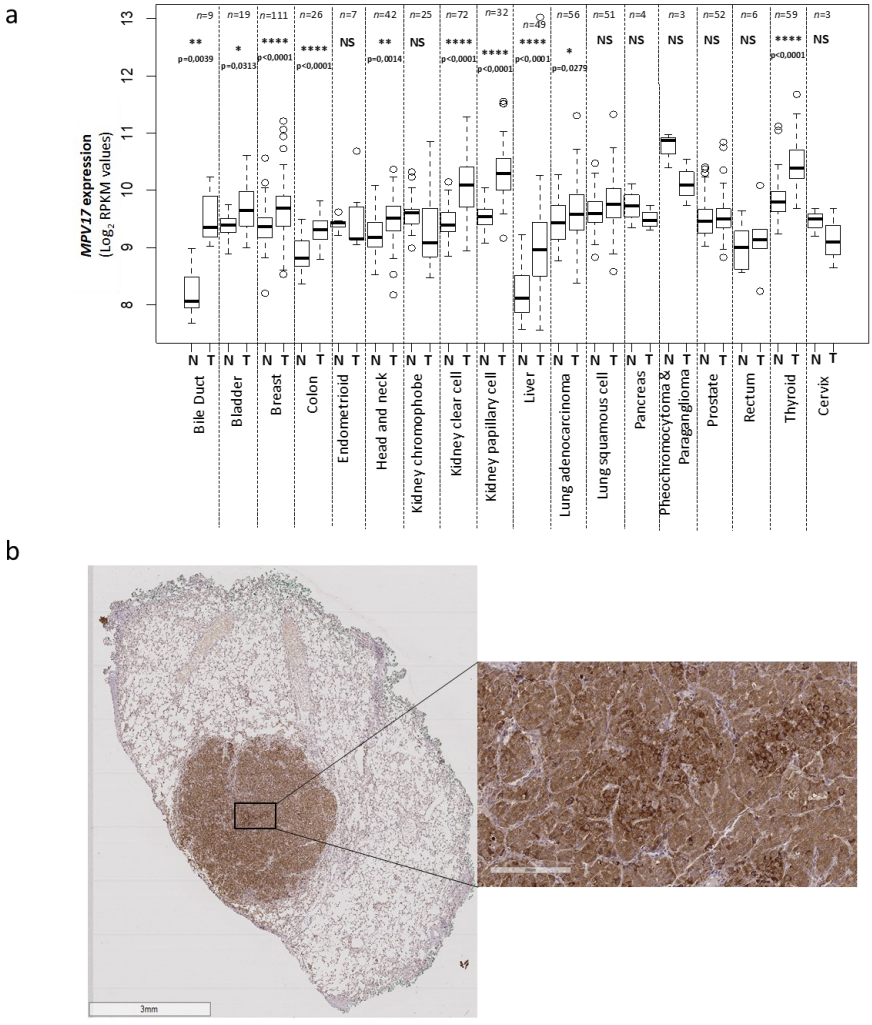

Figure 14 : Analysis of MPV17 expression in cancer tissues.

The Cancer Genome Atlas (TCGA), a public platform allowing the analysis of gene expression data sets generated by RNA sequencing (http://cancergenome.nih.gov), has been used to determine the expression level of *MPV17* in various tumour tissues (T) versus healthy tissues (N). P values were calculated with the two-tailed Wilcoxon signed

rank Test (α = 5 %; *: p<0.05; **: p<0.01; ***: p<0.001; ****: p<0.0001; NS: not significant) (a). Detection of MPV17 by immunohistochemistry in a paraffin-embedded biopsy of a liver adenocarcinoma (kindly provided by Professors Mustapha Najimi and Etienne Sokal, UCL). A strong signal for MPV17 is associated with the tumour, while the abundance of the protein is low in adjacent normal tissue (b).

MPV17 silencing is robustly associated with a decreased proliferation rate in different cancer cell lines.

In this study, we first assessed the effects of three commercially available shRNAs targeting *MPV17* mRNA: sh129921, sh127649 and sh131038. Using western blot analysis, the efficiency of gene silencing was evaluated by assessing the abundance of MPV17 in Huh7 cells transduced with these three shRNA-encoding lentiviral vectors. Both sh129921 and sh127649 led to an efficient knockdown of the gene while sh131038 did not efficiently induce *MPV17* silencing (Fig 15a).

We then demonstrated that Huh7 cells silenced for *MPV17* with sh129921 and sh127649 displayed a severely decreased proliferation rate, as quantified by three different proliferation assays, namely the doubling time (Fig 15b), the MTT assay (Fig 15c), and the total protein content (Fig 15d). The reduced cell proliferation phenotype was correlated with *MPV17* knockdown efficiency as no decreased proliferation rate was observed in Huh7 cells transduced with the vector encoding sh131038, the only shRNA that turned out to be inefficient in the knockdown induction.

To discard the possibility of a putative cell type or cancer type-specific phenotype, we next assessed the impact of sh129921 on the proliferation of two other human hepatoma cell lines, Hep3B and HepG2 cells, and two non-liver cancer cell lines, A549 cells, derived from a human pulmonary adenocarcinoma and SQD9 cells, a human squamous cell carcinoma cell line. Interestingly, Hep3B (Fig 15e), A549 (Fig 15f), SQD9 (Fig 15g) and HepG2 (data not shown) cells transduced with sh129921-encoding vector also displayed a reduced proliferation phenotype.

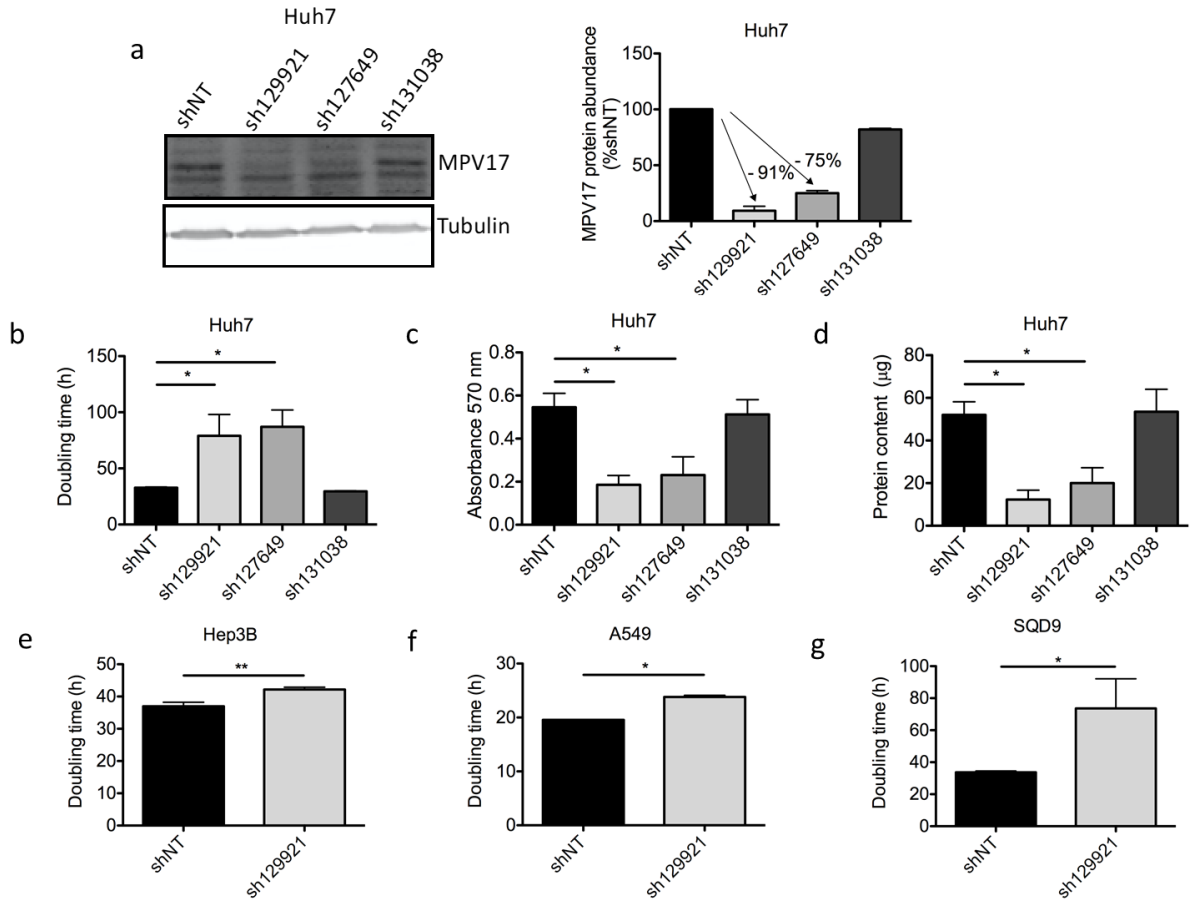

Figure 15 : Effect of shRNA-mediated *MPV17* knockdown on the proliferation of cancer cell lines.

Huh7 cells were transduced with non-target shRNA lentiviral vectors (shNT) or with shRNA lentiviral vectors targeting *MPV17* expression (sh129921, sh127649, sh131038). Hep3B, A549 and SQD9 cells were transduced with lentiviral shNT- or sh129921-containing vectors. Cells were selected for 6 days with puromycin (2.5 µg/mL). Cells were seeded at 8×10^3 cells/cm^2 (a, b, c, d, Huh7; g, SQD9), 5×10^3 cells/cm^2 (e, Hep3B) and 2.7×10^3 cells/cm^2 (f, A549) and grown for 4 days. MPV17 protein abundance was assessed by western blot analysis (a, Huh7). A representative western blot of 3 independent biological replicates (2 for sh131038) is shown (left) along with the western blot quantification of all the biological replicates (quantification with Image J software, data expressed as relative protein abundance to cells transduced with shNT-encoding vectors, right). Proliferation was then assessed by manual counting to calculate the doubling time (b, Huh7; e, Hep3B; f, A549; g, SQD9), by MTT assay (c, Huh7) and by the total protein content (d, Huh7). Data are presented as mean ± S.E.M of 3 independent biological replicates (2 for sh131038). P values were calculated with the one-tailed Mann-Whitney Test (α = 5 %; *: $p<0.05$; **: $p<0.01$; ***: $p<0.001$).

MPV17 silencing is not associated with mtDNA copy number depletion.

As MPV17 deficiency is associated with MDDS, we assessed whether *MPV17* silencing was accompanied by depletion in the mtDNA content or not, possibly accounting for the associated

decreased proliferation rate. Indeed, such mitochondrial defect has been shown to impair cell cycle progression (Mineri *et al.*, 2009). However, *MPV17* silencing did not lead to a reduction of mtDNA content in any of the tested cancer cell lines (Fig 16). This result is in agreement with observations from the literature regarding studies performed on other proliferating cancerous and non-cancerous cell types. Indeed, Alonzo and collaborators did not find any reduction of mtDNA content in *MPV17*-silenced HeLa cells (Alonzo *et al.*, 2018). Also, Dalla Rosa and collaborators showed that fibroblasts from *MPV17*-deficient patients did not display any reduced mtDNA content when proliferating (Dalla Rosa *et al.*, 2016).

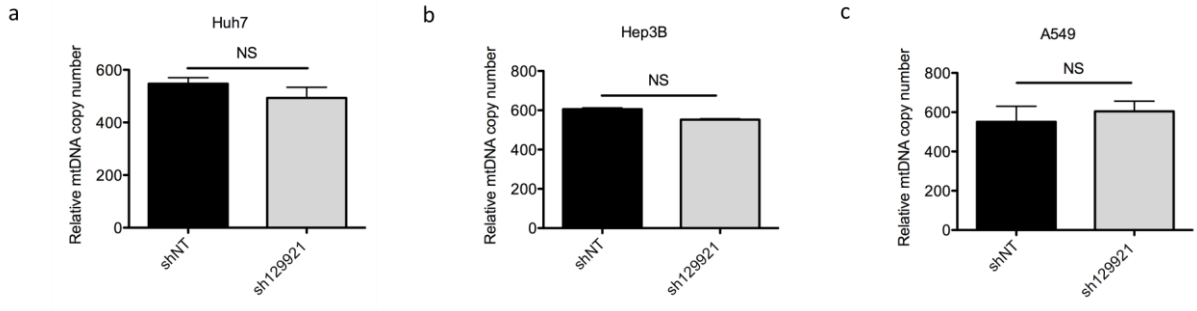

Figure 16 : Assessment of mtDNA content in *MPV17*-silenced cancer cell lines.

Huh7 (a), Hep3B (b) and A549 (c) cells were transduced with non-target shRNA- (shNT) or sh129921-containing lentiviral vectors. Transduced cells were selected for 6 days with puromycin (2.5 µg/mL). DNA was then extracted and mtDNA content was assessed by qPCR using NADH dehydrogenase 2 as a specific marker of mtDNA content and beclin for normalization with nuclear DNA. Results are presented as mean ± S.E.M of 3 independent biological replicates and are expressed in relative copy number to the nuclear DNA. P values were calculated with the one-tailed Mann-Whitney Test (α = 5 %; NS; *: $p<0.05$; **: $p<0.01$; ***: $p<0.001$).

The decreased proliferation rate in *MPV17*-silenced cells is associated with a decrease in the abundance of ATF4.

In order to determine the molecular mechanisms underlying the decreased proliferation rate in *MPV17*-silenced cancer cells, a transcriptomic analysis was performed. The RNA sequencing analysis was conducted on Huh7 cells transduced with sh129921- or shNT-encoding vectors. We performed an Ingenuity Pathway Analysis (IPA) on the RNA sequencing results, focusing on transcriptional regulators potentially responsible for a reduced proliferation capacity. In this

regard, the functional activities of ATF4 and MYC were predicted to be the most strongly inhibited as illustrated by their negative Z-scores (-2.792 and -4.635, respectively). The Z-score reflects the activation state of an upstream regulator by taking account "of known directional effects of one molecule on another or on a process, and the direction of change of molecules in the dataset" (Fakiola *et al.*, 2019). ATF4, frequently upregulated in cancer cells (Wortel *et al.*, 2017), is an attractive candidate in the attempt to elucidate the molecular mechanisms underlying the reduced proliferation phenotype in *MPV17*-silenced cancer cells as it has been shown that ATF4 not only up-regulates the expression of genes encoding actors implicated in amino acid uptake and metabolism (Harding *et al.*, 2003) (Malmberg and Adams, 2008) (Shu Wang *et al.*, 2015) but also promotes, indirectly, nucleotide synthesis (Ben-Sahra *et al.*, 2016), two essential aspects for cell proliferation. Therefore, its decreased abundance could readily explain a reduced proliferation rate, as exemplified in the literature and presented in the introduction (Ye *et al.*, 2010) (Huggins *et al.*, 2016) (Harding *et al.*, 2003).

The MYC proto-oncogene is also of great interest as it promotes cell cycle progression (Bouchard, Staller and Eilers, 1998) (Dang, 2013). We therefore decided to investigate both these transcription factors. While MYC western blotting analysis was technically challenging and so far inconclusive, the reduction of *ATF4* transcript abundance was readily confirmed at the protein level in sh129921 and sh127649-encoding vector transduced Huh7 cells (Fig 17a) as well as in sh129921-encoding vector transduced Hep3B (Fig 17b) and A549 (Fig 17c) cells, when compared with control cells transduced with shNT-containing vector.

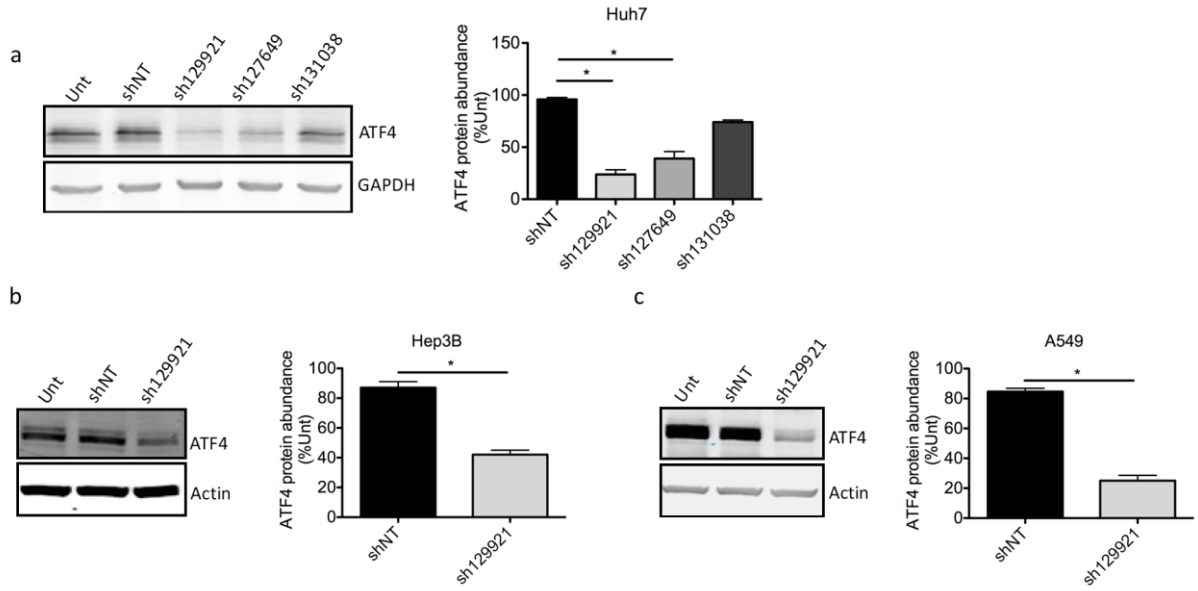

Figure 17 : ATF4 protein abundance following *MPV17* knockdown in Huh7, Hep3B and A549 cells.

Huh7 cells (a) were transduced with non-target shRNA lentiviral vectors (shNT) or with shRNA lentiviral vectors targeting *MPV17* expression (sh129921, sh127649, sh131038). Hep3B (b) and A549 (c) cells were transduced with lentiviral shNT- or sh129921-containing vectors. Cells were selected for 6 days with puromycin (2.5 µg/mL) before assessing ATF4 protein abundance by western blot analysis. For each cell line, a representative western blot of 3 (2 for sh131038) independent biological replicates is shown (left) along with the western blot quantification of all the biological replicates (quantification with Image J software, data expressed as relative protein abundance to untransduced (unt) cells, right). P values were calculated with the one-tailed Mann-Whitney Test (α = 5 %; *: $p<0.05$; **: $p<0.01$; ***: $p<0.001$).

Altogether, these results seem to strongly support an involvement of MPV17 in cancer cell proliferation as *MPV17* silencing is consistently accompanied by a reduction of both cell proliferation rate and ATF4 protein abundance. We therefore further investigated the ATF4-dependent cellular pathways potentially responsible for the reduced proliferation phenotype. During our investigation, we noticed that *SHMT2, MTHFD2* and *MTHFD1L* transcript expression levels were reduced in sh129921-mediated *MPV17*-silenced Huh7 cells (Fig 18a, b, c), suggesting an ATF4-dependent impairment of the folate cycle, a consequential shortage of formate supply and, *in fine*, a reduced nucleotide synthesis. However, a formate supplementation had no effect on the proliferation of *MPV17*-silenced cells (Fig 18d).

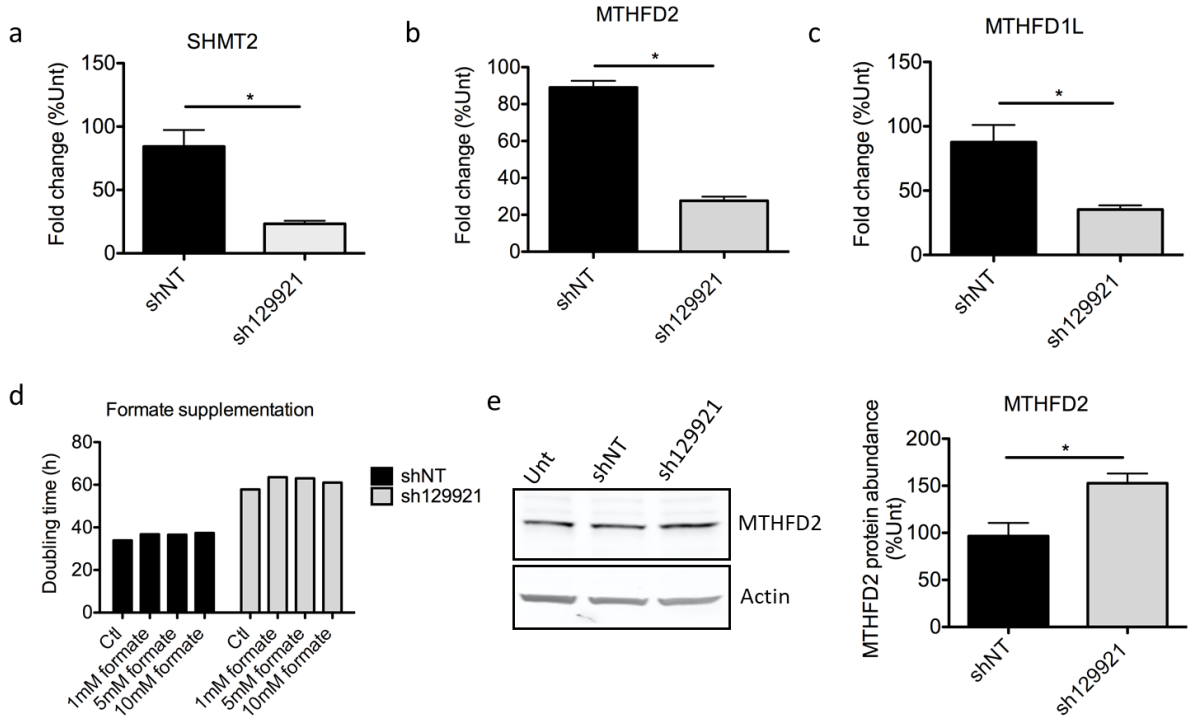

Figure 18 : Despite a downregulation of several transcripts involved in the folate cycle in *MPV17*-silenced cells, a formate supplementation does not rescue the reduced proliferation rate.

Huh7 cells were transduced with non-target shRNA- (shNT) or sh129921-containing lentiviral vectors. Transduced cells were selected for 6 days with puromycin (2.5 µg/mL). RNA was extracted and RT-qPCR was performed to assess *SHMT2* (a), *MTHFD2* (b) and *MTHFD1L* (c) transcript levels (data expressed relatively to untransduced cells (Unt)). Results are presented as mean ± S.E.M for 3 independent biological replicates. MTHFD2 protein abundance was also assessed by western blot analysis. A representative western blot of 3 independent biological replicates is shown (left) along with the quantification with Image J software of all three biological replicates (right) and data are expressed as relative protein abundance to untransduced cells (Unt) (e). Cells were seeded at 8×10^3 cells/cm^2 and grown for 4 days in the presence/absence of increasing formate concentration. Proliferation was then assessed by manual counting to calculate the doubling time, n=1 (d). P values were calculated with the one-tailed Mann-Whitney Test (α = 5 %; *: $p<0.05$; **: $p<0.01$; ***: $p<0.001$).

An explanation could lie in the observation that while *MTHFD2* mRNA expression is strongly downregulated in *MPV17*-silenced cells, this is not the case at the protein level. It is in fact the opposite as the protein abundance is significantly higher in *MPV17*-silenced cells compared to control (Fig 18e), suggesting either a translational compensation, or an increased stability of MTHFD2 protein in these cells.

Nonetheless, a potential proper formate supply does not necessarily exlude a depletion in nucleotide synthesis. Indeed, *MPV17*-silenced cells could suffer from a shortage of an upstream actor of the folate cycle, serine. Enticingly, sh129921-mediated *MPV17*-silenced Huh7 cells display reduced transcript expression levels of the three ATF4-controlled genes encoding for the enzymes driving the serine biosynthesis, namely *PHGDH*, *PSAT1* and *PSPH* (Fig 19a, b, c). As serine can also be taken up by the cell from the extracellular environment in an asparagine-dependent way, we also investigated the availability of this critical amino acid for the cells. As the Huh7 cells culture medium (DMEM) does not contain asparagine, the latter would be most likely synthetized under the ASNS activity. Interestingly, ASNS protein abundance is decreased in *MPV17*-silenced cells (Fig 19d). These results could suggest a depletion in serine in *MPV17*-silenced cells, leading to a depletion in glycine and a consequent decrease in purine synthesis. Thus, an asparagine supplementation was conducted in an attempt to restore the normal proliferation phenotype in *MPV17*-silenced cells. Although it resulted in a mild enhancement of the proliferation rate for *MPV17*-silenced cells, this effect was also observed in the control condition, indicating no net restoration of the proliferation of *MPV17*-silenced cells relatively to control (Fig 19e).

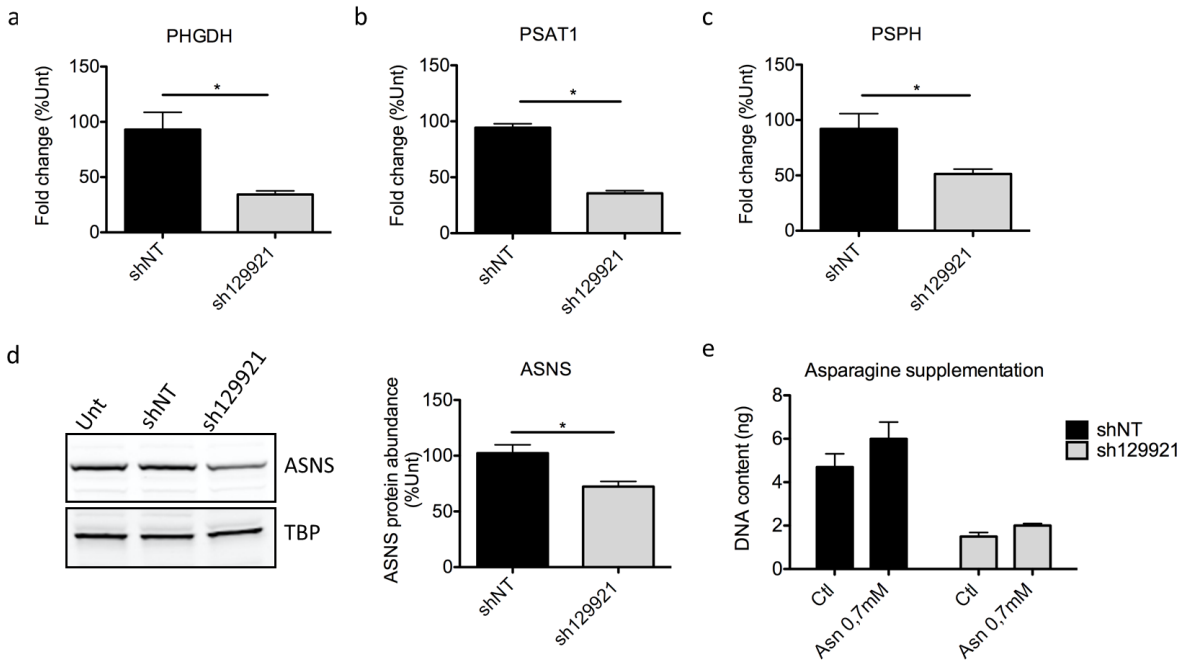

Figure 19 : Effect of *MPV17* silencing on key actors regulating serine supply.

Huh7 cells were transduced with non-target shRNA- (shNT) or sh129921-containing lentiviral vectors. Transduced cells were selected for 6 days with puromycin (2.5 µg/mL). RNA was extracted and RT-qPCR was performed to assess *PHGDH* (a), *PSAT* (b) and *PSPH* (c) transcript levels (data expressed relatively to untransduced cells (Unt). Results are presented as means ± S.E.M for 3 independent biological replicates. ASNS protein abundance was also assessed by western blot analysis. A representative western blot of 3 independent biological replicates is shown (left) along with the quantification with Image J software of all three biological replicates (right) and data are expressed as relative protein abundance to untransduced cells (Unt) (d). Cells were seeded at 8×10^3 cells/cm^2 and grown for 4 days in the presence/absence 0.7 mM Asparagine (Asn). Proliferation was then assessed by Cyquant assay. n=1, 3 technical replicates (e). P values were calculated with the one-tailed Mann-Whitney Test (α = 5 %; *: $p<0.05$; **: $p<0.01$; ***: $p<0.001$).

As neither formate nor asparagine supplementations succeeded to restore the reduced proliferation phenotype, even partially, and because deoxynucleotide synthesis is dependent on plethora of actors, controlled or not by ATF4, we decided to directly supplement the cells with deoxynucleosides to circumvent any hurdle. However, sh129921-mediated *MPV17*-silenced Huh7 cells showed no improvement in proliferation rate under this treatment (Fig 20a).

As ATF4 is also an important regulator of glutathione-related redox homeostasis, we hypothesized that the reduced abundance of ATF4 may lead to a disturbance in the redox balance and therefore a decreased cell proliferation that could be alleviated by supplementation

with an antioxidant like NAC. This hypothesis is supported by the literature (Huggins *et al.*, 2016), by the suspected shortage of actors implicated in glutathione biosynthesis, namely serine and glycine, and by data provided by the RNA sequencing on *MPV17*-silenced cells. Indeed, reduced transcript levels of enzymes implicated in the synthesis of glutathione such as cysthationine gamma-lyase (log2 fold change = -1,456 ; p-value = 2,14E-0,8) and cysthationine synthase (log2 fold change = -0,584 ; p-value = 2,34E-0,6) have been observed in *MPV17*-silenced cells compared to control. However, a NAC supplementation was not able to restore the proliferation phenotype of *MPV17*-silenced Huh7 cells (Fig 20b).

As a single supplementation may not be sufficient to restore the reduced proliferation rate (Harding *et al.*, 2003), in the way that ATF4 drives several important pathways, we attempted a double supplementation allying a cocktail of NEAA and the antioxydant BME. This double supplementation was however unsuccessful (Fig 20c).

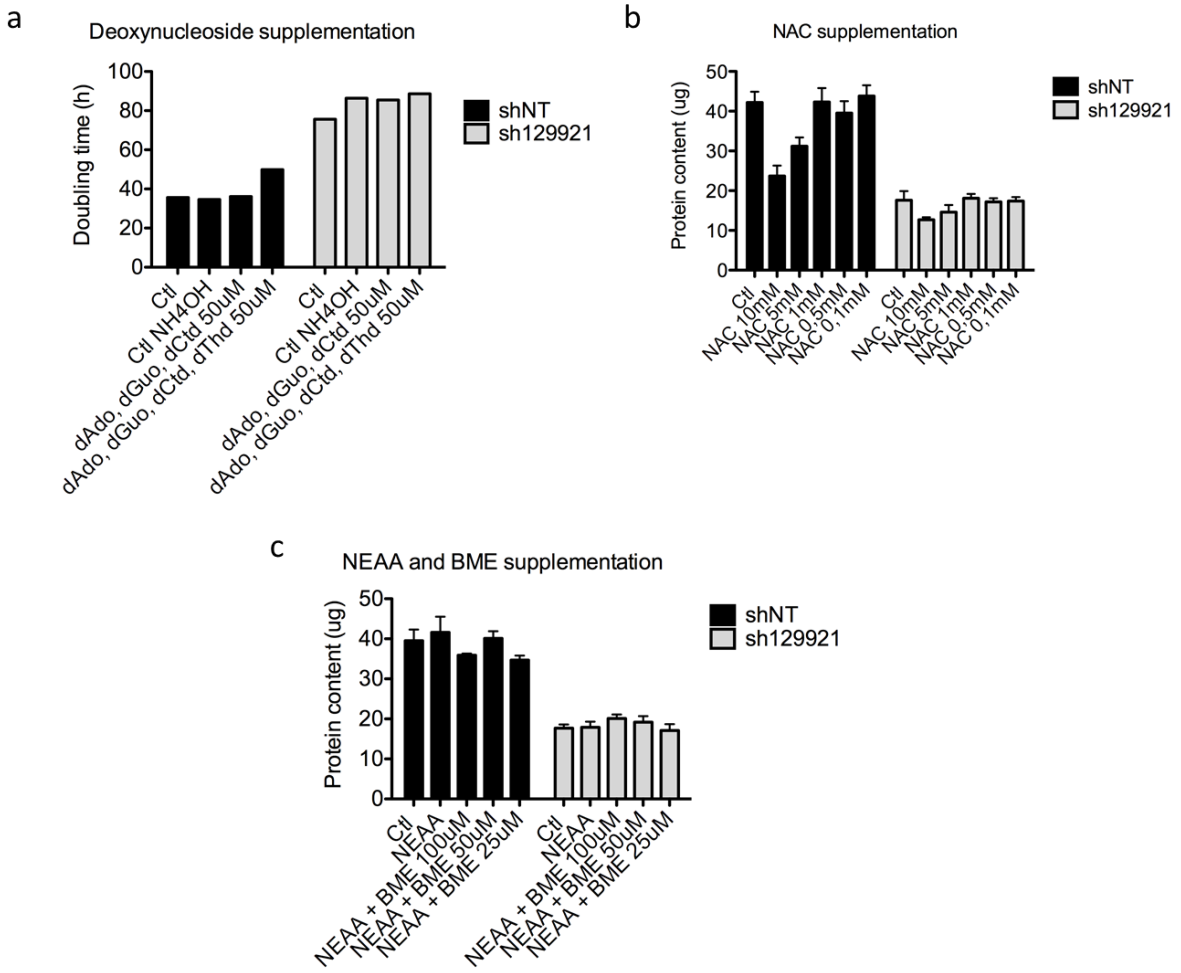

Figure 20 : Effect of deoxynucleoside, N-AcetylCysteine (NAC) and Non-Essentiel Amino Acid/ ß-Mercaptoethanol (NEAA/BME) supplementations on *MPV17*-silenced cells proliferation.

Huh7 cells were transduced with non-target shRNA- (shNT) or sh129921-containing lentiviral vectors. Transduced cells were selected for 6 days with puromycin (2.5 µg/mL). Cells were seeded at 8×10^3 cells/cm^2 and grown for 4 days in the presence/absence of 50µM of deoxyThymidine (dThd), deoxyCytidine (dCtd), deoxyAdenosisne (dAdo) and deoxyGuanosine (dGuo) diluted in ammonium hydroxide (NH_4OH) 1M or 50 µM of dCtd, dAdo, dGuo (a); in the presence/absence of increasing concentrations of NAC (b); in the presence/absence of increasing concentrations of BME and/or 100 µM of NEAA (c). Proliferation was then assessed by manual counting to calculate the doubling time (a; n=1), or by protein content dosage (b and c; n=1; 3 technical replicates).

Simultaneously to the rescue attempt of the ATF4-associated proliferation phenotype, we also investigated the upstream actors responsible for the reduced ATF4 abundance. The different hypothesis proposed are summarized in Figure 21.

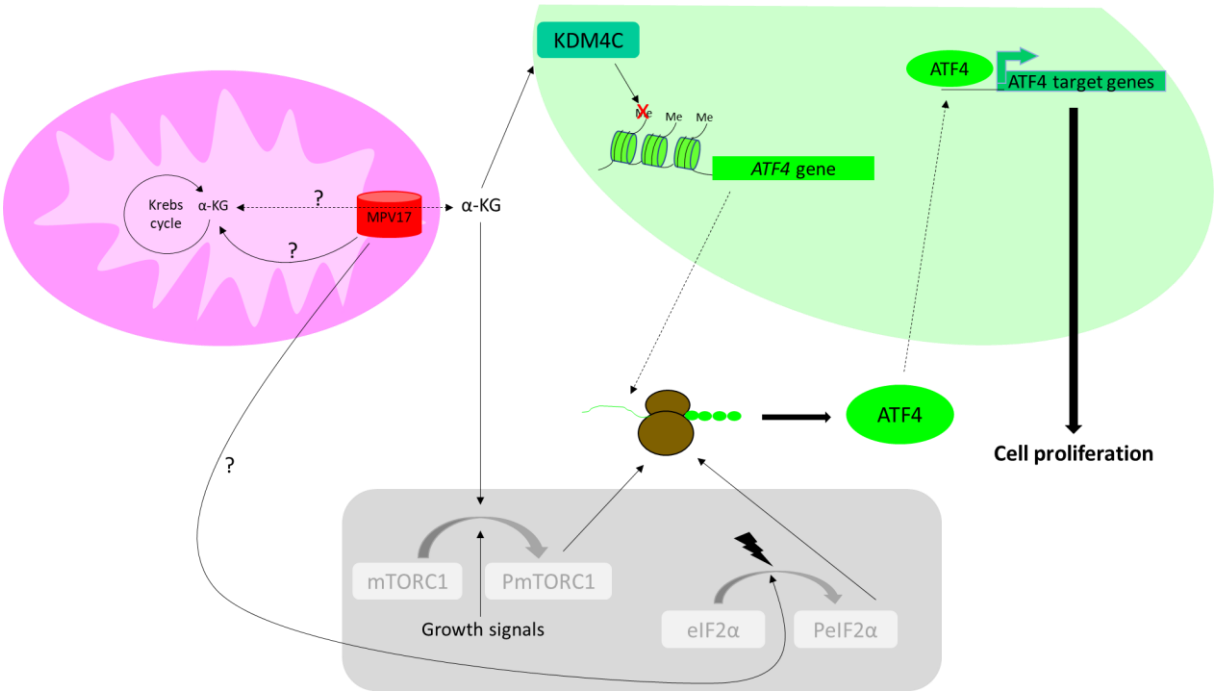

Figure 21 : How could MPV17 and ATF4 be functionally connected?

ATF4 abundance can be regulated either at the transcriptional level (Lysine DeMethylase 4C (KDM4C)) or at the translational level (active mTORC1 and PeIF2α). KDM4C is a histone modifying enzyme catalysing the removal of methyl groups (Me) from the trimethylated lysine 9 of histone 3, thereby activating the transcription of genes such as *ATF4*. The increased abundance of this transcription factor allows the expression of its target genes favouring cell proliferation. Noteworthy, MPV17 (Sym1) has been implicated in the homeostasis/transport (?) of Krebs cycle intermediates such as α-KetoGlutarate (α-KG). However, whether or not MPV17 is a direct transporter of metabolic intermediates still remains to be determined. As KDM4C is dependent on α-KG, its activity could be negatively affected by the functional loss of MPV17. α-KG has also been shown to induce mTORC1 activation. Therefore, a shortage in this intermediate could also hinder mTORC1 activity, resulting in a decrease in *ATF4* translation. The phosphorylation of eIF2α following a cellular stress (symbolized by a thunderbolt) leads to an increased translation of *ATF4*. One could speculate that, in cancer cells, the homeostasis keeper MPV17 and the integrated stress response positively regulate each other and ensure coping with bioenergetically demanding processes. Among those three upstream regulators of ATF4, the ones that we showed not implicated in the ATF4 reduced abundance observed in *MPV17*-silenced cells are greyed. Only the KDM4C-dependent mechanism is therefore left coloured but its implication in ATF4 reduced abundance and its direct functional link with MPV17 are in need of further investigations. Dashed arrows symbolize flux.

As a reminder, a decreased abundance of ATF4 could be due to a reduced activation of the ISR, resulting in lower level of eIF2α phosphorylated form (itself leading to a decrease in *ATF4* translation). The uncontrolled growth of cancer cells demands a strong adaptive response to cope with the increased metabolic load. In this regard, cancer cells often exploit the ISR

(Nguyen *et al.*, 2018). For example, in response to nutrient deprivation, a fibrosarcoma cell line has been shown to activate the GCN2-PeIF2α-ATF4 pathway to maintain metabolic homeostasis and survival (Ye *et al*., 2010). As MPV17 is described as a homeostasis keeper, one could hypothesize that the increased expression of *MPV17* observed in cancer cells (Fig 14a) participates in their accommodation to such substantial resource expenditure. One could also speculate that the ISR and MPV17 are, in this regard, positively interconnected. Interestingly, it has been shown that Sym1 is activated by the mitochondrion-nucleus retrograde response, a homeostasis-driven signaling pathway inducing nuclear genes expression in response to mitochondrial stress (Dallabona *et al.*, 2010). However, our results showed no change in PeIF2α level, excluding an upstream role of this particular actor in ATF4 reduced abundance (Fig 22a).

As a reminder, Sym1 has been described as a stress-induced bioenergetic modulator and suspected to be implicated in Krebs cycle intermediates homeostasis (Dallabona *et al.*, 2010), notably regarding α-ketoglutarate. Interestingly, it has been described that α-ketoglutarate stimulates mTORC1 activation (Durán *et al.*, 2012). One could therefore hypothesize that a shortage of α-ketoglutarate in *MPV17*-silenced cells is the underlying cause of a mTORC1-dependent ATF4 reduced protein level (Fig 21). However, the mTORC1 phosphorylation state in *MPV17*-silenced cells did not seem to predict a decreased activation of the complex (Fig 22b).

Of interest, both *ATF4* and *KDM4C* transcript expression levels were significantly downregulated in *MPV17*-silenced cells (Fig 22c). Even though the transcript level is not necesseraly representative of the protein abundance/activity, these preliminary results suggest that a decreased level of KDM4C could be responsible for the ATF4 reduced abundance in *MPV17*-silenced cells. In addition, the activity of KDM4C could be hindered by a putative

MPV17 knockdown-dependent shortage of α-ketoglutarate as KDM4C requires α-ketoglutarate as a substrate (Mosammaparast and Shi, 2010) (Fig 21).

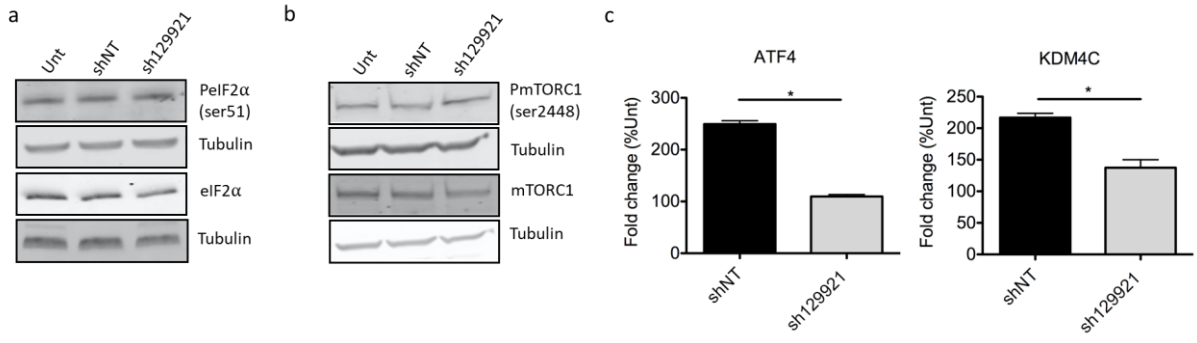

Figure 22 : Assessment of mTORC1 and eIF2*α* phsophorylation and *ATF4* and *KDM4C* transcript abundances in *MPV17*-silenced cells.

Huh7 cells were transduced with non-target shRNA- (shNT) or sh129921-containing lentiviral vectors. Transduced cells were selected for 6 days with puromycin (2.5 µg/mL). PmTORC1(ser2448) and mTORC1 (a), PeIF2*α*(ser51) and eIF2*α* (b) protein abundances were assessed by western blot analysis. A representative western blot of 3 independent biological replicates is shown. In parallel, RNA was also extracted and RT-qPCR was performed to assess *ATF4* and *KDM4C* transcript levels (data expressed relatively to untransduced cells (Unt)). Results are presented as mean ± S.E.M for 3 independent biological replicates. P values were calculated with the one-tailed Mann-Whitney Test (α = 5 %; *: $p<0.05$; **: $p<0.01$; ***: $p<0.001$).

As the supplementations we performed in order to restore the reduced proliferation rate in *MPV17*-silenced cells were all unsuccessful, we intended to directly restore *ATF4* expression in these cells, in order to definitely conclude whether the proliferation phenotype settlement is conditional on ATF4 abundance, or not. In the affirmative case, the supplementation experiments would be performed again and this time we would ensure that the supplemented molecules are indeed properly taken-up by the cell.

We however eventually did not pursue neither with this experiment nor with further investigation of ATF4 upstream regulators in light of the unforeseen results we simultaneously obtained and that are presented hereafter.

***MPV17* silencing is not always consistently associated with a reduced proliferation phenotype.**

Pursuing our analysis further, we observed that the sh129921-encoding vector transduced Huh7 cells were able to adapt along the passages and progressively restored the proliferation rate (Fig 23a), although MPV17 protein abundance was still strongly reduced (Fig 23b).

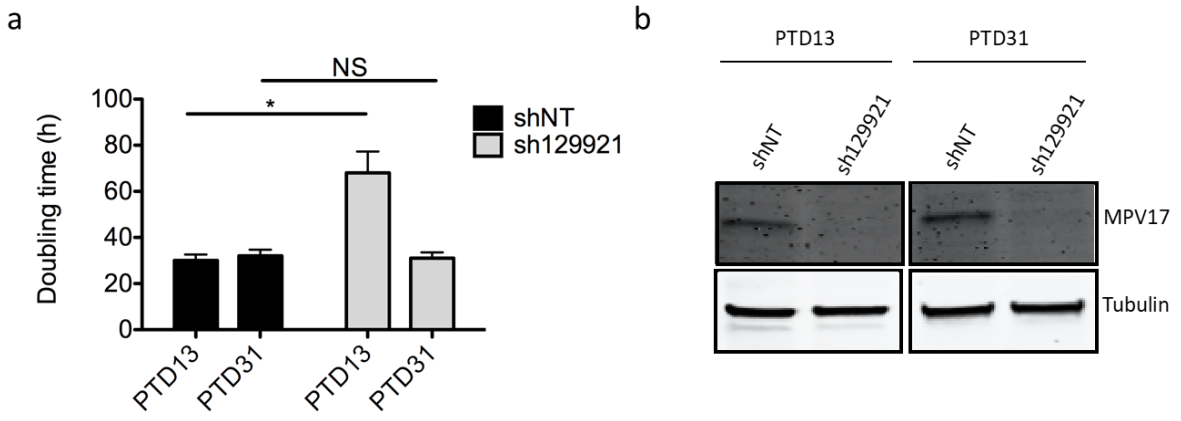

Figure 23 : Evolution of Huh7 proliferation rate and MPV17 protein abundance in sh129921-mediated *MPV17* knockdown.

Huh7 cells were transduced with non-target shRNA- (shNT) or with sh129921-containing lentiviral vectors. Transduced cells were selected for 6 days with puromycin (2.5 µg/mL). At 13 and 31 days after the transduction (PTD: post-transduction day), cells were seeded at 8×10^3 cells/cm^2 and grown for 4 days. Proliferation was then assessed by manual counting to calculate the doubling time (a) and MPV17 protein abundance was analysed by western blot (b). P values were calculated with the one-tailed Mann-Whitney Test (α = 5 %; NS; *: $p<0.05$; **: $p<0.01$; ***: $p<0.001$). n=3.

As we observed a progressive recovery of the decreased proliferation rate along passages, we therefore aimed at generating an IPTG-inducible sh129921 expression model in Huh7 cells. Strikingly, while we observed a strong *MPV17* knockdown in this inducible expression model, with a silencing efficiency comparable to the one observed in the constitutive silencing model (Fig 24a, b), the cell proliferation rate was unchanged (Fig 24d). Moreover, ATF4 did not display a decreased protein abundance (Fig 24c).

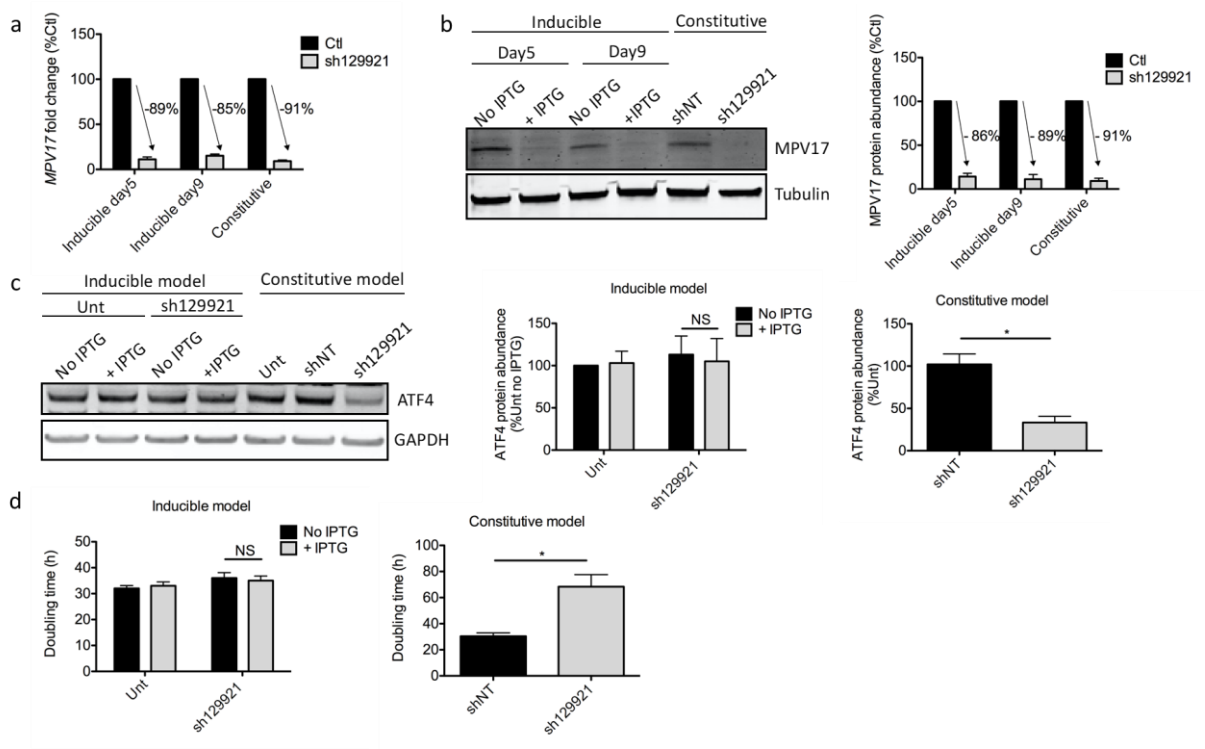

Figure 24 : MPV17 and ATF4 abundances and Huh7 cell proliferation rate following inducible sh129921-mediated *MPV17* knockdown.

Huh7 cells were transduced, or not (Unt), with inducible sh129921 lentiviral vector. Transduced cells were selected for 6 days with puromycin (2.5 µg/mL). Cells were then incubated for 5 days in the presence of 0.1 mM of IPTG to induce *MPV17* silencing. Cells were seeded at 8×10^3 cells/cm^2 and grown for 4 days in daily-renewed medium containing IPTG. RNA was extracted and RT-qPCR was performed to assess *MPV17* transcript level (data expressed relatively to respective control (Ctl), n=3) (a). MPV17 (b) and ATF4 (c) protein abundances were also assessed by western blot analysis after 5 days (MPV17) and 9 days (MPV17; ATF4) of IPTG induction. For each protein, a representative western blot of 3 independent biological replicates is shown (left) along with the western blot quantification of all the biological replicates (quantification with Image J software, data expressed as relative protein abundance to respective controls (Ctl) for MPV17 and untransduced (unt) cells for ATF4, right). Proliferation was then assessed by manual counting to calculate the doubling time (d). As a comparison, we performed at the same time and on the same cells a similar experiment with the constitutive expression of sh129921 (mediating *MPV17* knockdown) as described in Fig 12. P values were calculated with the one-tailed Mann-Whitney Test (α = 5 %; *: $p<0.05$; **: $p<0.01$; ***: $p<0.001$). n =3.

This absence of effect of *MPV17* silencing on the cell proliferation rate in the inducible expression system could have several origins. First, the IPTG molecule itself could have an unexpected effect on Huh7 cells proliferation, even though IPTG is not known to be metabolized (Politi *et al.*, 2014). Second, the reduced proliferation phenotype in the inducible

expression system might need more time to settle down. Indeed, in the constitutive system, *MPV17* is silenced for a total of 9 days before assessing the cell proliferation, as opposed to only 5 days in the inducible model (see "Materials and Methods" Fig 12). A third difference between the two approaches is that in order to ensure a proper knockdown of *MPV17* in the inducible model, the culture medium was changed every day in order to renew the IPTG, as opposed to every two or three days in the constitutive silencing model. One could thus hypothesize that this daily medium renewal could prevent the settling of the reduced proliferation phenotype by discontinuing the putative intercellular communication. These three hypotheses were tested but failed to explain the different phenotypical outcomes observed for the constitutive or inducible expression models (Fig 25 and 26).

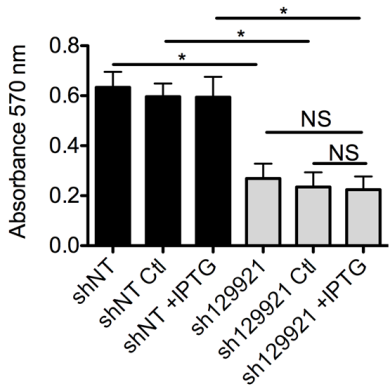

Figure 25 : Effect of IPTG on Huh7 cells proliferation following constitutive sh129921-mediated *MPV17* knockdown.

Huh7 cells were transduced with non-target shRNA- (shNT) or with sh129921-containing lentiviral vector. Transduced cells were selected for 6 days with puromycin (2.5 µg/mL). Cells were seeded at 8×10^3 cells/cm^2 and grown in the presence or in the absence of 0.1 mM of IPTG. After 4 days, cell proliferation was assessed by MTT assay. To mimic the conditions found in the inducible model of expression, the IPTG-containing medium was renewed daily. We therefore included a control in which no IPTG was present while the medium was also changed every day (Ctl). Data are presented as mean ± S.E.M (3 biological replicates). P values were calculated with the one-tailed Mann-Whitney Test (α = 5 %; NS; *: $p<0.05$; **: $p<0.01$; ***: $p<0.001$).

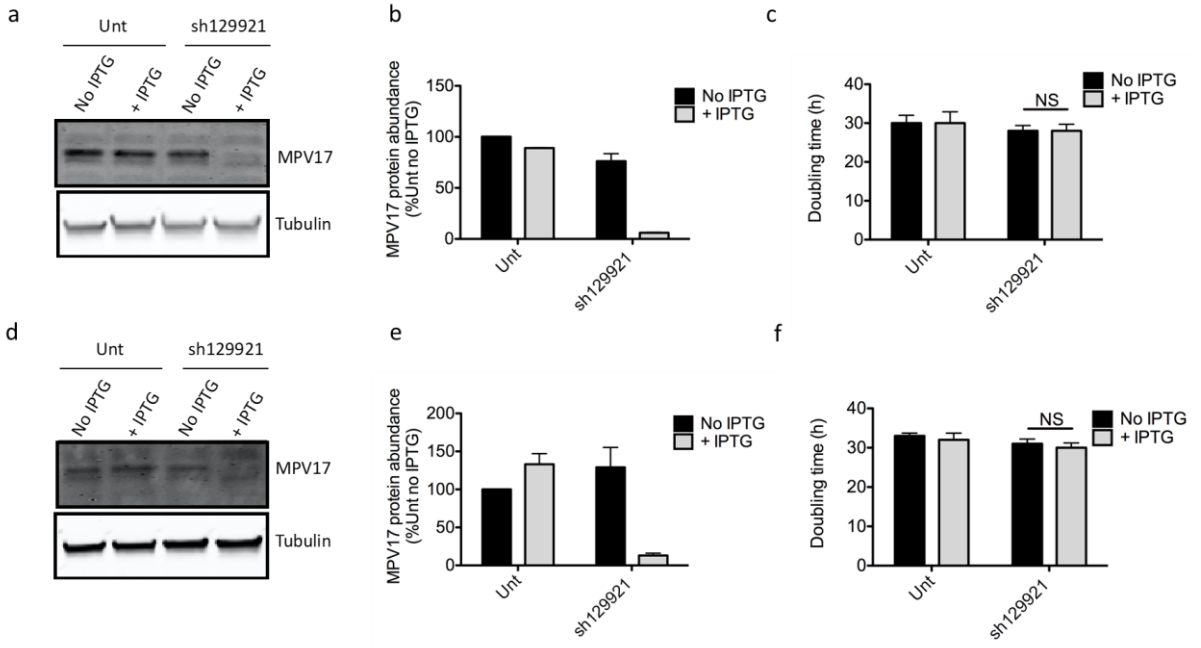

Figure 26 : Effect of the duration of the IPTG pre-treatment and the medium change frequency on Huh7 cells proliferation in response to inducible sh129921-mediated *MPV17* knockdown.

Cells were transduced, or not (Unt), with inducible sh129921 lentiviral vectors and selected for 6 days with puromycin (2.5 µg/mL). Cells were then incubated for 14 days in the presence of 0.1 mM of IPTG to induce *MPV17* silencing and culture medium was changed daily (a, b, c) or every 2 days (d, e, f). Cells were seeded at 8×10^3 cells/cm^2 and grown for 4 days in the presence of IPTG in the same conditions. MPV17 protein abundance was assessed by western blot analysis (a, d) and quantified with Image J software (b, e). Proliferation was then assessed by manual counting to calculate the doubling time (c, f). Data are presented as mean ± S.E.M of 3 independent biological replicates. P values were calculated with the one-tailed Mann-Whitney Test (α = 5 %; NS; *: p<0.05; **: p<0.01; ***: p<0.001).

These considerations led us to evaluate on Huh7 cells the effect of two additional commercially available shRNAs, sh128669 and sh131201, targeting different regions of the *MPV17* transcript (Fig 27).

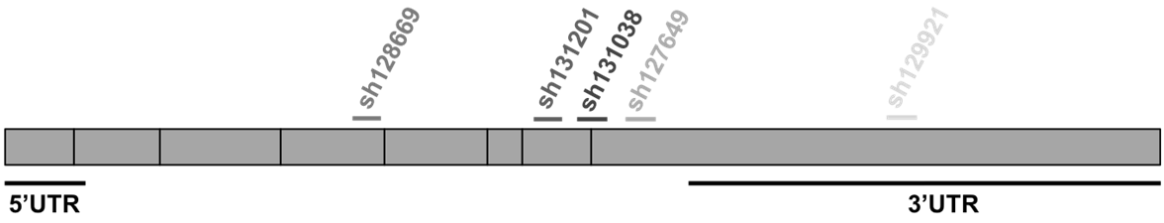

Figure 27 : Localisation of the shRNA-targeted sites on *MPV17* transcript.

The effects of several commercially available shRNAs directed against *MPV17* transcript were assessed in Huh7

cells. Each shRNA Sigma Aldrich reference (sh128669, sh131201, sh131038, sh127649 and sh129921) is indicated above its target site. Each grey box represents an exon of *MPV17* transcript (NM002437.5). A line indicates the 5'UTR and 3'UTR of the *MPV17* transcript.

Both shRNAs strongly reduce the abundance of MPV17 protein (Fig 28a) but no significant effect on the proliferation rate was observed (Fig 28c, d, e). Also, the abundance of ATF4 was not affected by *MPV17* knockdown mediated by either sh128669 or sh131201 (Fig 28b).

Thus, ATF4 reduced abundance does correlate with the proliferation rate but the putative link between the reduced proliferation phenotype (and therefore ATF4) and MPV17 protein abundance remains to be established.

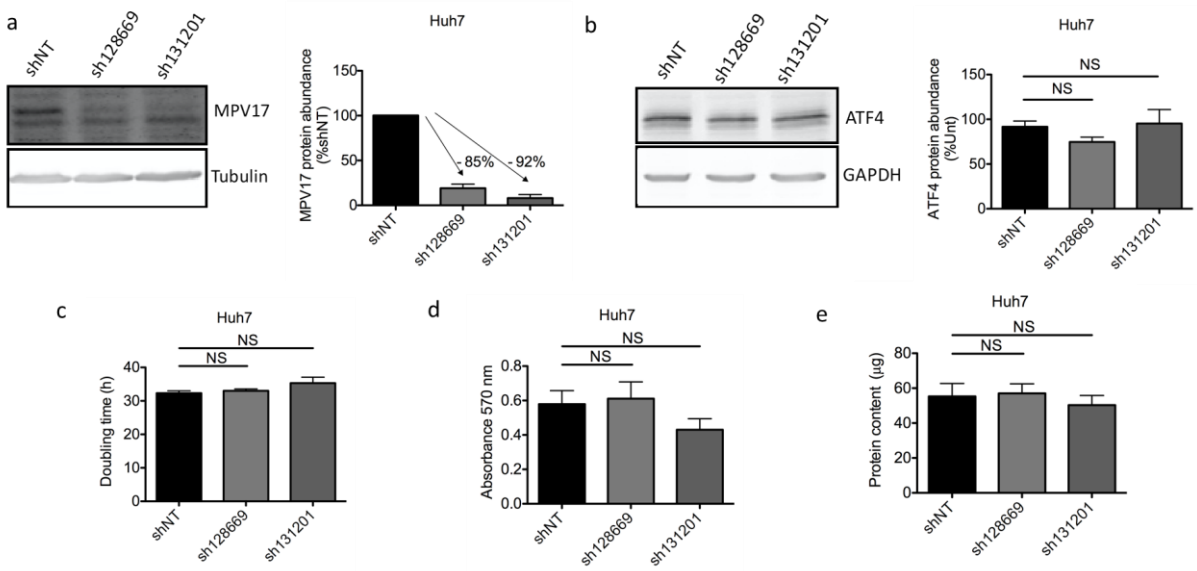

Figure 28 : Effect of *MPV17*-targeting sh128669 and sh131201 on Huh7 cells proliferation, MPV17 and ATF4 protein abundances.

Cells were transduced with non-target shRNA lentiviral vectors (shNT) or with shRNA lentiviral vectors targeting *MPV17* expression (sh128669 and sh131201). Transduced cells were selected for 6 days with puromycin (2.5 µg/mL). Cells were seeded at 8×10^3 cells/cm^2 and grown for 4 days. The abundance of MPV17 (a) and ATF4 (b) proteins was assessed by western blot analysis. For each protein, a representative western blot analysis of 3 independent biological replicates is shown (left) along with the western blot quantification of all the biological replicates (quantification with Image J software, data expressed as relative protein abundance to cells transduced with shNT-encoding vectors (a, MPV17) or untransduced (unt) cells (b, ATF4), right). Proliferation was then assessed by manual counting to calculate the doubling time (c), by MTT assay (d) and by the total protein content (e) and data are presented as mean ± S.E.M (3 biological replicates). P values were calculated with the one-tailed Mann-Whitney Test (α = 5 %; NS; *: $p<0.05$; **: $p<0.01$; ***: $p<0.001$).

In conclusion, we found that sh129921, sh127649, sh128669 and sh131201 all led to a strong *MPV17* knockdown while the resulting proliferation rates were highly variable. This lack of consistency led us to suspect a putative involvement of *MPV17* isoforms that would be differentially affected according to the shRNA used.

Therefore, we next interrogated the Genotype-Tissue Expression (GTEx) Consortium (2008, NIH) portal, that inventories the impact of genetic variations on gene expression within major tissues in the human body from *post mortem* donors. The GTEx Portal proposes 22 *MPV17* isoforms, including two major ones i.e. a short predominant isoform and a long one (first and second upper transcripts on Fig 29, respectively). This long isoform referenced in RefSeq as NM002437.5 encodes the MPV17 protein that we detected on western blot while the translation of all the other *MPV17* isoforms is not experimentally demonstrated, although some of them display the presence of an ORF. However, among the 22 isoforms, we observe that all the transcripts potentially targeted by sh129921 (1, 2, 3, 12, 13, 14, 15, 16 and 18) are also targeted by either sh128669 (15, 16) or sh131201 (1, 18) or both (2, 3, 12, 13, 14). The same kind of observation stands for the transcripts targeted by sh127649 (1, 2, 3, 5, 12, 13, 14, 15, 16, 18, 19, 21), providing no clear explanation about the different proliferation phenotypes observed for each pair of shRNAs (sh129921/sh127649 versus sh128669/131201) (Fig 29).

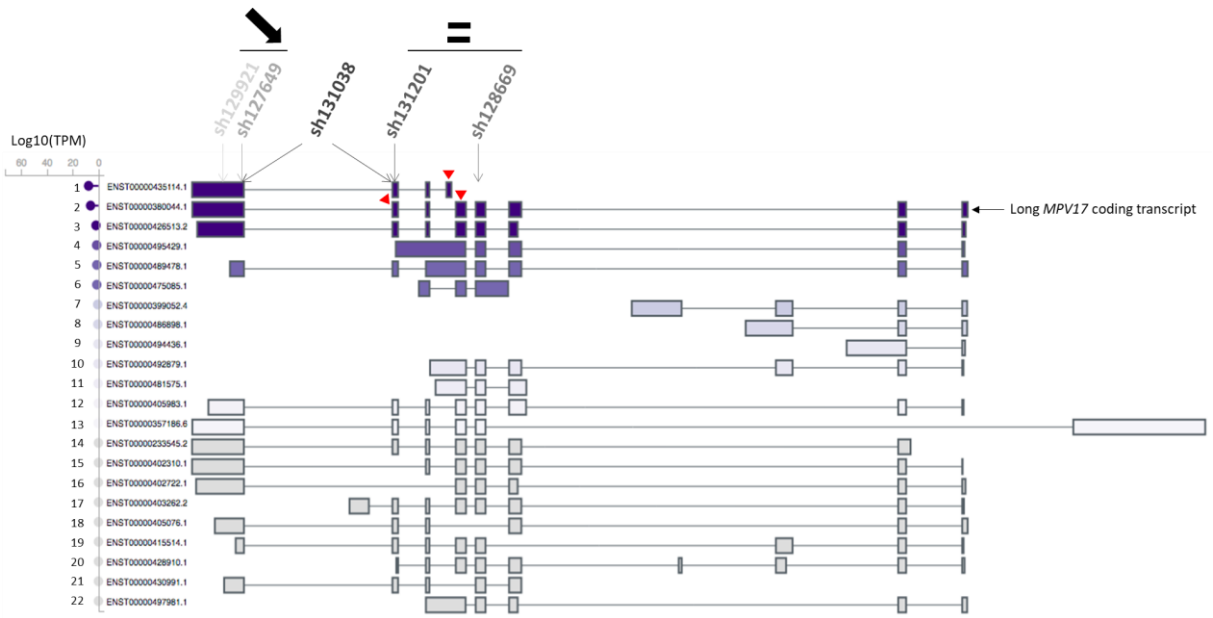

Figure 29 : Localisation of the shRNA-targeted sites on the *MPV17* transcript isoforms referenced in human liver. The Genotype-Tissue Expression (GTEx) Project was supported by the Common Fund of the Office of the Director of the National Institutes of Health, and by NCI, NHGRI, NHLBI, NIDA, NIMH, and NINDS. The data used for the analysis described in this manuscript and this Fig. were obtained from the GTEx Portal on 02/05/19. We indicated the Sigma Aldrich reference of each shRNA targeting *MPV17* transcripts (sh128669, sh131201, sh131038, sh127649 and sh129921) above its targeted site. Each box represents an exon in *MPV17* transcript isoforms. The darker the purple, the more abundant the transcript (as referred by Log 10 (Trancripts Per Million (TPM))). The 3'UTR is located on the left of the image, and the 5'UTR on the right. We added a down-oriented arrow that indicates both shRNAs providing the reduced proliferation phenotype, while " = " indicates both shRNAs leading to an unchanged proliferation rate. Red triangles indicate the localization of the divergent primers used in Fig 39 in the second part of this thesis.

Altogether, the absence of effect of the inducible sh129921 on the cell proliferation rate, combined with the observation that, at least, two different shRNAs targeting *MPV17* (sh131201 and sh128669) have no effect on the proliferation of Huh7 cells, despite a strong decrease in the MPV17 protein abundance, suggest that the decreased proliferation rate of transduced cells observed for two shRNAs (sh129921 and sh127649) is not related to a reduced MPV17 protein abundance. In an attempt to shed light on this question, we eventually performed a rescue experiment.

Rescuing MPV17 does not restore the proliferation phenotype.

As Huh7 cells could neither be efficiently transfected nor transduced with the *MPV17*-expressing vector, HepG2 cells were used for the rescue attempt. Indeed, as mentioned before, we also observed the reduced proliferation rate in this hepatoma cell line silenced for *MPV17*. This cell line turned out to be the most receptive to the lentiviral *MPV17*-expressing vector. Since a rescue experiment consists in re-introducing the shRNA-mediated silenced mRNA, it requires the use of a re-introduced mRNA lacking the shRNA targeted sequence (in this case, the 3'UTR region).

We were compelled to perform *MPV17* overexpression before inducing the constitutive knockdown mediated by sh129921. The justification of this chronology resides in the observation that, on the contrary to shNT-encoding vector transduced cells, sh129921-encoding vector transduced cells were not able to stand a second round of transduction due to cell death. This suggests that *MPV17*-silenced cells are distressed, in accordance with their decreased proliferation rate. This aspect is therefore not compatible with a short-term assessment of cell proliferation.

MPV17 knockdown was properly induced in the overexpression control. Indeed, cells double transduced with pLenti GFP, as a control, and then with pLKO.1 sh129921, displayed a strong reduction of MPV17 abundance accompanied by the decreased proliferation rate (Fig 30a, b, c). As expected, the reduced proliferation phenotype was absent in pLenti GFP and pLKO.1 shNT double-transduced cells (Fig 30b, c). Cells double-transduced with pLenti MPV17 and pLKO.1 shNT suitably overexpressed MPV17 (Fig 30a). It is interesting to emphasize the fact that MPV17 overexpression, on its own, has no significant effect on cell proliferation (Fig 30b, c). This observation can be reconciled with the idea that MPV17 is described as a channel. Thus, the qualitative state of MPV17 (open/closed) would be more relevant than its quantitative state. Finally, cells double-transduced with pLenti MPV17 and pLKO.1 sh129921

overexpressed MPV17 but lost the expression of the endogenous protein (Fig 30a). Remarkably, these cells exhibited the reduced proliferation phenotype (Fig 30b, c).

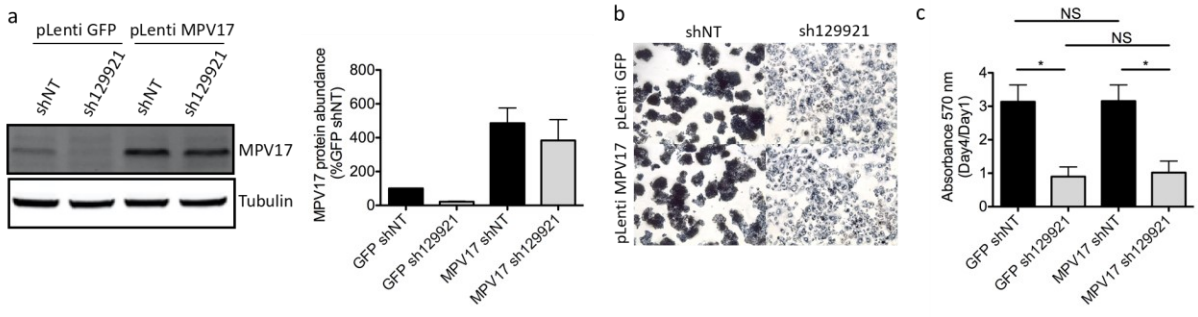

Figure 30 : Effect of MPV17 rescue on the proliferation of *MPV17*-silenced HepG2 cells.

Cells were first transduced with pLenti *GFP* or pLenti *MPV17* and selected for 6 days with puromycin (2.5 µg/mL). Cells were then transduced with shNT or sh129921-encoding lentiviral vectors and let to recover for 5 days to allow *MPV17* silencing. Cells were then seeded at 1.5×10^4 cells/cm^2 and grown for 4 days before assessing MPV17 protein abundance (a). A representative western blot analysis of 3 independent biological replicates is shown (left) along with the western blot quantification of all the biological replicates (quantification with Image J software, data expressed as relative protein abundance to cells transduced with shNT and GFP-encoding vectors, right). Cell proliferation assessment by MTT assay was also performed at day 1 and day 4. The ratio day 4/day 1 is then calculated in order to correct any putative seeding differences that could mask or mislead to a partial phenotype rescue (c). Micrographies were taken at the phase contrast microscope before adding the lysis buffer for the MTT assay on day 4 (b). Data are presented as mean ± S.E.M (3 biological replicates). P values were calculated with the one-tailed Mann-Whitney Test (α = 5 %; NS; *: $p<0.05$; **: $p<0.01$; ***: $p<0.001$).

The results obtained in this first part of this thesis work were puzzling and while not implicating the protein MPV17 in cancer cell proliferation, they do not exclude a role of putative *MPV17* non-coding transcripts. This aspect is further discussed in the part "General discussion, conclusion and perspectives". Beyond the important biological message that MPV17 protein is not involved in cancer cell proliferation, these results enlightened an equally essential technical message, also further discussed, related to the caution required in terms of result interpretation when working with shRNA-mediated knockown as well as the requirement to perform a rescue experiment. These valuable messages resulted in a recent publication in PLOS One (Canonne et al., 2020).

PART II: INVESTIGATION OF *MPV17* CIRCULAR RNAs

INTRODUCTION

CiRNAs, seemingly present in all eukaryotic species (Wang *et al.*, 2014), originate from non-canonical backsplicing and consists in the circularization of a pre-mRNA following the covalent joining of a downstream splice donor with an upstream splice acceptor. These cyclisation events lead to a variety of ciRNAs composed of one or more exons and even introns and lacking the conventional 5'and 3' ends of linear RNAs (Barrett and Salzman, 2016) (Lasda and Parker, 2014) (Xu *et al.*, 2018) (Jeck *et al.*, 2013) (Fig 31).

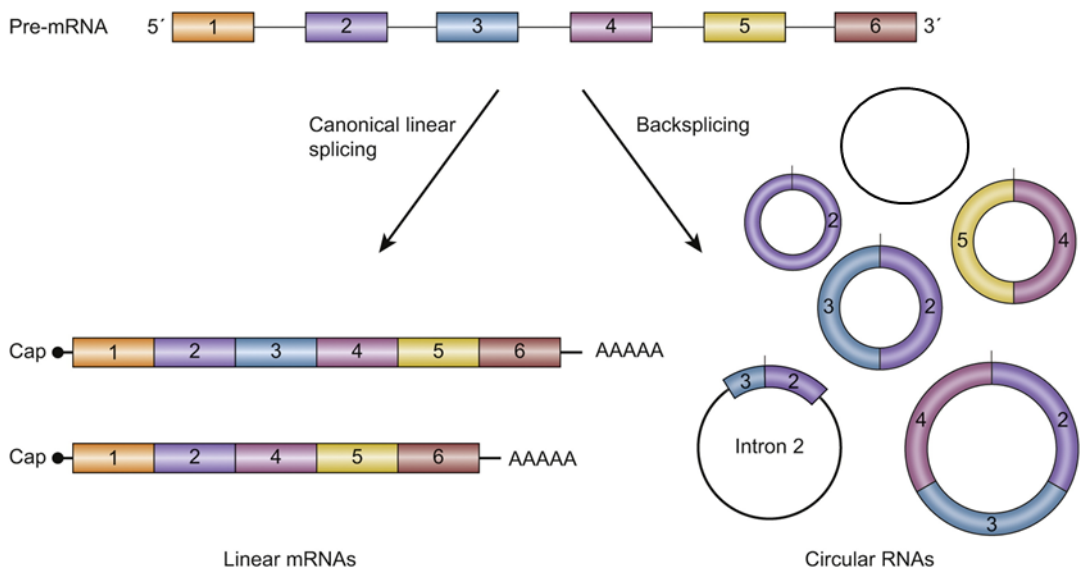

Figure 31 : Possible structural combinations of circular RNAs (ciRNAs).
CiRNAs originate from the non-canonical backsplicing of pre-mRNAs. This process results in a heterogeneous population of cyclized molecular entities, exclusively exonic, intronic or exonic-intronic. The colored boxes represent different exons of a pre-mRNA and the dark line symbolizes introns bordering these exons. Adapted from (Huang *et al.*, 2017).

First disregarded by the scientific community and considered as biologically irrelevant splicing artefacts constituting transcriptional noise, ciRNAs are now actively studied and ever-growing evidence suggest their functional importance in core biological processes.

1. CiRNA biogenesis

The observation that ciRNAs are not expressed in the same abundance as their cognate linear form (Memczak *et al.*, 2013) (Jeck *et al.*, 2013) (Salzman *et al.*, 2012) suggests that their biosynthesis is dependent on specific mechanisms. Bioinformatic analyses on human genome revealed that ciRNA generation seems to be favoured by several pre-mRNA features. First, ciRNA-forming exons tend to be threefold longer than non-circularizing exons (Jeck *et al.*, 2013). Second, flanking introns of circularizing exons also tend to be threefold longer than those flanking non-circularizing exons. Of note, the average size of a human exon is 145 bp while the one of an intron is 3.4 kbp (Tropp, 2012). Third, there is a twofold stronger possibility to encounter *Alu* inverted repeat elements in the flanking introns of circularized exons than in those of non-circularized exons (Jeck *et al.*, 2013). *Alu* elements are 55-million-year-old most abundant repetitive elements in primate's genomes, with an average length of 300 bp (Häsler and Strub, 2006). The base-pairing of *Alu* inverted repeat elements in the flanking introns of ciRNA-forming exons promote ciRNA generation by bringing closer backsplicing sites (Lasda and Parker, 2014) (Fig 32A, left).

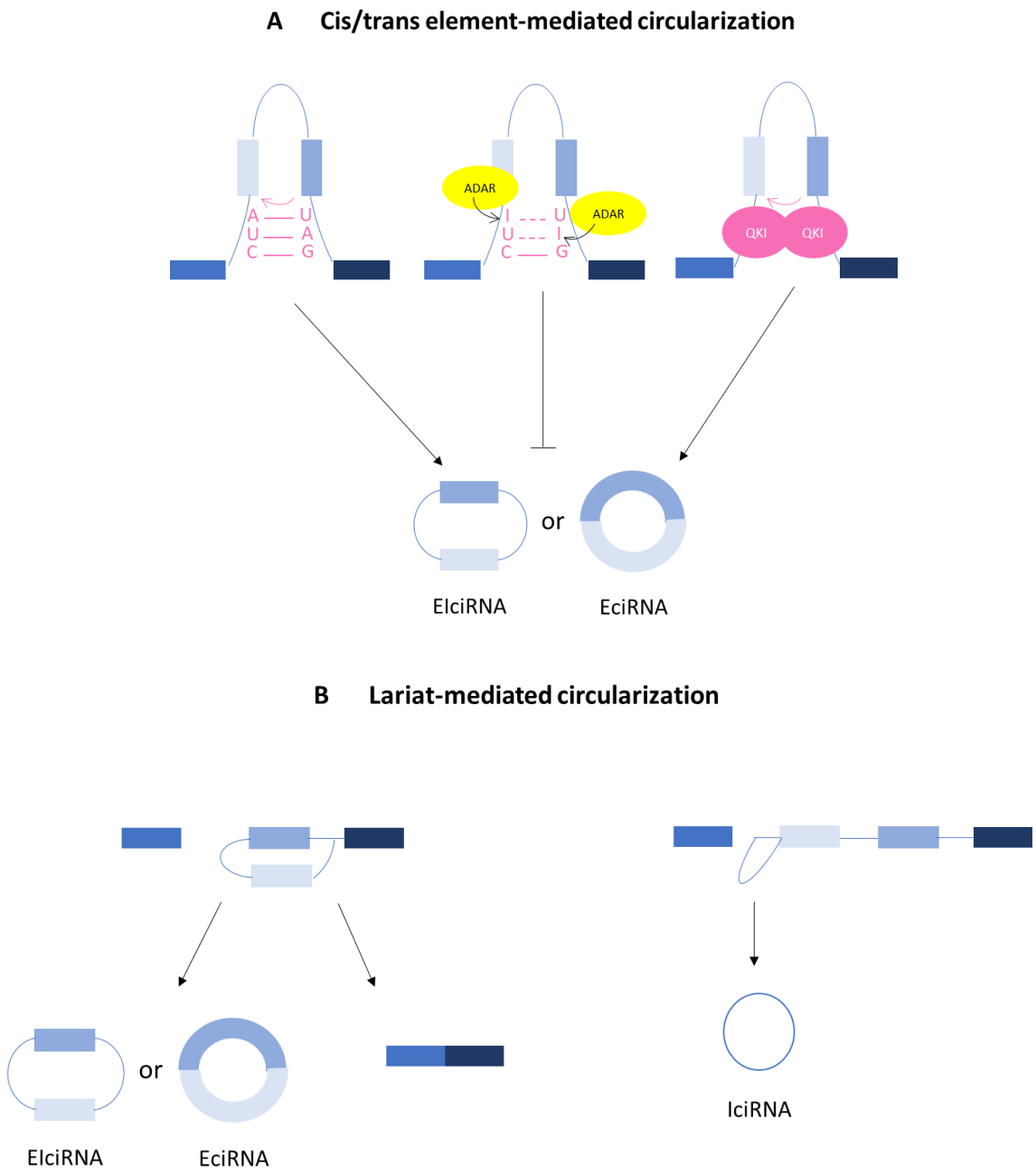

Figure 32 : Molecular mechanisms driving circular RNAs (ciRNAs) biosynthesis.

(A) CiRNA biogenesis can be molecularly driven in *cis* by intron-pairing of inversely oriented complementary sequences such as *Alu* sequences (left). These events are finely regulated by RNA binding proteins in *trans*. Thus, by catalyzing the Adenosine to Inosine (A-I) conversion in *Alu* sequences, Adenosine Deaminase Acting on RNA (ADAR) weakens the duplex interaction in the base-pairing event and inhibits the subsequent ciRNA formation (middle). RNA binding proteins can also act positively on ciRNA generation. Indeed, QuaKIng (QKI), by forming homodimers, brings closer backsplicing sites and thereby allows ciRNA formation (right).

(B) Lasso-like structures generated during conventional linear splicing can favour backsplicing. For example, a lariat composed of introns and exons following exon skipping event can undergo backsplicing-mediated circularization and give rise to an exon-intron containing ciRNA (EIciRNA) or an exonic ciRNA (EciRNA) when

further linear splicing is taking place (left). An intron-containing lariat failing to be 2'-5'-debranched and subsequently degraded can also generate a ciRNA (right).

RNA Binding Proteins (RBP) have also been implicated in ciRNA biogenesis. Indeed, Conn and collaborators demonstrated that QuaKIng (QKI) actuates the circularization of pre-mRNAs in immortalized human mammary epithelial cells during Epithelial to Mesenchymal Transition (EMT). QKI binds recognition motifs present in the adjacent introns of ciRNA-forming exons, thereby creating a bridge necessary to the circularization event (Conn *et al.*, 2015) (Fig 32A, right). In this study, QKI is likely responsible for the biogenesis of around one third of all ciRNAs differentially expressed during EMT. Strikingly, the engineered incorporation of these consensus binding sites in introns flanking exons that are not ordinarily undergoing circularization is sufficient to induce ciRNA formation (Conn *et al.*, 2015).

Whether enabled by consensus sequences and/or mediated by proteins, the generation of a ciRNA is favoured by the spatial proximity of the backsplicing sites. Jeck and collaborators proposed a third ciRNA biogenesis model allowing this proximity and in which the intermediate step of a lariat generation during conventional linear splicing of a pre-mRNA favours the formation of ciRNAs. More specifically, canonical splicing of a pre-mRNA involving exon skipping events could lead to the circularization of those skipped exons in the way that the lasso-like structure they form allows a spatial proximity between potential backsplicing sites (Jeck *et al.*, 2013) (Fig 32B, left). On a similar note, intronic ciRNAs (IciRNAs) biogenesis constitutes a particular case since it can be exempt of the backsplicing step. Thus, during conventional linear splicing, the generation of an intron-containing lariat can escape degradation and be trimmed of its 3'-single strand, giving rise to a ciRNA (Zhang *et al.*, 2013) (Fig 32B, right). The resistance to degradation of some intronic lariats is dependent on specific

GU-rich consensus sequences near their 5' splice site and C-rich consensus sequences near their 2'-5'-phosphodiester branchpoint (Zhang *et al.*, 2013).

However, as ciRNA expression appears to be cell-type/developmental-stage specific (Conn *et al.*, 2015) (Rybak-Wolf *et al.*, 2015) (Salzman *et al.*, 2013), a simple spatial proximity of the backsplicing sites does not seem to be sufficient to control by itself ciRNA formation and suggests the existence of other *trans*-acting regulatory factors. Hence, studies have implicated RBP in the fine regulation of this process, as illustrated by Adenosine Deaminase Acting on RNA (ADAR). ADAR catalyses the hydrolytic deamination reaction supporting the Adenosine to Inosine (A-I) conversion in RNA (Häsler and Strub, 2006). Interestingly, A-I editing essentially occurs in *Alu* elements (Häsler and Strub, 2006). In this manner, ADAR weakens the base pairing of inversely oriented *Alu* sequences in flanking introns of ciRNA-forming exons and thereby reduces ciRNA biogenesis (Fig 32A, middle). Accordingly, RNA interference and shRNA-based ADAR1 knockdown has been shown to increase the biogenesis of some ciRNAs in human HEK293T and SH-SY5Y cells (independently from their cognate linear mRNAs) as well as in P19 mouse cells, wherein introns bordering circularized exons also harbour reverse complementary matches (Ivanov *et al.*, 2015) (Rybak-Wolf *et al.*, 2015).

Literature also describes some proteins as (back)splicing regulators of their own pre-mRNA. As an example, Ashwal-Fluss and collaborators demonstrated that Muscleblind (Mbl), a protein involved in both muscle and ocular system development in *Drosophila* (Begemann *et al.*, 1997), promotes the biosynthesis of the ciRNA (*ciMbl*) originating from its own pre-mRNA through binding specific consensus sites localized in the exon 2 and exon 2-flanking introns and thereby favouring a looping structure (Ashwal-Fluss *et al.*, 2014). This ability of Mbl to promote circular over linear splicing of its own pre-mRNA in a protein-dependent manner constitutes

an original way to exert a negative feedback control on its linear transcript/protein abundance. Moreover, Mbl is in turn sequestered by *ciMbl*, further regulating *Mbl* splicing isoforms and protein expression (Fig 33).

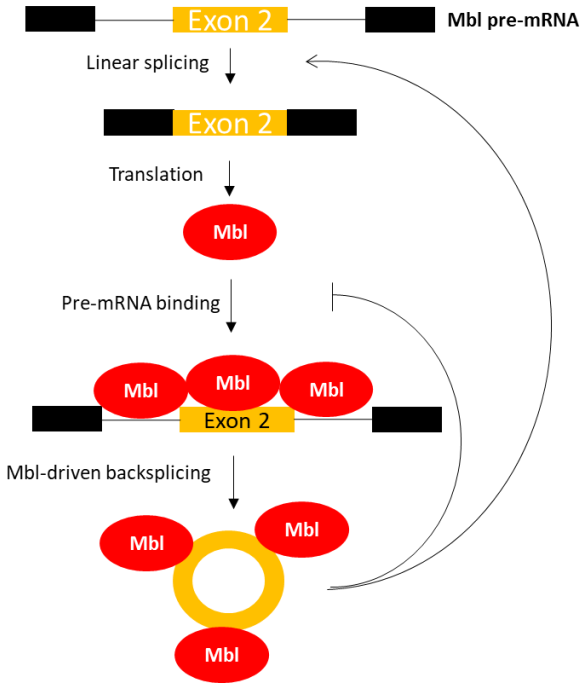

Figure 33 : Muscleblind (Mbl) promotes the circularization of its own pre-mRNA.
Muscleblind (Mbl) protein controls the generation of its own circular RNA transcript isoform by binding specific sequences localized on exon 2 and exon 2-adjacent introns. Thus, a low Mbl protein level is favourable to the linear splicing of the pre-mRNA while a high protein level induces its backsplicing. Moreover, *ciMbl* offers a second level of negative feedback by tethering Mbl. Inspired from (Barrett and Salzman, 2016)

Gene promoters are also able to preferentially drive the expression of ciRNAs over their linear cognates. As an example, murine Sex-determining region Y (*Sry)* gene gives rise to both linear and circular RNAs. The former is localized in the developing genital ridge and is involved in male sex determination, and the latter is found in the germ cells of adult testis. The discriminative use of a distal promoter instead of a proximal one in adult testis cells allows the specific generation of the ciRNA as it produces a long inverted-repeat-containing transcript capable of circularization (Hacker *et al.*, 1995).

CiRNA biogenesis is thought to implicate the spliceosome. First, canonical splicing signals have been found adjacently to the backsplicing sites of ciRNAs (Jeck *et al.*, 2013) (Memczak *et al.*, 2013). Second, mutations of these signals suppress circularization (Ashwal-Fluss *et al.*, 2014), and third, isoginkgetin-mediated spliceosome inhibition drastically decreases ciRNA biogenesis (Starke *et al.*, 2015). In a recent study however, Liu and collaborators detected a substantial number of ciRNAs with no canonical splicing sites in HeLa cells and human brain (Liu *et al.*, 2020). Moreover, they also discovered particular ciRNAs for which the junction point does not occur at a typical exon/intron or exon/exon junction but rather resides inside an intron and/or an exon (Liu *et al.*, 2020). Noteworthy, the authors found that these interior ciRNAs (int ciRNAs) are more abundant than canonical ciRNAs. Moreover, beyond the canonical splicing signal AG/GU, they enlightened the presence of a novel motif adjacent to the backsplicing site of both canonical ciRNAs and int ciRNAs, namely AC/CU (Liu *et al.*, 2020). Interestingly, they also uncovered the existence of Short Homologous Sequences (SHS) adjacent to the backsplice site of both canonical ciRNAs and int ciRNAs, up to 34 nt in size. Overall, the discovery of both SHS and the novel AC/CU motif support the existence of a more complex mechanism underlying ciRNA biogenesis, and possibly distinct ones according to the type of ciRNAs (Liu *et al.*, 2020). Specifically, the authors hypothesize that the biogenesis mechanism dependent on SHS could be based on template switching (Fig 34).

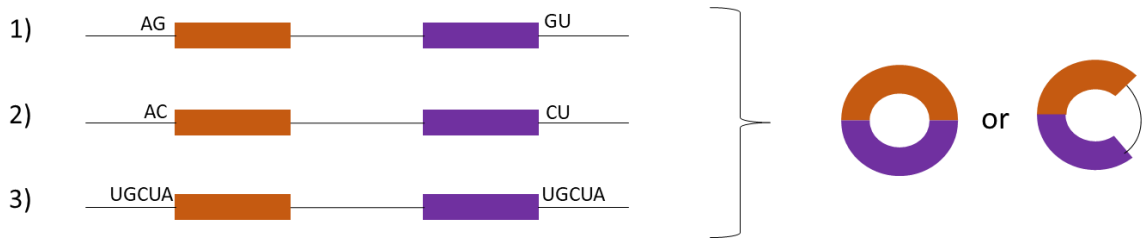

Figure 34: Pre-mRNA sequence features driving circular RNAs (ciRNAs) backsplicing.

CiRNAs are thought to be generated 1) via a specific canonical splicing signal (AG/GU) under the action of the spliceosome, 2) through an unknown mechanism implicating the newly discovered signal AC/CU, 3) following

template switching enabled by short homologous sequences located on either side of the back-fusion point. Inspired from (Liu *et al.*, 2020).

Studies show that there are thousands of ciRNAs in human cells and that they emerge from roughly 15-20% of the transcriptome (Jeck *et al.*, 2013) (Conn *et al.*, 2015) (Glažar, Papavasileiou and Rajewsky, 2014). This information, together with their dynamic expression discussed above, their extended half-lives (up to 48h) (Jeck *et al.*, 2013) and the fact that they are evolutionary conserved (Rybak-Wolf *et al.*, 2015) (Memczak *et al.*, 2013) (Jeck *et al.*, 2013), are compelling evidence that they are more than random inactive splicing by-products and that they bear important biological functions.

2. CiRNA functions

Concrete information regarding the biological functions of ciRNAs are multiplying but still remain limited and cannot be extrapolated to all ciRNAs. The biological functions of ciRNAs currently proposed are presented in Fig 35 and detailed hereafter.

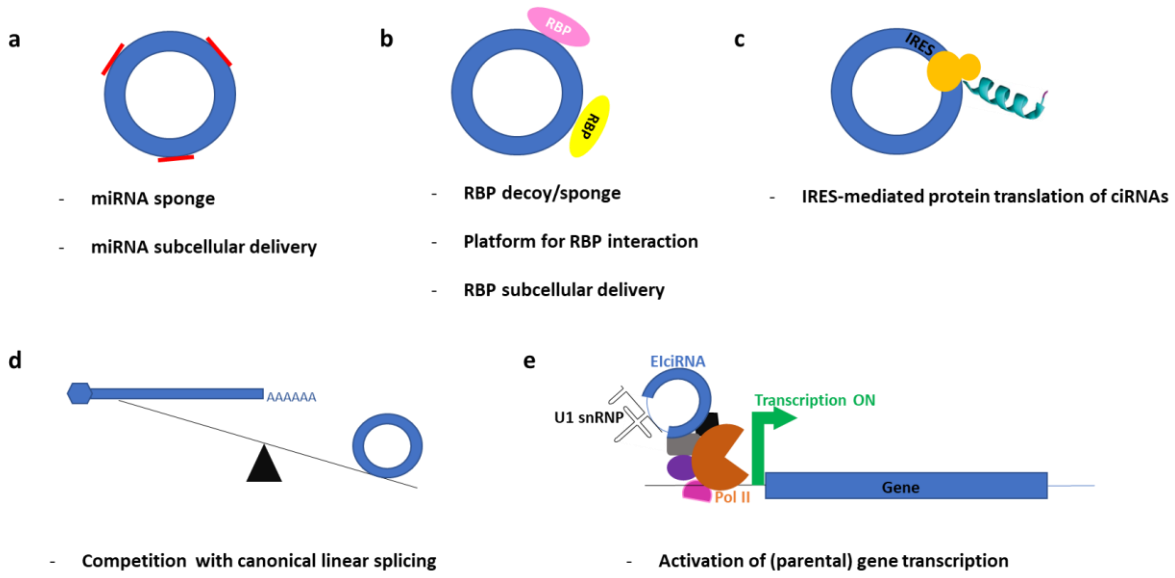

Figure 35 : Proposed biological functions of circular RNAs (ciRNAs).

CiRNAs can indirectly increase mRNA translation by sequestering miRNAs (a). Similarly, ciRNAs can also interact with proteins, constituting RNA Binding Protein (RBP) sorting/scaffolding/tethering agents (b). Recently, it was reported that ciRNAs can be translated into proteins with a functional domain (c). CiRNAs are generally

thought to compete with the production of their cognate linear mRNA (d). Finally, ciRNAs have been shown to act as transcriptional regulators increasing gene expression. This has been specifically described for Exonic-Intronic ciRNAs (EIciRNAs) whose intronic part would bind U1 small nuclear RiboNucleoProtein particle (U1 snRNP) and further interact with RNA polymerase II (pol II), enhancing the expression of their parental genes (e).

The structure of ciRNAs tends to inform about their biological functions. While Exonic ciRNAs (EciRNAs), the most prevalent class of ciRNAs, are more associated with an activity of miRNA sponges in the cytoplasm, Exon-Intron containing ciRNAs (EIciRNAs) and IciRNAs seem more prone to act as transcription regulators in the nucleus (Xu *et al.*, 2018).

The miRNA sponge function of ciRNAs was first uncovered with circular RNA Sponge for miR-7 (*ciRS-7*). Antisense *ciRS-7* derives from the *Cerebellar Degeneration Related 1* (CDR1) gene and is highly expressed in mammalian brain (Hansen *et al.*, 2011). Its potent miR-7 sponge function was first illustrated by the work of Memczak and collaborators, wherein either morpholino-driven inhibition of miR-7 or human *ciRS-7* overexpression in *Danio rerio* both led to a similar phenotype of impaired brain development (Memczak *et al.*, 2013). In various studies, the *ciRS-7/* miR-7 axis has been shown to carry out diverse biological functions, ranging from osteoblastic differentiation through Growth Differentiation Factor 5 (GDF5) upregulation (X. Li *et al.*, 2018) to the promotion of oesophageal cancer cell proliferation and metastasis via HomeobOX 13 (HOXB13) upregulation (R. Li *et al.*, 2018). Interestingly, as much as *ciRS-7* is able to act as a miRNA sponge, it can be as easily targeted and degraded by one miRNA, namely miR-671 (Hansen *et al.*, 2011). As such, Memczak and collaborators hypothesised that *ciRS-7* could act as a miR-7 transporter, whose scheduled delivery in specific subcellular compartments would be dependent on miR-671 action (Memczak *et al.*, 2013).
This is only one example of an ever-expanding list of ciRNAs acting as miRNA sponges, thereby *trans*-regulating the expression of their own cognate linear forms or, in most cases so far uncovered, the expression of separate actors (Yu and Kuo, 2019).

CiRNAs generally interact with proteins (Hentze and Preiss, 2013) (Huang *et al.*, 2020). More specifically, they can display RBP-sponge abilities, illustrated earlier with the *ciMbl*-Mbl interaction (Ashwal-Fluss *et al.*, 2014), and also exemplified by the *ciForkhead bOX O3* (*ciFOXO3*)- Cyclin Dependent Kinase 2 (CDK2)- p21 complex. Indeed, *ciFOXO3* sequesters CDK2, thereby preventing its binding to cyclin E, an interaction essential for the G1-S transition of the cell cycle. Moreover, *ciFOXO3* also binds p21 and therefore enhances the innate inhibitory effect of p21 on CDK2. Thus, the formation of this ternary complex blocks the progression of the cell cycle (Du *et al.*, 2016). The scaffolding properties of ciRNAs are also illustrated by *ciAngiomotin-like 1* (*ciAmotl*) that has been shown to bind and assist Phosphoinositide-Dependent Kinase1 (PDK1)-mediated phosphorylation of Protein Kinase B (PKB) in Murine Cardiac Fibroblasts (MCF), leading to its nuclear translocation and subsequent cardioprotective action (Zeng *et al.*, 2017). In another study, *ciAmotl1* has been shown to act as a sorting agent and promote tumorigenesis by retaining c-myc in the nucleus (Q. Yang *et al.*, 2017).

CiRNAs are also described as gene transcription regulators. Indeed, Li and collaborators demonstrated in HeLa cells that some EIciRNAs are nucleus-localized and interact with RNA Polymerase II (Pol II), U1 small nuclear ribonuclear particle and the promoter of their parental genes, thereby inducing their transcription (Li *et al.*, 2015). In addition, Zhang and collaborators have shown in human cells (HeLa and H9) that antisense-oligonucleotide-mediated knockdown of several IciRNAs also led to a diminished transcription of their parental genes seemingly via modulation of Pol II activity (Zhang *et al.*, 2013). Moreover, ciRNAs transcriptional activity is not restricted to their parental genes as demonstrated by a multifaceted approach for *ciRas Homolog family member bT1 (ciRHOT1).* Indeed, *ciRHOT1,* overexpressed in HepatoCellular Carcinoma (HCC), associates with Tip60, a histone acetyltransferase involved in chromatin

remodelling, to promote the expression of *Nuclear Receptor subfamily 2 group F member 6 (NR2F6)*, a transcription factor of poor prognosis in HCC (L. Wang *et al.*, 2019).

Interestingly, ciRNAs have also been shown to act on the translational level, as exemplified by *ciAntisense Non-coding RNA in the Inhibitor of cyclin-dependent kinase 4 Locus (ciANRIL)* in HEK293T cells. By binding Pescadillo homolog 1, an assembly factor involved in rRNA processing, *ciANRIL* is able to decrease ribosome biogenesis (Holdt *et al.*, 2016).
In addition, Abdelmohsen and collaborators demonstrated in HeLa cells that the translation of Poly(A)-Binding Protein Nuclear 1 (PABPN1), involved in the poly(A) tail formation of mRNAs, is modulated by its cognate circular form. More precisely, *ciPABPN1* competes for the binding of the translational activator HuR, thereby reducing its availability and leading to the inhibition of *PABPN1* mRNA translation (Abdelmohsen *et al.*, 2017).

It is only very recently that ciRNAs revealed their fascinating ability to encode proteins, until then only imagined based on computational analysis (Chen *et al.*, 2016) and studies on engineered ciRNAs (Wang and Wang, 2015) (Chen and Sarnow, 1995). Since ciRNAs are inherently deprived of 5'-cap, the translation of the circular transcript is driven by Internal Ribosome Entry Sites (IRES) that allows recruitment of ribosomes internally (Hellen and Sarnow, 2001). Additionally, ciRNA translation has been shown to be mediated by the base modification N^6-methyladenosine (Y. Yang *et al.*, 2017).
Using artificial expression-vector constructs and CRISPR-based flagging techniques as well as dual luciferase vector system, Legnini and collaborators demonstrated that mono-exonic *ciZiNc Finger protein 609 (ciZNF609)*, differentially expressed during human and murine myogenesis, has a potential for an IRES-dependent translation. However, the function of the protein encoded by *ciZNF609* remains to be fully characterized.

Similarly, bi-exonic *ciF-BoX/WD repeat-containing protein 7* (*ciFBXW7)* has been shown to encode a 185-amino-acid protein able to reduce the proliferation of glioma cells (U251 and U373) both *in vitro* and *in vivo* (Yang *et al.*, 2018). The protein encoded by *ciFBXW7* (ciFBXW7185) performs its anti-proliferative function by antagonizing c-myc stabilization. C-myc stabilization is mediated by the de-ubiquitinating enzyme Ubiquitin Specific Peptidase 28 (USP28) by inhibiting FBXW7α, a component of the Skp1-Cul1-F Box (SCF) ubiquitin ligase encoded by the linear form of *FBXW7* pre-mRNA. Through competing for USP28 binding, ciFBXW7185 prevents USP28-mediated FBXW7α inhibition, thereby allowing the subsequent FBXW7α-dependent degradation of c-myc (Yang *et al.*, 2018).

This example of a translated ciRNA playing a role of decoy for its linear cognate is also illustrated by *ciß-catenin*. As shown in immortalized liver cancer cells, the 370-amino-acid protein encoded by *ciß-catenin* acts as a competitive bait for Glycogen Synthase Kinase 3ß (GSK3ß), thereby preventing the GSK3ß-induced degradation of ß-catenin (Liang *et al.*, 2019). ß-catenin is then free to translocate in the nucleus and promote the transcription of pro-oncogenic genes, placing ciß-catenin as a central pro-malignancy actor.

To date, ten ciRNAs have been shown to translate into proteins. Among those functionally characterized, the majority act as tumour suppressors (Huang *et al.*, 2020).

The functional research regarding ciRNAs is nascent, making the points discussed above only the tip of the iceberg in term of biological importance of ciRNAs. It clearly appears that ciRNAs embody a powerful class of molecular actors with obvious relevance in terms of cell physiology but also pathology, with proven decisive implications in diseases ranging from atherosclerosis and neurogenerative diseases to diabetes and cancer (Xu *et al.*, 2018) (Holdt, Kohlmaier and Teupser, 2018b). Standardized and robust genome-wide approaches as well as stringent

biochemical techniques are therefore essential to properly identify and characterize those central players.

3. CiRNA identification

RNA-sequencing dataset analysis using specific computational methods is generally the first approach used to identify ciRNAs (Salzman *et al.*, 2012). In principle, ciRNA detection is achieved by identifying reads matching a putative backsplice junction, as exons would then appear in a non-colinear order (Zhang *et al.*, 2014). In order to exclude false positives, RNA-sequencing analysis are performed in a paired-end fashion.

The burst in ciRNA research in the last decades led to plethora of data from RNA-sequencing analyses that are now gathered in databases. To name only one, circBase is an exhaustive and user-friendly database unifying collected ciRNAs (Glažar, Papavasileiou and Rajewsky, 2014).

Samples destined for ciRNA identification are generally enriched/purified beforehand. Common strategies, for example, consist in depleting ribosomal RNAs and/or treating the samples with 3'-5' exoribonuclease RNAse R which decays linear mRNAs (Iparraguirre *et al.*, 2019). Notably, the latter step allows the degradation of specific chimeric transcripts that can be filtered in by mapping algorithms and constitute false positives. Those particular transcripts can originate from trans-splicing, when a pre-mRNA is spliced with another, or genome (tandem) duplication which results in exon(s) repetitions (Fig 36) (Jeck and Sharpless, 2014). In both cases, an apparent resulting backsplice sequence would in fact not arise from a ciRNA but from a linear transcript. However, RNAse R treatment entails some limitations. Indeed, some linear mRNAs may be resistant to such treatment (Vincent and Deutscher, 2006) (Szabo and Salzman, 2016). Also, a more disturbing observation is that some ciRNAs are degraded by

the enzyme, although lacking 3'end, as it is observed for *ciRS-7* (Jeck *et al.*, 2013) (Szabo and Salzman, 2016).

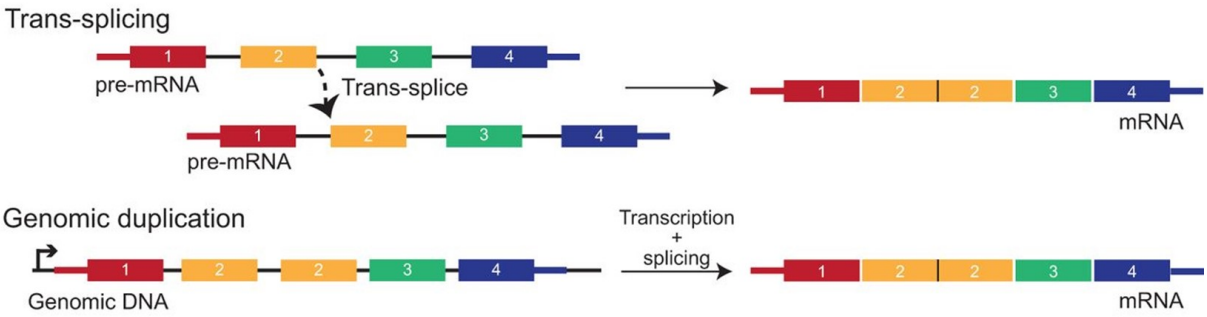

Figure 36 : The different origins of spurious backsplice junctions that might occur and complicate circular RNA (ciRNA) identification.

Trans-splicing and genomic duplication might lead to products displaying a misleading backsplice junction erroneously associated with ciRNAs. In these examples, one might mistakenly consider the existence of a single-exon ciRNA originating from the exon 2 of the presented transcript. (Barrett and Salzman, 2016)

The putative ciRNAs identified/predicted by high throughput methods like RNA-sequencing are generally validated by RT-qPCR using primers targeting the backsplice junction. Those primers are called "outward-facing" or "divergent" as their 3'ends oppose each other when mapped on the genome/linear transcript. This common and potent biochemical method is however not devoid of bias. More specifically, artefactual products due to template switching can arise during the Reverse Transcription (RT) step. A template switching event consists in the dissociation of the extending cDNA strand from its RNA template followed by a homology-driven re-hybridation of the cDNA on another RNA template (Fig 37) (Jeck and Sharpless, 2014) (Barrett and Salzman, 2016). Later amplified during PCR, this aberrant product is easily misconstrued for a ciRNA as it gives rise to a spurious backsplice junction. Template-switching artefacts are quite treacherous in the way that they have shown replicability properties and sometimes a higher abundance than experimentally validated products of interest (Wu *et al.*, 2014).

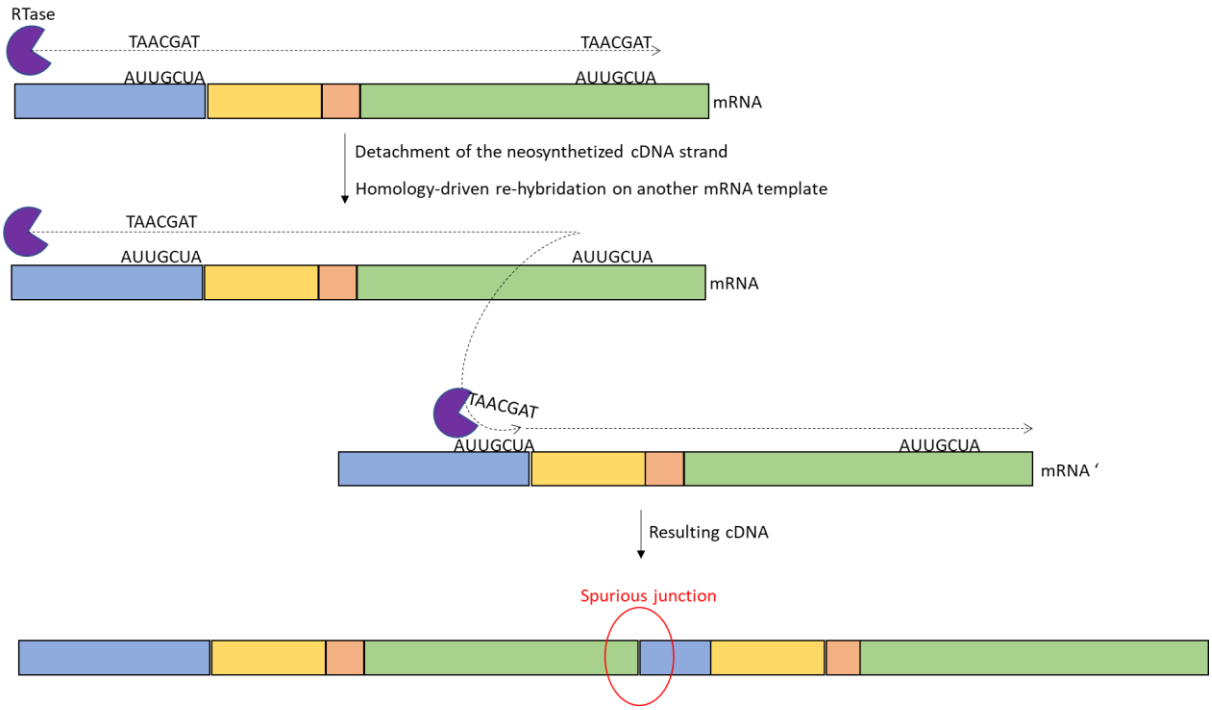

Figure 37 : Mechanism of homology-driven template-switching event.

During the reverse transcription step, the reverse transcriptase (RTase) can switch from one template to another. This phenomenon is favored by the presence of homologous sequences in the mRNA template and the resulting product can be misinterpreted as a circular RNA due to the generation of an apparent backsplice junction.

OBJECTIVES

This second axis of the thesis is focused on the exploration of *MPV17* ciRNAs. Indeed, ciRNAs are a research hotspot, notably as therapeutic agents and targets. Moreover, the putative existence of *MPV17* ciRNAs might provide some clues for yet unexplained observations performed in the first part of the thesis, where different *MPV17* shRNAs have been associated with various proliferation phenotypes, despite a similar effect on the MPV17 protein abundance.

Thus, this work aims at 1) investigating the putative existence of *MPV17* ciRNAs, which would, in and of itself, already constitute a valuable finding and 2) exploring their function(s) and relevance in terms of pathology, if any. Indeed, as mentioned in the introduction, ciRNAs dysregulation bears substantial pathological impact. Also, in regard to the hepatocerebral phenotype associated with MPV17 pathology, the mammalian brain has been shown to be the richest organ in terms of ciRNA abundance and variety, suggesting a critical regulatory role of ciRNAs in brain development and function (You *et al.*, 2015) (Sekar and Liang, 2019) (cf introduction, *ciRS-7* and *ciFBXW7*). Moreover, liver ciRNAs seem to be involved in hepatic proliferation as well as energy metabolism (Li *et al.*, 2017), suggesting that the loss of a ciRNA could have a negative impact on liver integrity. Around 40 % of total ciRNAs present in an organ are specific to this organ (Xu *et al.*, 2017), explaining how the loss of one ciRNA could give rise to tissue-specific pathologies. Finally, ciRNAs have been implicated in mitochondrial function and dynamics (Zhao *et al.*, 2019) (Wang *et al.*, 2017).

This work is realised in collaboration with URVI (University of Namur), under the supervision of Dr. Damien Coupeau and Prof. Benoît Muylkens, as their team is more qualified and experienced in term of circular RNA research.

MATERIALS AND METHODS

RNA extraction

Total RNA was extracted from 90% confluent cells (T75 flask) with TRI Reagent (Sigma, T9424) according to manufacturer's recommendations. Briefly, 1 mL of TRI Reagent was added to the cells. After complete lysis, 200 µL of chloroform were then added to the samples which were vigorously shaken, allowed to stand 10 min at room temperature and centrifuged for 15 min at 12 000g at 4 °C. The aqueous phase was retrieved and 500 µL of isopropanol were added. Samples were allowed to stand 10 min at room temperature and centrifuged for 15 min at 12 000g at 4 °C. Pellets were then washed twice with ethanol 75 %, air-dried and dissolved in 50 µL of distilled water.

DNase and RNase treatments

An amount of 20 µg of RNA was incubated for 20 min at 37 °C in the presence of 4 µL of DNase I (NEB, M0303S) and 10 µL of DNase I 10 X reaction buffer (NEB, B0303S) in a total volume of 100 µL. A volume of 2 µL of DNase I was then added once more to the mix and another 20 min incubation at 37 °C was performed. DNase I treatment was followed by a purification step. More specifically, the solution volume was adjusted to 300 µL with distilled water and an equal volume of phenol-chloroform-isoamyl alcohol mixture (Sigma-Aldrich, 77618) was added. The solution was vortexed for 30 sec and then centrifuged at 12 000 g for 15 min at 4 °C. A volume of 300 µL of chloroform: 3-methylbutanol (49: 1) (Sigma-Aldrich, 19392) was then added to the retrieved upper aqueous phase (approximately 300 µL). The solution was then vortexed for 30 sec and centrifuged at 12 000 g for 15 min at 4 °C. Volumes of 600 µL of 100 % ethanol and 100 µL of 3 M sodium acetate were then added to the retrieved upper aqueous phase (approximately 300 µL). The solution was incubated for 1h at -80 °C and

centrifuged at 15 000 g for 20 min at 4 °C. The pellet was then washed with 75% ethanol, centrifuged at 12 000 g for 5 min at 4 °C, quickly air-dried and resuspended in 50 µL of distilled water. An amount of 7 µg of RNA was then incubated for 1 h at 37 °C with 2 µL of RNase R (Lucigen, RNR07250) and 10 µL of 10 X reaction buffer (Lucigen, RNR07250) in a total volume of 100 µL. The sample was then re-purified as described above and ultimately resuspended in 11 µL of distilled water.

Reverse Transcription (RT)

Volumes of 2 µL of dNTPs mix (Eurogentec, NU-0010) and 1 µL of random primers (NEB, S1230) were added to the 11 µL of purified sample enriched in ciRNAs. The sample was incubated for 3 min at 94 °C and then immediately placed on ice for at least 1 min. Volumes of 1 µL of dithiothreitol (Uptima, 054721), 1 µL of SuperScript IV (Thermo Fisher, 00789728) and 4 µL of its 5X buffer (Thermo Fisher, LT-00789839) and 1 µL of RNase OUT (Thermo Fisher, 10777019) were added to the sample. The mix was incubated for 10 min at room temperature, for 1 h at 53 °C and finally for 10 min at 80 °C. One µL of RNase H (Thermo Fisher, 18021014) was then added to the sample, before an incubation at 37 °C for 20 min.

For *MPV17* specific RT, 1 µL of a mix of two *MPV17*-targeting primers (5'-AATGTCACCCAGGCCCATCA- 3' and 5' -GAGAAAGCAGCCTAGAAAACACG- 3') was used instead of random hexamers. The rest of the protocol is identical to what is described above except that the step which consists in incubating the samples 10 min at room temperature is excluded.

Nested PCR

For the first PCR and for each condition, the reaction mix was composed of 27.25 µL of distilled water, 1.5 µL of dNTPs mix (Eurogentec, NU-0010), 5 µL of forward primer at 2 µM, 5 µL of

reverse primer at 2 µM (see Table 4), 0.25 µL of GoTaq DNA Polymerase (Promega, M3001), 10 µL of 5X Green GoTaq Reaction Buffer (Promega, M7911) and 1 µL of cDNA (pure or diluted, as stated). The programmed conditions for cDNA amplification consisted in an initial denaturation at 94 °C for 3 min, followed by 25 cycles consisting in 30 sec at 94 °C, 30 sec at 56 °C, 1min 30 sec at 72 °C and a final extension at 72 °C for 7 min. For the second PCR, 1 µL of the first PCR product (pure or diluted, as stated) was further amplified (see Table 4 for primers) for 35 cycles in the same conditions described above.

ID	Forward primer (5'→3')	Reverse primer (5'→3')	Company
pGEM® -T Easy	TGTAAAACGACGGCCAGTG (PU)	CAGGAAACAGCTATGACCA (RPU)	Eurogentec
Fig39 ciRNA 1 First level nested PCR	TAATGGACTGTCAGCCCAGGAC	GAGAAAGCAGCCTAGAAAACACG	IDT
Fig39 ciRNA 1 Second level nested PCR	GACTGTCAGCCCAGGACAACTG	CTAGAAAACACGGGGCAAAGC	IDT
Fig39 ciRNA 2 First level nested PCR	GGTTTTACAGGGATAAAAAAGGG	GTCTTCTTCCCCTGGGCTGT	IDT
Fig39 ciRNA 2 Second level nested PCR	CAGGGATAAAAAAGGGGGATT	TTCTTCCCCTGGGCTGTCAG	IDT
Fig39 ciRNA 3 First level nested PCR	TTCTACCTGGTCCCCCTTCA	GTTGGCTAACTGCACAGCAGG	IDT
Fig39 ciRNA 3 Second level nested PCR	CTACCTGGTCCCCCTTCATTA	TGCACAGCAGGCCATAGAT	IDT

Table 4: List of primers used for nested PCR.

The primers sequence, identification and provenance are specified.

PCR screening for sequencing

PCR amplification products were recovered using the NucleoSpin Gel and PCR Clean-up kit (Macherey-Nagel, 740609.250) according to manufacturer's recommendations. A volume of 3 µL of cleaned-up PCR products was incubated overnight at 12 °C with 1 µL of pGEM®-T Easy (Promega, A137A), 5 µL of 2X ligation buffer (Promega, C671X) and 1 µL of T4 DNA ligase (Promega, M180A). The next day, 50 µL of competent TG1 *E. coli* in LB were electroporated 5 msec at 2500 V with 1.5 µL of ligation product using the ECM 399 Electroporation System (BTX). Bacteria were then immediately resuspended in 150 µL of LB medium, spread on LB-agar (Sigma Aldrich, L2897) Petri dishes (Greiner bio-one, 664160)) containing 100 µg/mL of ampicillin (PanReacApplichem, A0839), 160 µg/mL of IPTG (VWR, 43714) and 120 µg/mL of X-Gal (5-bromo-4-chloro-3-indolyl-β-D-galactopyranoside) (VWR, IN115A) and incubated overnight at 37 °C. The next day, several white bacteria colonies were randomly picked with a sterile toothpick that was then plunged into a 96-well plate for PCR amplification. The reaction mix was composed of 11.5 µL of distilled water, 0.4 µL of dNTPs mix (Eurogentec, NU-0010), 2 µL of Universal Primer (PU) at 2 µM, 2 µL of Universal Reverse Primer (RPU) at 2 µM (see Table 4), 0.1 µL of GoTaq DNA Polymerase (Promega, M3001) and 4 µL of 5X Green GoTaq Reaction Buffer (Promega, M7911) and 1 µL of cDNA. The programmed conditions for cDNA amplification consisted in an initial denaturation at 94 °C for 3 min, then 94 °C for 30 sec, 55 °C for 30 sec, 72 °C for 1 min for 35 cycles and a final extension at 72 °C for 7 min. PCR products were then run on a 1.5 % agarose gel containing 0.005% Midori green (Nippongenetics, MG04) and bacteria containing PCR amplicons of interest were then sent for sequencing at Eurofins Genomics (Les Ulis, France).

RESULTS

Three potential ciRNAs originating from the *MPV17* gene are listed in CircBase (http://www.circbase.org/) (Fig 38), although not being experimentally validated yet. Among them, two long *MPV17* ciRNAs were identified by the group of Salzman in H1 human embryonic stem cells and/or in human keratinocytes, after applying an improved computational method on publicly available RNA sequencing data from the ENCODE database (Salzman *et al.*, 2013). In a similar way, the group of Rybak-Wolf enlighted the putative existence of a third small *MPV17* ciRNA in human cerebellum (Rybak-Wolf *et al.*, 2015).

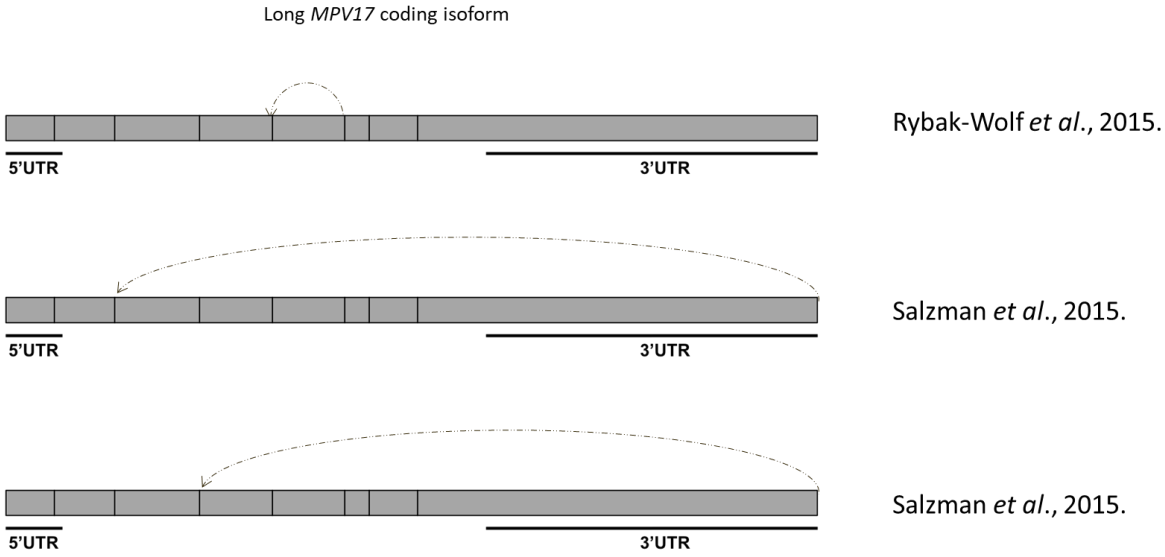

Figure 38 : *MPV17* circular RNAs (ciRNAs) predicted by RNA-sequencing followed by computational analysis. Three ciRNAs derived from the *MPV17* gene are reported in CircBase. Each grey box represents an exon of the long *MPV17* coding transcript. A dashed arrow delimits and indicates the circular nature of each ciRNA sequence.

Our first approach did not consist in specifically designing primers flanking the backsplice junction of those ciRNAs. Instead, as we were interested in having a full overview of the potential ciRNA landscape in Huh7 cell line, divergent primers were strategically placed inside selected exons of *MPV17* transcripts, thereby allowing the full-length amplification of various putative ciRNAs, comprising not only those described in CircBase but also other putative

unidentified ciRNAs. Specifically, we designed two sets of outward-facing primers in two different exons of the long *MPV17* coding transcript and one in a specific exon of the short *MPV17* non-coding transcript, described in GTEx Portal as the most abundant *MPV17* non-coding transcript in human healthy liver (Fig 29).

Only one set of primers allowed the amplification of a putative ciRNA (Fig 39a, ciRNA 3, red arrow) as shown by the enriched presence of a single band in Huh7 sample treated with RNAse R compared to untreated sample. PCR product sequencing indicated that this presumed ciRNA spreads over five exons on the long *MPV17* transcript and that the circularization event would take place in the fourth and the last exons (5'→ 3') (Fig 39b). Interestingly, the junction point is located inside these exons and is flanked by the SHS "GCCCU", overall reminiscent of an int ciRNA.

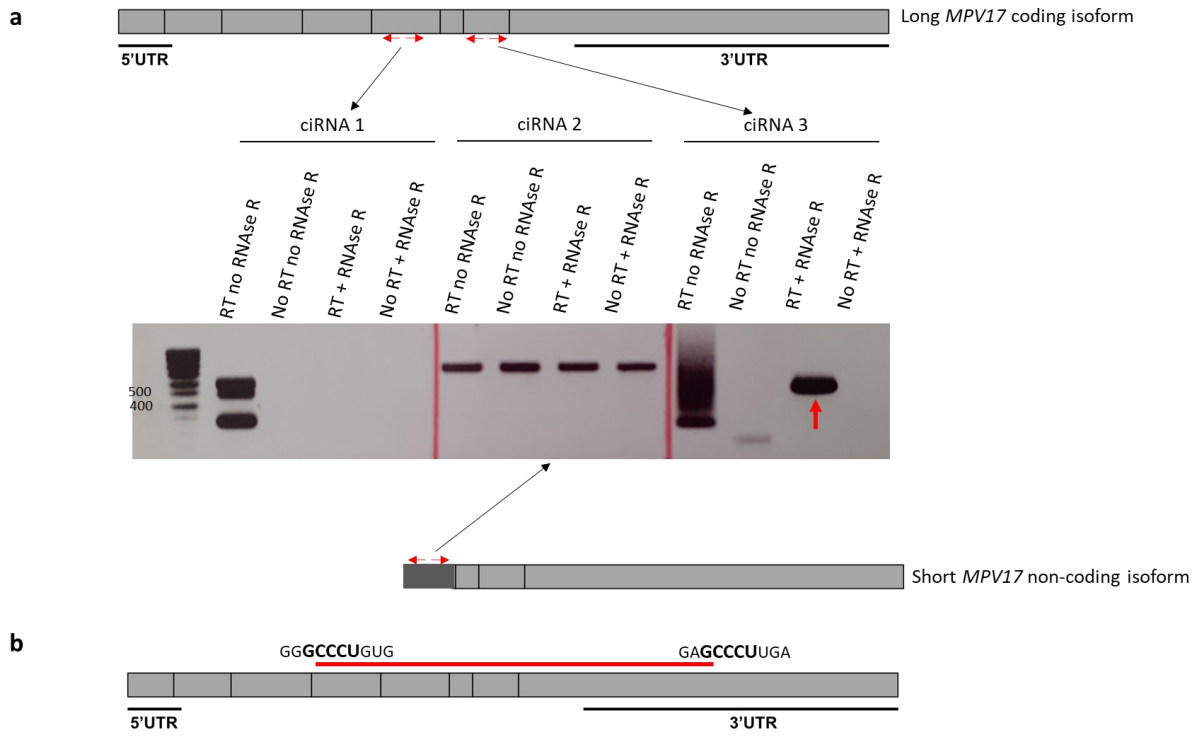

Figure 39 : Detection of putative *MPV17* circular RNAs (ciRNAs) in Huh7 cells.

(a) RNA was extracted from Huh7 cells and treated or not with RNAse R to eliminate linear RNAs. RNA was then reverse transcribed (RT) or not. Nested PCR was then performed (Ta= 56 °C) using different pairs of primers in order to detect putative ciRNAs and PCR products were resolved on agarose gel. The *MPV17* transcript regions targeted by the primers (red arrows) are indicated by a black arrow, pointing the exon (grey box) in which the

primers are localized. For the ciRNA 2, the primers are localized in an exon that is not shared with the long isoform, therefore distinguished and appearing in darker grey. (b) Localization on the long *MPV17* coding isoform of the putative ciRNA detected with the third set of primers (ciRNA 3) (shown by the red arrow in (a)). The two end points of the red line should be imagined joined to form a circularized structure. The detail of the sequence around the supposed backsplice junction is indicated in order to outline the existence of a Short Homologous Sequence (SHS) flanking the circularization event (in bold).

Unfortunately, we were not able to replicate this result on another biological Huh7 sample (originating from the same frozen cell vial, passage +1). Instead, we detected another putative ciRNA, that we originally thought to be similar to the first one we previously amplified (Fig 40a, blue arrow). Furthermore, diverse starting dilutions of cDNA material and various annealing temperatures both led to the amplification of different putative ciRNAs (Fig 40a, b). Noteworthy, most of the detected putative ciRNAs are also int ciRNAs. Most of them (except number 2) also display the presence of SHS in the flanking sequence of their backsplice junction. Two of them, number 1 and 2, share one upstream backsplicing site as well as the presence of the canonical splicing signal AG/GU (red triangles) (Fig 40b). Noteworthy, the third exon of *MPV17* transcript (5' → 3') is predicted to be alternatively spliced (NCBI, transcript ID: XM_017004152.1). This event would occur at the exact same position of the upstream backsplicing site shared by ciRNAs number 1 and 2.

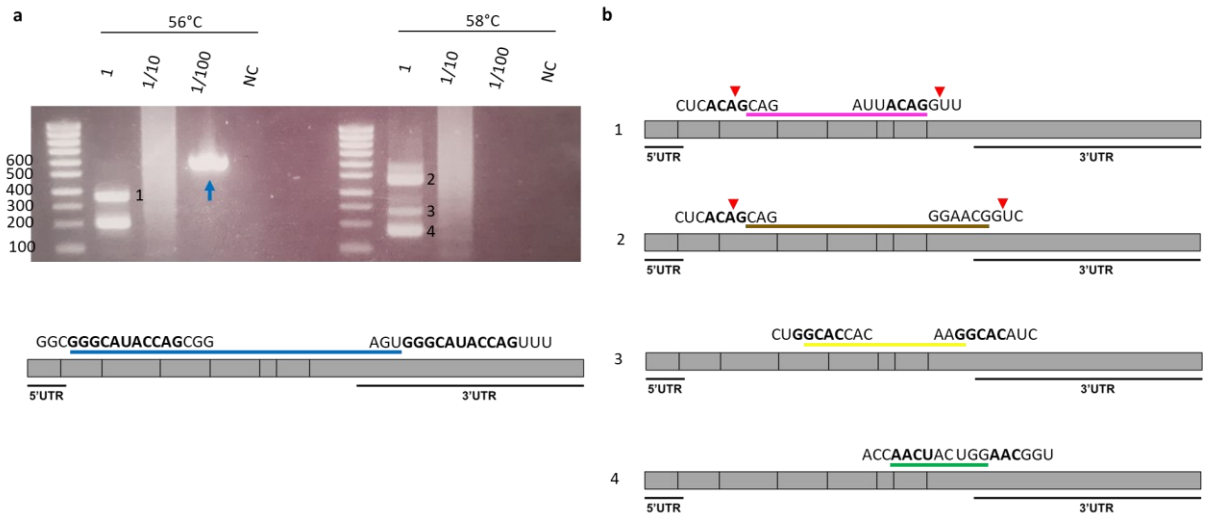

Figure 40 : Second replicate for the detection of putative *MPV17* circular RNAs (ciRNAs) in Huh7 cells.
(a) RNA was extracted from Huh7 cells and treated with RNAse R to eliminate linear RNAs. RNA was then reverse transcribed and a nested PCR was performed (Ta= 56 °C or 58 °C) on different dilutions of starting cDNA material (1, 1/10 or 1/100). PCR products were then resolved on agarose gel. The blue arrow shows a putative ciRNA whose localization on the long *MPV17* coding transcript is indicated by a blue line. The two end points of the blue line should be imagined joined to form a circularized structure. The detail of the sequence around the supposed backsplice junction is indicated in order to outline the existence of a Short Homologous Sequence (SHS) flanking the circularization event (in bold). NC: negative control (PCR performed on water). (b) The localization on the long *MPV17* coding transcript of other detected putative ciRNAs (1, 2, 3 and 4) are also indicated as well as the detail of the sequence around the supposed backsplice junction. A red triangle outlines the existence of the canonical splicing signal AG/GU.

To shed more light on *MPV17* ciRNAs existence and robustness, we decided to investigate the potential expression of the ciRNAs detected in Huh7 cells in other different human cell lines, namely AICS cells (induced pluripotent stem cells), HEK293T cells (embryonic kidney), HeLa cells (cervix adenocarcinoma), HepG2 cells (hepatocellular carcinoma), PANC1 cells (pancreatic epithelioid carcinoma), KP4 cells (pancreatic ductal carcinoma) and T98G cells (brain glioblastoma). Huh7 cells were still investigated as well and another putative ciRNA (Fig 41a, 1), although not previously detected, was amplified in these cells, adding more variability to the existing results, since this biological sample comes from the same extracted RNA material used in Fig 40 but originates from independent RNAse R treatment and RT.

Enticingly, although not previously detected in Huh7 cells, the same putative ciRNA was amplified in both Huh7 and T98G cells (Fig 41a, 2 and 3), leaning the balance towards a genuine existence. Its circularization event occurs at a typical exon/exon junction, constituting the only ciRNA in this work presenting this particular feature.

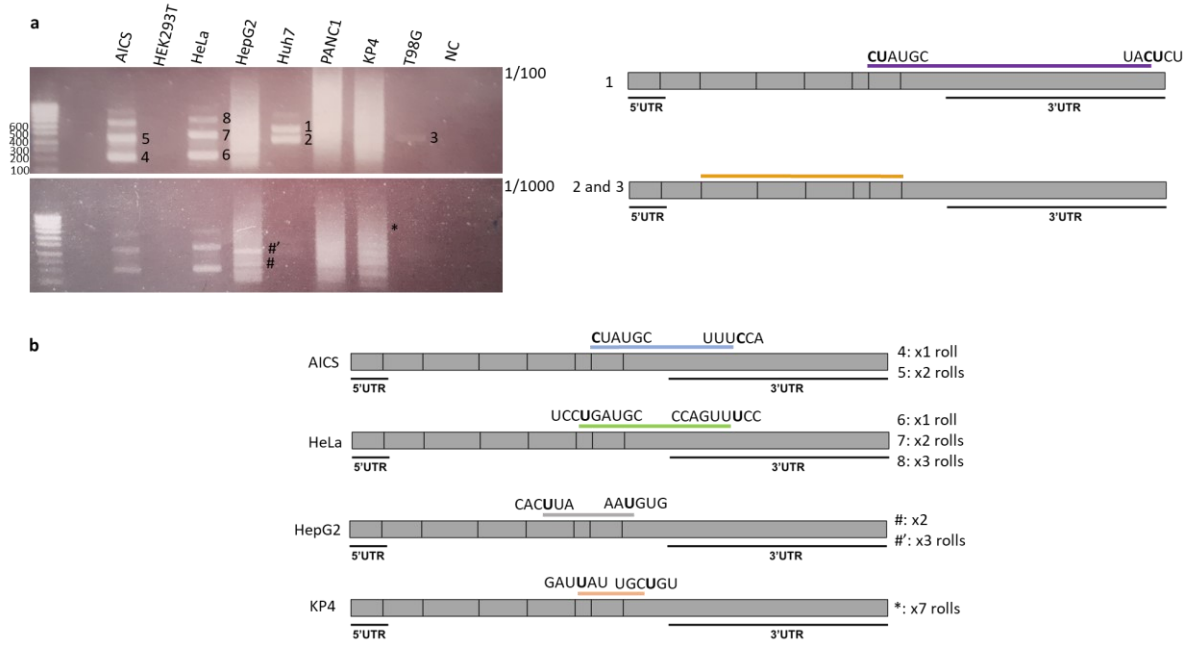

Figure 41 : Detection of putative *MPV17* circular RNAs (ciRNAs) in several human cell lines.

(a) RNA from eight different cell lines was extracted and treated with RNAse R to eliminate linear RNAs. RNA was then reverse transcribed and a nested PCR was performed (Ta= 56 °C) on different dilutions of material (1/100 or 1/1000 of the first PCR product engaged in the second round of the nested PCR). PCR products were then resolved on agarose gel, purified, screened and sequenced. The localization on the long *MPV17* coding transcript of detected ciRNAs (1, 2 and 3) is indicated as well as the detail of the sequence around the supposed backsplice junction. NC: negative control (PCR performed on water). (b) The localization on the long *MPV17* coding transcript of putative ciRNAs presenting multi-rolling reverse transcription characteristics is indicated as well as the detail of the sequence around the supposed backsplice junction. For each putative ciRNA (4, 5, 6, 7, and 8), the number of detected rolls (see Fig 42) is indicated on the right of their corresponding localization on the *MPV17* transcript. For the particular case of HepG2 and KP4 cells, where clear bands are not particularly visible because of the smear aspect, the detected ciRNAs are referred as « # », « #' » for HepG2 cells and « * » for KP4 cells.

AICS and HeLa cells display the same electrophoretic profile but with a slight shift in size (Fig 41a). This ladder-like profile is reminiscent of RT multi-rolling events, which could constitute a strong sign in favour of the presence of ciRNAs. Indeed, divergent primers like the ones used

in this study lead to ciRNA amplification providing that rolling events occur during the RT, a common occurrence when dealing with ciRNAs. Thus, thanks to strand displacement, the enzyme reverse transcribes several times in a row the ciRNA sequence, leading to a linear cDNA composed of several repetitions of the ciRNA sequence. Depending on the number of rolls during RT and the random targeting of the primers during PCR, this event gives rise to a ladder-like aspect on agarose gel, composed of several multimers (Fig 42).

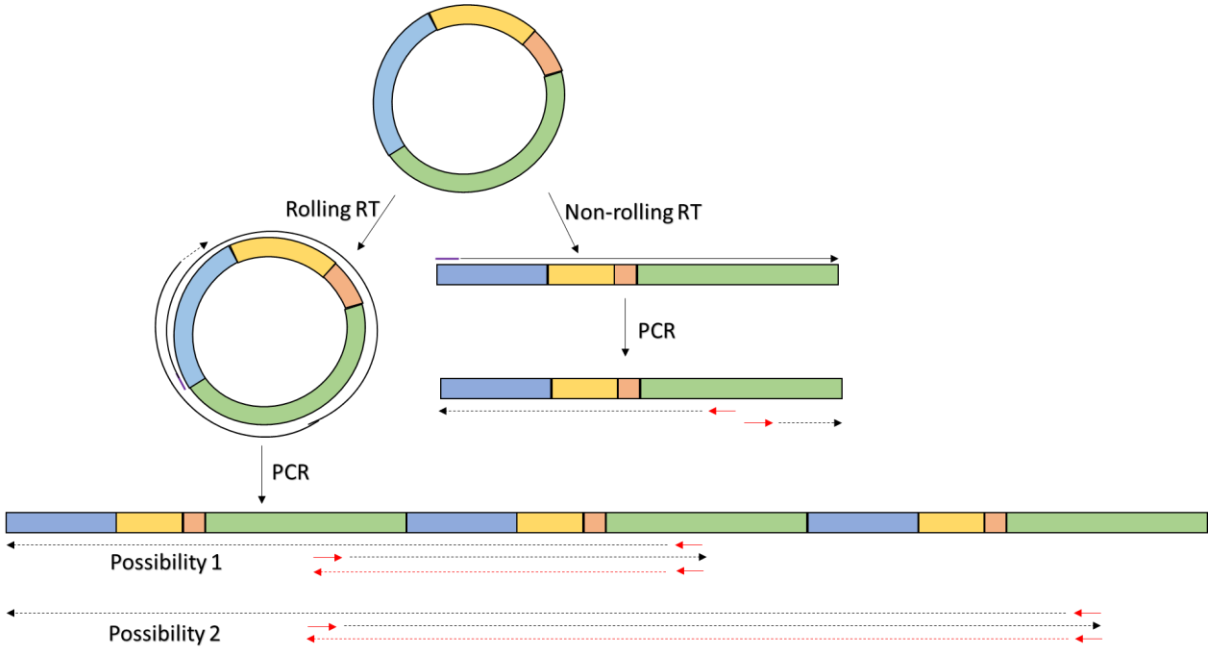

Figure 42 : Rolling Reverse Transcription (RT) is necessary for the detection of complete circular RNAs (ciRNAs). Since the final RT product of a ciRNA is a linear cDNA, only an event of rolling during RT would enable the amplification of a ciRNA with divergent primers (red arrows). Depending on the number of rolls and the random placement of the primers during PCR, this amplification results in diverse products composed of various repetitions of the same ciRNA sequence (possibility 1 and 2).

The cloning and sequencing of these PCR products indeed revealed that the ladder-like profiles of AICS and HeLa cells are due to rolling events, highlighting the possible existence of one ciRNA in each cell type. While these two ciRNAs are inherently different, they are closely overlapping and present one downstream backsplicing site that varies only by one nucleotide in terms of position (Fig 41b). AICS ciRNA also shares an upstream backsplicing site with one ciRNA detected in Huh7 cells (Fig 41a, 1).

While the electrophoretic profiles of HepG2, PANC1 and KP4 cells appeared smeared, we nonetheless decided to attempt cloning and sequencing the PCR products, as a ladder-like profiles can sometimes be discerned (Fig 41a, 1/1000, HepG2 and KP4). While most of the results were *MPV17*-specific but seemingly irrelevant and due to technical artefacts, some amplified products displayed rolling characteristics. Thus, in HepG2 cells, two PCR products (“ # ” and “ #’ ”) are different concatemers of the same sequence. In the KP4 cells, one PCR product (“ * ”) display seven repetitions of the same sequence (Fig 41b).

In order to “clean” the smeared signal obtained for HepG2, KP4 and PANC1 cell lines, we performed, on the same RNA samples, an RT using primers specifically targeting *MPV17*.

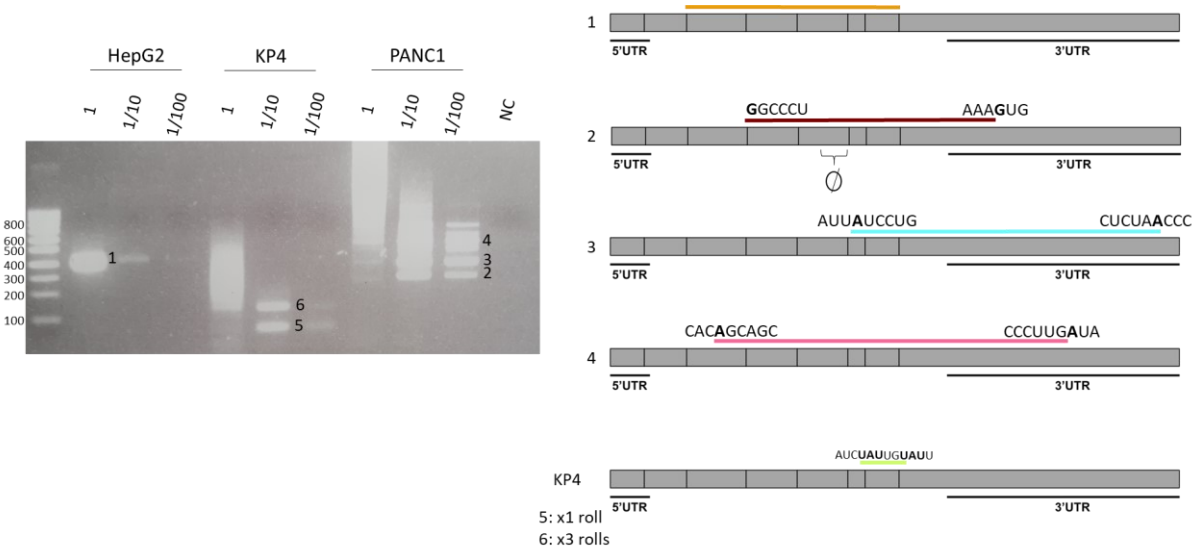

Figure 43 : Detection of putative *MPV17* circular RNAs on HepG2, KP4 and PANC1 cells following specific *MPV17* Reverse Transcription (RT).

RNA from HepG2, KP4 and PANC1 cell lines was extracted and treated with RNAse R to eliminate linear RNAs. RNA was then reverse transcribed using two specific *MPV17*-targeting primers and a nested PCR was performed (Ta= 56 °C) on different dilutions of material (1, 1/100 or 1/1000 of the first PCR product engaged in the second round of the nested PCR). PCR products were then resolved on agarose gel, purified, screened and sequenced. The localization on the long *MPV17* coding transcript of detected ciRNAs is indicated as well as the detail of the sequence around the supposed backsplice junction. When present, multi-rolling RT events are detailed. NC: negative control (PCR performed on water). The empty symbol represents the absence of the indicated sequence.

The specific RT successfully allowed the amplification of distinct products for each cell line (Fig 43). Enticingly, we detected in HepG2 cells (Fig 43, 1) the same putative ciRNA previously amplified in both Huh7 and T98G cell lines (Fig 41, 2 and 3).

Among the diverse putative ciRNAs identified in PANC1 cells (Fig 43, 2 and 3 and 4), one of them presents an exon missing around half of its canonical sequence (Fig 43, 2). However, no alternative splicing of this particular exon has been described/predicted so far.

Finally, we detected once more multi-rolling RT events in KP4 cells, originating from the putative presence of a ciRNA that, while closely resembling the ciRNA detected in Fig 41, remains a distinct ciRNA species.

GENERAL DISCUSSION CONCLUSION AND PERSPECTIVES

In this thesis work we studied the putative role of MPV17 in cancer cell proliferation. While *MPV17* silencing did not lead to depletion in mtDNA content in the tested cancer cell lines, in accordance with the literature (Dalla Rosa *et al.*, 2016) (Alonzo *et al.*, 2018), the resulting proliferation phenotypes associated with *MPV17* shRNA-mediated knockdown were unsettling and inconclusive, leading us to perform a rescue experiment that eventually excluded a role of MPV17 protein in cancer cell proliferation. The intriguing and somewhat misleading results we obtained during this investigation clearly demonstrate the need to systematically perform a rescue experiment in order to ascertain the specific nature of the experimental results.

In our study, we tested five shRNAs targeting *MPV17*. The shRNA-dependent variable phenotypical outcomes in Huh7 cells led us to consider a putative contribution of *MPV17* transcript isoforms and/or the possible existence of off-target effects.

Despite the fact that we could not find any correlation between the shRNA-targeted *MPV17* transcript isoforms and the proliferation phenotype, it is not sufficient to preclude this hypothesis as there is no guaranty that the *MPV17* transcript isoforms spectrum described in GTEx portal in human healthy liver is conserved in the Huh7 cell line.

It is also interesting to note that the predictive alignment (BLAST, ncbi) of sh129921 and sh127649, the two shRNAs associated with a reduced proliferation phenotype, on human transcripts did not highlight the putative existence of a shared off-target mRNA. Again, this observation is however not sufficient to exclude a putative off-target effect as it could be taking place through separate effectors for each shRNA. Noteworthy, a cross-analysis between the predicted off-target mRNAs (obtained from the BLAST alignment of sh129921 sequence on

human transcripts) and the RNA sequencing analysis put into light two mRNAs slightly downregulated in sh129921-encoding vector transduced Huh7 cells compared to shNT-encoding vector transduced cells. One of them, with a fold change of 0.7, codes for ADhesion G protein-coupled Receptor A3 (ADGRA3). This cell membrane receptor is associated with a good outcome regarding colorectal cancer as it inhibits the Wnt/β-catenin signaling pathway (Wu *et al.*, 2018). The second mRNA, with a fold change of 0.77, codes for Nuclear Factor 1-A type (NF1-A). Knowing that this transcription factor increases a glioblastoma cell line proliferation by repressing p21 (Lee *et al.*, 2014), its downregulation could explain the reduced proliferation rate that we observed. However, it is intricate to predict the biological impact of such a moderate mRNA downregulation. Also, whether the downregulation of those mRNAs is indeed due to a direct off-target effect from sh129921 or if it is just a secondary consequence of *MPV17* silencing is difficult to foresee.

However, the most intriguing observation in this work was that the same shRNA (sh129921), expressed either constitutively or induced with IPTG, resulted in different effects on cell proliferation. The emergence of the inducible lentiviral vectors, which enable a reversible and fine tuning of gene knockdown, allows further characterization of gene function, a better ease in studying genes for which knockdown ends up being too deleterious or lethal for the cell, as well as timeframe selection in a developmental process (Martínez, 2010). In this study, we resorted to this tool to overcome a progressive compensation/adjustment of the cells following *MPV17* knockdown. The transient nature of the inducible knockdown would theoretically prevent this compensation to settle.

Cell adaptation following gene tampering is not surprising in itself, especially coming from cancer cells as they are well-known plasticity masters. Upon gene invalidation, cells strive to achieve a new equilibrium which, when attained, is outlined by a gene expression readjustment

(El-Brolosy and Stainier, 2017). In trivial cases, the compensation comes from the (over)expression of a paralog or another actor possessing overlapping function with the repressed gene (Dooley *et al.*, 2019) (O'Leary *et al.*, 2013). For example, upon KInesin Family member 11 (KIF11) inhibition in mammalian cells, KIF15 compensates for the absence of the motor protein to drive bipolar spindle assembly during cell mitosis, although KIF15 is not essential when KIF11 is fully active (Tanenbaum *et al.*, 2009). Sometimes, the cell adaptation is more challenging and compels more complex cellular networks. This is exemplified in the *epidermal growth factor like 7* (*egfl7*) zebrafish mutants, in which a phenotype of vascular defect is prevented by the upregulation of a set of genes and proteins, including several family members of the extracellular matrix elastin microfibril interfacer (*emilin*) gene (Rossi *et al.*, 2015) (Cerikan *et al.*, 2016). Depending on a study objective, this concept of cellular adjustment is important in driving the relevant choice of a gene invalidation method, i.e. acute (e.g. siRNA-mediated knockdown) or prolonged (e.g. shRNA-mediated knockdown or CRISPR/Cas9-driven KnockOut (KO)). Indeed, the resulting phenotypes from one or the other method have often been reported as diverging because of genome remodelling occurrence (Rossi *et al.*, 2015) (Cerikan *et al.*, 2016) (Hall *et al.*, 2013) (Williams *et al.*, 2015). For example, while a fasting condition is necessary to induce phenotypes of hypoglycaemia and hypertriglyceridemia in *Ppara* KO mice, those phenotypes are already visible in normally fed mice depleted in *Ppara* via siRNA. Peroxisome Proliferator-Activated Receptor α (PPARα) is a ligand-activated transcription factor regulating fatty acid metabolism. During fasting, the energy supply greatly relies on fatty acid oxidation in the liver. While the acute knockdown model demonstrates that PPARα function is impactful regardless of the fed state, the chronic knockdown model suggests the settlement of compensatory mechanisms during development allowing lipid and glucose homeostasis to a certain extent, i.e. in stress-less non-fasting conditions (De Souza *et al.*, 2006). Thus, while acute gene depletion does not usually let enough time to the cells to adapt and

therefore allows a direct view of a potential gene function, this approach does not authentically reflect (compensatory) phenotypes that might take place over time in *in vivo* disease models. On the contrary, during prolonged gene invalidation, although cell adaptation in response to a gene loss may hinder the study of the gene function, it can also enlighten important adaptive mechanisms (Cerikan *et al.*, 2016). Thus, while it is reasonable to consider all those techniques based on their advantages/drawbacks in terms of specificity/off-target risks, invalidation gene potency/homogeneity and their associated technical challenges, one should also not lose sight from the fact that these techniques lead to different cell states in terms of subsequent genome intervention. Furthermore, when this genome intervention is simple, meaning when the gene invalidation releases a negative feedback loop resulting in a compensatory expression of a paralog for example, the same compensatory phenotypes may be visible in both acute and prolonged gene invalidation approaches. For example, the cell cycle regulatory protein RetinoBlastoma Like 1 (RBL1) compensates for the absence of its family member RBL2 in both acute and prolonged gene invalidation in T lymphocytes and breast cancer cells (Jackson and Pereira-Smith, 2006) (Mulligan, Wong and Jacks, 1998) (El-Brolosy and Stainier, 2017). On the contrary, when a compensatory phenotype, if present, is only visible in the prolonged gene invalidation model, a more complex set of actors/course of events is probably at play. This is exemplified by the opposed phenotypes obtained in Dedicator Of CytoKinesis 6 (*DOCK6)*-KO versus siDOCK6-treated HeLa cells. The loss of the guanine nucleotide exchange factor encoded by this gene leads to a severe collapse of the actin cytoskeleton in the acute knockdown model. This dramatic defect is however not visible in the KO model, in which elaborate compensatory mechanisms are triggered following the time-dependent accumulation of G-actin (Cerikan *et al.*, 2016). Also, in the particular case of the KO approach, it could reveal that an upstream trigger, like the genomic lesion or the mutant RNA, is necessary for the settlement of the cell compensatory mechanisms (El-Brolosy and Stainier, 2017). As an example, the

knockout of β-actin in primary MEFs is accompanied by a compensatory expression of γ-actin which remains upregulated even after the re-introduction of β-actin, suggesting that the cells accommodate in response to an upstream trigger (Tondeleir *et al.*, 2012).

An explanation for the opposed proliferation phenotypes observed in the constitutive and inducible sh129921-expression models could reside in the fact that the shRNA is expressed at a higher level in the constitutive model. Indeed, it is recommended by Sigma Aldrich to ensure a minimum of 70 % knockdown in a constitutive model, before switching to an inducible one. This recommendation reflects the risk of obtaining a less potent gene silencing with an inducible vector when compared to a constitutive one due to a lower shRNA expression.
In our experimental conditions, the observation that MPV17 knockdown at the protein level was quite comparable in both expression models does not preclude a higher expression of the shRNA in the constitutive expression system, which could either increase the risk of off-targeting or favour a better targeting of some non-coding *MPV17* transcript isoforms. A working perspective for this matter is to quantify the expression of sh129921 in both constitutive and inducible expression models. However, while a confirmed higher expression of sh129921 in the constitutive expression model compared to the inducible one would definitely strengthen both these hypotheses, it would not allow to discriminate which one is likely responsible for the reduced proliferation phenotype.

While most researchers are confident in their interpretation of a particular gene function when a consistent phenotype is observed with at least two different shRNA sequences targeting a transcript, we and others experienced that this is not sufficient and that a rescue experiment is an all-encompassing insurance of the veracity of the scientific conclusions (Peretz *et al.*, 2018). However, as properly reported by Peretz and collaborators, “Rescue experiments are a good

way to ensure specificity and are being added to an increasing number of studies, although, based on a survey of scientific literature, this is probably limited to less than 0.1 % of studies" (Peretz *et al.*, 2018). Our work stresses the imperative necessity to perform a rescue experiment in each study carrying out shRNA-mediated gene knockdown. Nevertheless, the benefit of a rescue experiment often matches its technical complexity. In terms of limitations while performing a rescue experiment, we can mention that the re-expression of the silenced gene, generally at a higher level than the normal endogenous one, might, in itself, lead to undesired effects (Peretz *et al.*, 2018). In addition, the random integration of the vector can also lead to additional off-target effects. A rescue experiment is also stressful for the cells as they undergo another round of lentiviral transduction as well as the action of a second selective antibiotic. In this study, for the rescue experiment, we had to perform the overexpression of MPV17 before the actual knockdown of the protein, as the combined stresses due to *MPV17*-silencing and the second round of transduction repeatedly led to severe cell death. We were also compelled to perform the rescue experiment on HepG2 cells instead of Huh7 cells as the efficiency of transduction with the overexpression plasmid was very low in the last cell type.

Although the rescue experiment should undeniably be an indispensable control in every experiment based on shRNA-induced knockdown, it is not totally dependable as the absence of rescue of a particular observed phenotype does not necessarily mean that the effect observed with the shRNA was due to off-target effects. Indeed, in ideal circumstances, every splice variant targeted by the shRNA should be restored in the rescue experiment, which might not always be realistic (Peretz *et al.*, 2018). In this work, the reintroduction of the only known MPV17-coding transcript refuted any role of the protein in cancer cell proliferation.

On a side note, we would like to mention that we could have performed this work on a three-dimensional (3D) cell culture model as it ensures more realistic cell responses compared to a

two-dimensional (2D) model (Chaicharoenaudomrung, Kunhorm and Noisa, 2019). This is especially relevant regarding cancer cells since 3D cell culture can better mimic cell architecture and interaction as well as microenvironment. Notably, 2D cell culture fails to reproduce the differential zones inside a tumor, typically composed of a necrotic centre, an intermediate quiescent viable zone and a proliferating periphery. Stress-responsive MPV17 could therefore be of particular importance in the deeper layers of the tumor, more deprived in nutrients, oxygen and growth factors. However, this natural gradient is not represented in a 2D cell culture model (Chaicharoenaudomrung, Kunhorm and Noisa, 2019).

In a nutshell, our work demonstrates that MPV17 does not induce depletion in mtDNA content in cancer cell lines and that MPV17 does not control their cell cycle/proliferation. Importantly, in the future, rescue experiments should be a requirement in any study involving shRNA in order to silence a gene and analyse its subsequent effects on a particular phenotype. While the absence of rescue of the phenotype is not a strict indicator of specificity of the results, the restoration of the phenotype surely is a strong argument in favour of the specificity of any shRNA-induced phenotype of interest.

These results however do not exclude the fact that the observed reduced proliferation phenotype might still be *MPV17*-dependent although the protein itself would not be at play. Indeed, as discussed above, *MPV17* non-coding transcript isoforms might be accountable for the reduced proliferation phenotype, as consolidated by their large diversity proposed by the GTEx Portal. A work perspective would therefore be to exhaustively characterize the population of *MPV17* non-coding transcripts in Huh7 cells (paired-end RNA sequencing analysis) and determine if they are indeed differentially targeted by each shRNA as well as in the two sh129921-expression models. However, the implication of another class of *MPV17* non-coding

transcripts, namely ciRNAs, should also be considered. Despite being both referenced in databases (GTEx Portal and CircBase), the genuine existence of either linear and/or circular *MPV17* non-coding transcripts has not been experimentally demonstrated yet. While both categories are relevant regarding our study and definitely in need of further characterization, we decided, within the time imparted that we had left, to pursue with the investigation of *MPV17* circular transcripts. Indeed, considering the ever-growing evidence that ciRNAs regulate various, if not all, biological processes, we deemed the characterization of *MPV17* ciRNAs appealing and promising. Also, studies extensively associated ciRNAs and cell proliferation (Feng *et al.*, 2019) (X. Wang *et al.*, 2019) (Yang *et al.*, 2019). For example, the silencing of ciHomeodomain-Interacting Protein Kinase 3 (ciHIPK3), which sponges miR-149, suppresses A549 cell proliferation (Lu *et al.*, 2020). The second part of this work was therefore focused on exploring the *MPV17* ciRNA landscape.

The investigation of *MPV17* ciRNAs led to the detection of many and in several cell types. A majority of the ciRNAs detected in Huh7 cells presented SHS in the flanking sequences of the backsplice junction. This feature could be a sign of template-switching-driven biogenesis or might as well be a technical artefact. The lack of reproducibility of the results, at both technical and biological levels, could be an indicator of non-specificity or, on the contrary, highlight the complexity and diversity of existing *MPV17* ciRNAs. Indeed, it has been described that a single gene can express one to ten different ciRNA isoforms (Holdt, Kohlmaier and Teupser, 2018a) (Szabo and Salzman, 2016) as exemplified, for the first time, with the *Deleted in Colorectal Carcinoma* (*DCC*) gene which displays four potential ciRNA splice variants (Nigro *et al.*, 1991). One could also presume a finely-tuned expression of each ciRNA, down to the single cell level. All of this would therefore lead to random PCR-amplification preference.

In other investigated cell types (AICS, HeLa, KP4, PANC1 cells), signs of multi-rolling events during the RT strengthened the legitimate existence of the detected ciRNAs but no shared ciRNA was identified. Noteworthy, we did not validate, in the particular cell types explored in this study, the *MPV17* ciRNAs listed in CircBase. Remarkably, none of the putative ciRNAs detected in Huh7 cells is selectively targeted by the two shRNAs leading to a reduced proliferation phenotype, offering no possible candidate accountable for the different phenotypical outcomes obtained with the different shRNAs used.

Hepatocerebral MPV17-related MDDS is still enigmatic in the way that affected individuals present a broad spectrum of clinical manifestations, even when bearing the same mutation, offering no clear genotype-phenotype correlation (El-Hattab *et al.*, 2018). However, the survival rate is slightly higher for individuals with biallelic missense pathogenic variants, notably for the particular mutation p.R50Q (El-Hattab *et al.*, 2018). Recently, the group of Gilberti conducted a valuable study in a yeast model enlightening the molecular/functional consequences of seven *MPV17* missense point mutations (equivalent to the ones found in affected human individuals) (Gilberti *et al.*, 2018). Expectedly, they confirmed that all pathogenic variants displayed mtDNA instability and a severely compromised growth at 37°C in the presence of ethanol as previously described and discussed in the introduction (Trott and Morano, 2004) (Dallabona *et al.*, 2010). Similarly to what is observed in patients, the respiratory phenotype of the p.R50Q mutant was the mildest, closely followed by the p.G24W mutant. While all mutants displayed the presence of Sym1 protein, its relative abundance was highly variable among the different mutants. Specifically, Sym1 abundance in the p.R50Q mutant remained unchanged compared to control, while the p.G24W mutant displayed an extreme instability/degradation of the protein. Interestingly however, the residual protein in p.G24W mutant turned out to be the most capable one, if not the only one, to assemble with its

interacting partners, with no information however regarding the resulting functionality of the complex.

Altogether, these observations reflect the intricacy in attempting to determine the specific consequences of a particular genotype. Thus, it appears legitimate to wonder if other players than the protein, at the transcript level, could also be differentially affected by the diverse mutations and further modulate the phenotype variability. Moreover, the tissue-specific manifestation of the disease, despite the ubiquitous MPV17 expression, is also puzzling. CiRNAs are attractive candidates to consider in attempt to shed light on those interrogations, as evidenced by the specific and enthralling presence of one common ciRNA in Huh7, HepG2 and T98G cells. The tissues from which these cancer cell lines are derived (liver for Huh7 and HepG2 and brain for T98G) are reminiscent of the hepatocerebral form associated with MPV17-dependent MDDS. Following a mutation on the *MPV17* gene, one could therefore speculate that the functional loss of this particular ciRNA could partake in the settlement of the tissue-restricted phenotype observed in *MPV17*-mutated patients, providing that this particular ciRNA carries a crucial biological function in these organs. To further investigate this idea, we could attempt to detect this ciRNA expression in specific healthy human and mice tissues as well as patients/mutated mice tissues. In the case scenario that this ciRNA would be specifically detected in mice kidneys, this would constitute an exciting lead in understanding the species-specific phenotypes observed in MPV17 deficiencies. Also, the partake of this ciRNA in MPV17-related MDDS could be determined with a rescue experiment. The re-expression of a ciRNA has already been successfully performed, both *in vitro* and *in vivo*, in several studies in the context of heart failure and stroke (Zeng *et al.*, 2017) (K. Wang *et al.*, 2016) (Bai *et al.*, 2018). Astonishingly, in these studies, a local protective effect of the ciRNAs was noticed despite a systemic delivery.

In terms of work perspectives, a primary imperative step will be to validate the authenticity of this ciRNA, first by reaching reproducibility of the results, at both technical and biological levels and second, by ensuring its actual circularity. While the design of primers aiming at amplifying the backsplice junction of the putative ciRNA is an interesting work perspective, it would not exclude the possibility of RT-generated template-switching artefacts. For this purpose, the circular nature of the putative ciRNA will be further ascertain by Northern Blotting, with a probe specific to the ciRNA backsplice junction (Schneider *et al.*, 2018). The biochemical validation of a putative ciRNA is a critical step that should be ironclad and rigorous. However, the literature shows that a significant amount of studies only rely on RNAse R treatment and RT-qPCR-mediated amplification of the backsplice junction to validate the circularity of the ciRNA (Pfafenrot and Preußer, 2019). As discussed in the introduction of the second part of the thesis, those methods entail deceitful limitations, as illustrated by RT-generated template switching artefacts (Fig 37). Therefore, more stringent techniques like Northern Blotting should always be implemented during the experimental validation of a ciRNA, despite its recognized challenging realisation.

Once both the authenticity and the tissue/species-specific expression of the ciRNA are demonstrated, the deciphering of its function will be tackled. To do so, a first relevant approach could consist in an RNA sequencing analysis of cells presenting a knockdown or overexpressing the ciRNA (versus appropriate controls). Differentially expressed actors would then be examined in terms of pathologic/MDDS relevance and the ones displaying an expression (inversely) proportional to the one of the ciRNA in both conditions would be considered as the most relevant candidates. In the eventuality that the candidate and ciRNA expressions show a positive correlation, one could hypothesize that the ciRNA acts as a miRNA sponge. Binding sites of the miRNAs known to target the candidate would then be researched on the ciRNA sequence. If a miRNA sponge activity is suspected, this hypothesis would be

tested using dual luciferase reporter assay and RNA pull-down assay coupled with RT-qPCR. An RNA pull-down assay, using a specific ciRNA probe, coupled with mass-spectrometry analysis would also be a method of choice to identify putative interactions between the ciRNA and proteins. *MPV17* ciRNA could be critical for the functional regulation of actors involved in deoxynucleotide supply/synthesis or in mitochondrial integrity/homeostasis, either by stabilizing them, increasing their expression/translation or by determining their subcellular localization. Referring thereto, the localization of *MPV17* ciRNA will be determined by Fluorescence In Situ Hybridization and/or by cellular fractionation.

To conclude, over the last decades, the non-protein coding genome, and more particularly the emerging class of ciRNAs, has been gaining prominence, notably in the context of human diseases. Since more than 98% of the genome does not encode proteins (Lander, 2011), the relevance of non-coding RNAs in core biological processes is still likely largely underestimated. Along those lines, we decided to explore the existence of *MPV17* ciRNAs, as they might account for the different proliferation phenotypes observed in Huh7 cells successfully silenced for *MPV17* with different shRNAs. So far, none of the putative *MPV17* ciRNAs detected in Huh7 cells could explain the phenotypical differences. However, our data are highly preliminary and in need of further investigation/validation.

Because each organ possesses a specific functional subnetwork of genes, a mutation affecting an ubiquitous protein usually only impacts specific tissues (Kitsak *et al.*, 2016). The tissue and context-specific expression of ciRNAs make them potent players in terms of cell type-specific interactomes. Therefore, we suggest that *MPV17* ciRNA might partake in MPV17-related MDDS, as the selective expression of a putative ciRNA in Huh7, HepG2 (liver) and T98G (brain) cells might be a valuable preliminary observation in the attempt to explain the particular hepatic and neurologic damages observed in patients.

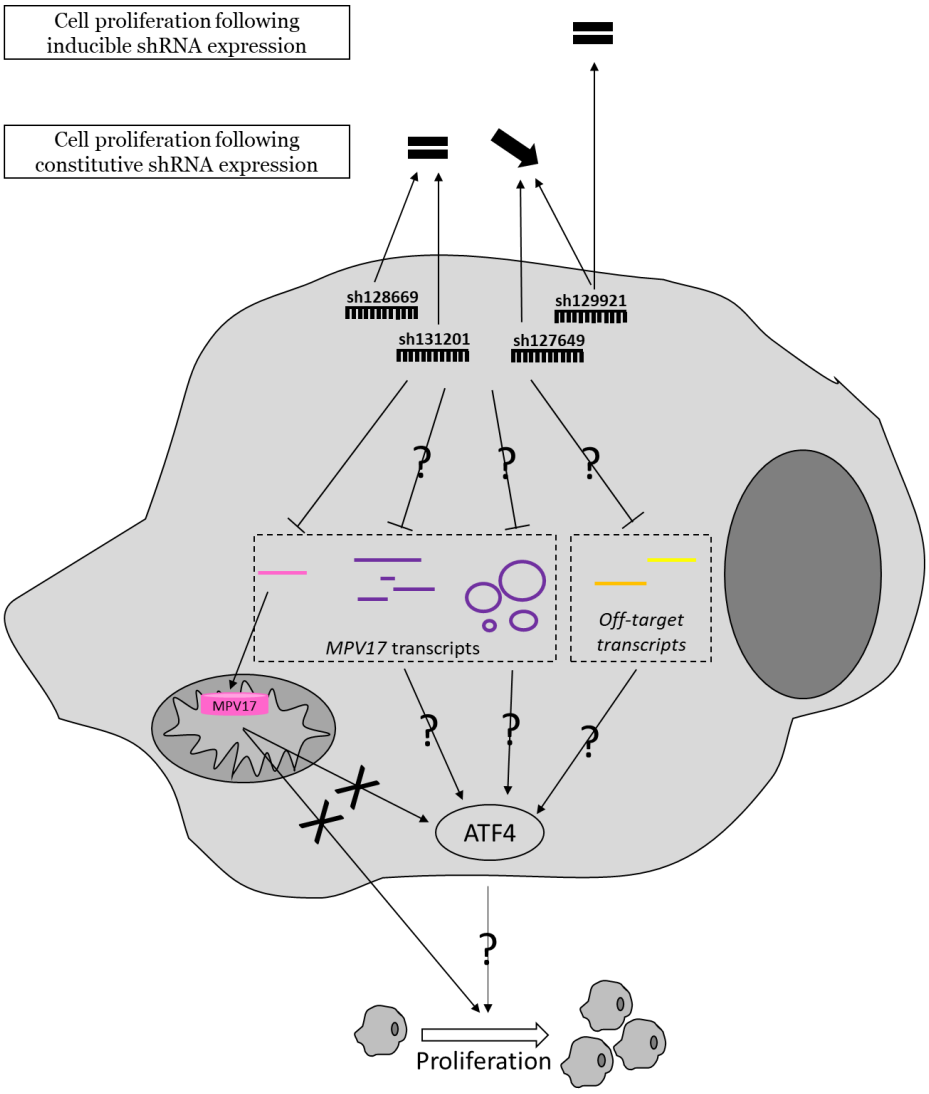

Figure 44 : Summary figure describing the main findings of this thesis.

In this work, we depleted MPV17 (pink) from the Huh7 cancer cell line using four different shRNAs and obtained confusing results. Indeed, MPV17 invalidation led to a reduced proliferation phenotype in only half of the cases (sh129921 and sh127649) and the inducible expression of one of the shRNA (sh129921) associated with the reduced proliferation phenotype resulted in the absence of this phenotype. We eventually excluded a role of MPV17 protein in cancer cell proliferation by performing a rescue experiment. Noteworthy, when present, the reduced proliferation phenotype was consistently associated with a reduced ATF4 abundance, which is consistent with its functional role as a master regulator of cellular pathways that are crucial for cell proliferation (nucleotide synthesis, amino acid metabolism). However, whether ATF4 decreased abundance is indeed the upstream causal event driving the reduced proliferation phenotype is yet undetermined. Two main hypotheses can be brought forward in the attempt to explain the disturbing results that we obtained, and so far, none of them can be completely infirmed or confirmed. First, the reduced proliferation phenotype associated with two different shRNAs can result from off-target effects that are common and well-known from the scientific community. Second, the reduced proliferation phenotype could still be a consequence of on-target effects but in this case, it would not be related to MPV17 protein but rather to a differential targeting of *MPV17* non-coding transcripts (purple). This later population can comprise both linear and circular transcripts but their respective genuine existence has not been validated yet.

REFERENCES

Abdelmohsen, K. *et al.* (2017) 'Identification of HuR target circular RNAs uncovers suppression of PABPN1 translation by CircPABPN1', *RNA Biology*. Taylor and Francis Inc., 14(3), pp. 361–369. doi: 10.1080/15476286.2017.1279788.

Alonzo, J. R. *et al.* (2018) 'The mitochondrial inner membrane protein MPV17 prevents uracil accumulation in mitochondrial DNA', *Journal of Biological Chemistry*, 293(52), pp. 20285–20294. doi: 10.1074/jbc.RA118.004788.

Ameri, K. and Harris, A. L. (2008) 'Activating transcription factor 4', *The International Journal of Biochemistry & Cell Biology*, 40(1), pp. 14–21. doi: 10.1016/j.biocel.2007.01.020.

Andersona, D. D., Quintero, C. M. and Stovera, P. J. (2011) 'Identification of a de novo thymidylate biosynthesis pathway in mammalian mitochondria', *Proceedings of the National Academy of Sciences of the United States of America*. National Academy of Sciences, 108(37), pp. 15163–15168. doi: 10.1073/pnas.1103623108.

Antonenkov, V. D. *et al.* (2015) 'The Human Mitochondrial DNA Depletion Syndrome Gene MPV17 Encodes a Non-selective Channel That Modulates Membrane Potential.', *The Journal of biological chemistry*. American Society for Biochemistry and Molecular Biology, 290(22), pp. 13840–61. doi: 10.1074/jbc.M114.608083.

Ashwal-Fluss, R. *et al.* (2014) 'circRNA Biogenesis Competes with Pre-mRNA Splicing', *Molecular Cell*. Cell Press, 56(1), pp. 55–66. doi: 10.1016/J.MOLCEL.2014.08.019.

Aslanian, A. M., Fletcher, B. S. and Kilberg, M. S. (2001) 'Asparagine synthetase expression alone is sufficient to induce L-asparaginase resistance in MOLT-4 human leukaemia cells', *Biochemical Journal*. Portland Press Ltd, 357(1), pp. 321–328. doi: 10.1042/0264-6021:3570321.

Ayala, A., Muñoz, M. F. and Argüelles, S. (2014) 'Lipid Peroxidation: Production, Metabolism, and Signaling Mechanisms of Malondialdehyde and 4-Hydroxy-2-Nonenal'. doi: 10.1155/2014/360438.

Bai, Y. *et al.* (2018) 'Circular RNA DLGAP4 ameliorates ischemic stroke outcomes by targeting miR-143 to regulate endothelial-mesenchymal transition associated with blood–brain barrier integrity', *Journal of Neuroscience*. Society for Neuroscience, 38(1), pp. 32–50. doi: 10.1523/JNEUROSCI.1348-17.2017.

Bao, X. R. *et al.* (2016) 'Mitochondrial dysfunction remodels one-carbon metabolism in human cells', *eLife*. eLife Sciences Publications Ltd, 5(JUN2016). doi: 10.7554/eLife.10575.

Barrett, S. P. and Salzman, J. (2016) 'Circular RNAs: analysis, expression and potential functions', *Development*, 143(11), pp. 1838–1847. doi: 10.1242/dev.128074.

Begemann, G. *et al.* (1997) 'muscleblind, a gene required for photoreceptor differentiation in Drosophila, encodes novel nuclear Cys3His-type zinc-finger-containing proteins.', *Development (Cambridge, England)*, 124(21), pp. 4321–31. Available at: http://www.ncbi.nlm.nih.gov/pubmed/9334280 (Accessed: 9 August 2019).

Begg, E. J. and Barclay, M. L. (1995) 'Aminoglycosides--50 years on.', *British journal of clinical pharmacology*. Wiley-Blackwell, 39(6), pp. 597–603. Available at: http://www.ncbi.nlm.nih.gov/pubmed/7654476 (Accessed: 3 June 2019).

Ben-Sahra, I. *et al.* (2016) 'mTORC1 induces purine synthesis through control of the mitochondrial tetrahydrofolate cycle', *Science*. American Association for the Advancement of Science, 351(6274), pp. 728–733. doi: 10.1126/science.aad0489.

Binder, C. J. *et al.* (1999) 'Glomerular overproduction of oxygen radicals in Mpv17 gene-inactivated mice causes podocyte foot process flattening and proteinuria: A model of steroid-resistant nephrosis sensitive to radical scavenger therapy.', *The American journal of pathology*. American Society for Investigative Pathology, 154(4), pp. 1067–75. doi: 10.1016/S0002-9440(10)65359-X.

Bottani, E. *et al.* (2014) 'AAV-mediated liver-specific MPV17 expression restores mtDNA levels and prevents diet-induced liver failure.', *Molecular therapy : the journal of the American Society of Gene Therapy*. American Society of Gene & Cell Therapy, 22(1), pp. 10–7. doi: 10.1038/mt.2013.230.

Bouchard, C., Staller, P. and Eilers, M. (1998) 'Control of cell proliferation by Myc', *Trends in Cell Biology*, pp. 202–206. doi: 10.1016/S0962-8924(98)01251-3.

Cerikan, B. *et al.* (2016) 'Cell-Intrinsic Adaptation Arising from Chronic Ablation of a Key Rho GTPase Regulator', *Developmental Cell*. Cell Press, 39(1), pp. 28–43. doi: 10.1016/j.devcel.2016.08.020.

Chaicharoenaudomrung, N., Kunhorm, P. and Noisa, P. (2019) 'Three-dimensional cell culture systems as an in vitro platform for cancer and stem cell modeling', *World J Stem Cells*, 11(12), pp. 1065–1083. doi: 10.4252/wjsc.v11.i12.1065.

Chen, C. and Sarnow, P. (1995) 'Initiation of protein synthesis by the eukaryotic translational apparatus on circular RNAs', *Science*, 268(5209), pp. 415–417. doi: 10.1126/science.7536344.

Chen, D. *et al.* (2017) 'ATF4 promotes angiogenesis and neuronal cell death and confers ferroptosis in a xCT-dependent manner', *Nature Publishing Group*, 36, pp. 5593–5608. doi:

10.1038/onc.2017.146.

Chen, X. *et al.* (2016) 'circRNADb: A comprehensive database for human circular RNAs with protein-coding annotations', *Scientific Reports*. Nature Publishing Group, 6(1), p. 34985. doi: 10.1038/srep34985.

Chiang, G. G. and Abraham, R. T. (2005) 'Phosphorylation of mammalian target of rapamycin (mTOR) at Ser-2448 is mediated by p70S6 kinase.', *The Journal of biological chemistry*. American Society for Biochemistry and Molecular Biology, 280(27), pp. 25485–90. doi: 10.1074/jbc.M501707200.

Choi, Y.-R. *et al.* (2015) 'A novel homozygous MPV17 mutation in two families with axonal sensorimotor polyneuropathy.', *BMC neurology*. BioMed Central, 15, p. 179. doi: 10.1186/s12883-015-0430-1.

Choudhury, F. K. *et al.* (2017) 'Reactive oxygen species, abiotic stress and stress combination', *The Plant Journal*. Blackwell Publishing Ltd, 90(5), pp. 856–867. doi: 10.1111/tpj.13299.

Conn, S. J. *et al.* (2015) 'The RNA Binding Protein Quaking Regulates Formation of circRNAs', *Cell*, 160(6), pp. 1125–1134. doi: 10.1016/j.cell.2015.02.014.

Dalla Rosa, I. *et al.* (2016) 'MPV17 Loss Causes Deoxynucleotide Insufficiency and Slow DNA Replication in Mitochondria', *PLOS Genetics*. Edited by N.-G. Larsson. Public Library of Science, 12(1), p. e1005779. doi: 10.1371/journal.pgen.1005779.

Dallabona, C. *et al.* (2010) 'Sym1, the yeast ortholog of the MPV17 human disease protein, is a stress-induced bioenergetic and morphogenetic mitochondrial modulator', *Human Molecular Genetics*. Narnia, 19(6), pp. 1098–1107. doi: 10.1093/hmg/ddp581.

Dang, C. V. (2013) 'MYC, metabolism, cell growth, and tumorigenesis', *Cold Spring Harbor Perspectives in Medicine*. Cold Spring Harbor Laboratory Press, 3(8). doi: 10.1101/cshperspect.a014217.

Dooley, C. M. *et al.* (2019) 'The gene regulatory basis of genetic compensation during neural crest induction', *PLoS Genetics*. Public Library of Science, 15(6). doi: 10.1371/journal.pgen.1008213.

Du, W. W. *et al.* (2016) 'Foxo3 circular RNA retards cell cycle progression via forming ternary complexes with p21 and CDK2', *Nucleic Acids Research*, 44(6), pp. 2846–2858. doi: 10.1093/nar/gkw027.

Ducker, G. S. and Rabinowitz, J. D. (2017) 'One-Carbon Metabolism in Health and Disease', *Cell Metabolism*, 25(1), pp. 27–42. doi: 10.1016/j.cmet.2016.08.009.

Durán, R. V. *et al.* (2012) 'Glutaminolysis Activates Rag-mTORC1 Signaling', *Molecular*

Cell. Cell Press, 47(3), pp. 349–358. doi: 10.1016/j.molcel.2012.05.043.
El-Brolosy, M. A. and Stainier, D. Y. R. (2017) 'Genetic compensation: A phenomenon in search of mechanisms', *PLoS Genetics*. Public Library of Science, p. e1006780. doi: 10.1371/journal.pgen.1006780.
El-Hattab, A. W. *et al.* (2009) 'MPV17-associated hepatocerebral mitochondrial DNA depletion syndrome: New patients and novel mutations'. doi: 10.1016/j.ymgme.2009.10.003.
El-Hattab, A. W. *et al.* (2018) '*MPV17* -related mitochondrial DNA maintenance defect: New cases and review of clinical, biochemical, and molecular aspects', *Human Mutation*, 39(4), pp. 461–470. doi: 10.1002/humu.23387.
Endo, J. *et al.* (2009) 'Metabolic remodeling induced by mitochondrial aldehyde stress stimulates tolerance to oxidative stress in the heart', *Circulation Research*. Circ Res, 105(11), pp. 1118–1127. doi: 10.1161/CIRCRESAHA.109.206607.
Ertel, I. J. *et al.* (1979) 'Effective dose of L-asparaginase for induction of remission in previously treated children with acute lymphocytic leukemia: a report from Childrens Cancer Study Group.', *Cancer research*, 39(10), pp. 3893–6. Available at: http://www.ncbi.nlm.nih.gov/pubmed/383278 (Accessed: 12 June 2019).
Fakiola, M. *et al.* (2019) 'Transcriptional blood signatures for active and amphotericin B treated visceral leishmaniasis in India', *PLOS Neglected Tropical Diseases*. Edited by H. Louzir. Public Library of Science, 13(8), p. e0007673. doi: 10.1371/journal.pntd.0007673.
Fels, D. *et al.* (2005) 'Activation of the Integrated Stress Response (ISR) is required for adaptation of tumor cells to hypoxic stress and contributes to tumor growth', *Cancer Research*, 65(9 Supplement).
Feng, Y. *et al.* (2019) 'Circular RNA circ0005276 promotes the proliferation and migration of prostate cancer cells by interacting with FUS to transcriptionally activate XIAP', *Cell Death and Disease*. Nature Publishing Group, 10(11), pp. 1–14. doi: 10.1038/s41419-019-2028-9.
Ferrari, G. *et al.* (2005) 'Infantile hepatocerebral syndromes associated with mutations in the mitochondrial DNA polymerase-gA Abbreviations: ad = autosomal dominant; ar = autosomal recessive; MDS = mitochondrial DNA depletion syndrome; mtDNA = mitochondrial DNA; PCR = polymerase chain reaction; PEO = progressive external ophthalmoplegia; POLG1 = gene encoding mitochondrial DNA polymerase-gA; pol-gA = DNA polymerase-gA; SANDO = sensory atactic neuropathy with dysarthria and ophthalmoplegia', *Brain*, 128, pp. 723–731. doi: 10.1093/brain/awh410.
Ferraro, P. *et al.* (2006) 'Mitochondrial deoxynucleotide pool sizes in mouse liver and evidence for a transport mechanism for thymidine monophosphate', *Proceedings of the*

National Academy of Sciences, 103(49), pp. 18586–18591. doi: 10.1073/pnas.0609020103.
Fujita, Y. *et al.* (2007) 'CHOP (C/EBP homologous protein) and ASNS (asparagine synthetase) induction in cybrid cells harboring MELAS and NARP mitochondrial DNA mutations', *Mitochondrion*, 7(1–2), pp. 80–88. doi: 10.1016/j.mito.2006.11.003.
Garaeva, A. A. *et al.* (2016) 'Mitochondrial dysfunction induces SESN2 gene expression through activating transcription factor 4', *Cell Cycle*. Taylor and Francis Inc., 15(1), pp. 64–71. doi: 10.1080/15384101.2015.1120929.
Gilberti, M. *et al.* (2018) 'Pathological alleles of MPV17 modeled in the yeast Saccharomyces cerevisiae orthologous gene SYM1 reveal their inability to take part in a high molecular weight complex', *PLoS ONE*. Public Library of Science, 13(10). doi: 10.1371/journal.pone.0205014.
Glažar, P., Papavasileiou, P. and Rajewsky, N. (2014) 'circBase: a database for circular RNAs', *RNA*, 20(11), pp. 1666–1670. doi: 10.1261/rna.043687.113.
zum Gottesberge Meyer, A.-M., Reuter, A. and Weiher, H. (1996) 'Inner ear defect similar to Alport's syndrome in the glomerulosclerosis mouse model Mpv17', *European Archives of Oto-Rhino-Laryngology*. Springer-Verlag, 253(8), pp. 470–474. doi: 10.1007/BF00179952.
Gustafsson Sheppard, N. *et al.* (2015) 'The folate-coupled enzyme MTHFD2 is a nuclear protein and promotes cell proliferation', *Scientific Reports*. Nature Publishing Group, 5(1), p. 15029. doi: 10.1038/srep15029.
Hacker, A. *et al.* (1995) 'Expression of Sry, the mouse sex determining gene.', *Development (Cambridge, England)*, 121(6), pp. 1603–14. Available at: http://www.ncbi.nlm.nih.gov/pubmed/7600978 (Accessed: 8 August 2019).
Hall, E. A. *et al.* (2013) 'Acute Versus Chronic Loss of Mammalian Azi1/Cep131 Results in Distinct Ciliary Phenotypes', *PLoS Genetics*, 9(12). doi: 10.1371/journal.pgen.1003928.
Hansen, T. B. *et al.* (2011) 'miRNA-dependent gene silencing involving Ago2-mediated cleavage of a circular antisense RNA', *The EMBO Journal*, 30(21), pp. 4414–4422. doi: 10.1038/emboj.2011.359.
Harding, H. P. *et al.* (2003) 'An Integrated Stress Response Regulates Amino Acid Metabolism and Resistance to Oxidative Stress', *Molecular Cell*. Cell Press, 11(3), pp. 619–633. doi: 10.1016/S1097-2765(03)00105-9.
Häsler, J. and Strub, K. (2006) 'Alu elements as regulators of gene expression.', *Nucleic acids research*. Oxford University Press, 34(19), pp. 5491–7. doi: 10.1093/nar/gkl706.
Hellen, C. U. T. and Sarnow, P. (2001) 'Internal ribosome entry sites in eukaryotic mRNA molecules', *Genes & Development*, 15(13), pp. 1593–1612. doi: 10.1101/gad.891101.

Hentze, M. W. and Preiss, T. (2013) 'Circular RNAs: splicing's enigma variations', *The EMBO Journal*, 32(7), pp. 923–925. doi: 10.1038/emboj.2013.53.

Holdt, L. M. *et al.* (2016) 'Circular non-coding RNA ANRIL modulates ribosomal RNA maturation and atherosclerosis in humans', *Nature Communications*. Nature Publishing Group, 7(1), p. 12429. doi: 10.1038/ncomms12429.

Holdt, L. M., Kohlmaier, A. and Teupser, D. (2018a) 'Circular RNAs as therapeutic agents and targets', *Frontiers in Physiology*. Frontiers Media S.A. doi: 10.3389/fphys.2018.01262.

Holdt, L. M., Kohlmaier, A. and Teupser, D. (2018b) 'Molecular roles and function of circular RNAs in eukaryotic cells', *Cellular and Molecular Life Sciences*, 75(6), pp. 1071–1098. doi: 10.1007/s00018-017-2688-5.

Hu, Y. L. *et al.* (2016) 'Glucose deprivation induces chemoresistance in colorectal cancer cells by increasing ATF4 expression', *World Journal of Gastroenterology*. Baishideng Publishing Group Co., Limited, 22(27), pp. 6235–6245. doi: 10.3748/wjg.v22.i27.6235.

Huang, A. *et al.* (2020) 'Circular RNA-protein interactions: Functions, mechanisms, and identification', *Theranostics*. Ivyspring International Publisher, pp. 3506–3517. doi: 10.7150/thno.42174.

Huang, M. L. H. *et al.* (2013) 'Molecular and functional alterations in a mouse cardiac model of friedreich ataxia: Activation of the integrated stress response, eIF2α phosphorylation, and the induction of downstream targets', *American Journal of Pathology*. Am J Pathol, 183(3), pp. 745–757. doi: 10.1016/j.ajpath.2013.05.032.

Huang, S. *et al.* (2017) 'The emerging role of circular RNAs in transcriptome regulation', *Genomics*. Academic Press Inc., pp. 401–407. doi: 10.1016/j.ygeno.2017.06.005.

Huggins, C. J. *et al.* (2016) 'C/EBPγ Is a Critical Regulator of Cellular Stress Response Networks through Heterodimerization with ATF4', *Molecular and Cellular Biology*, 36(5), pp. 693–713. doi: 10.1128/MCB.00911-15.

Hutson, R. G. *et al.* (1997) 'Amino acid control of asparagine synthetase: relation to asparaginase resistance in human leukemia cells', *American Journal of Physiology-Cell Physiology*, 272(5), pp. C1691–C1699. doi: 10.1152/ajpcell.1997.272.5.C1691.

Iparraguirre, L. *et al.* (2019) 'To Be or Not to Be: Circular RNAs or mRNAs From Circular DNAs?', *Frontiers in Genetics*. Frontiers Media S.A., 10, p. 940. doi: 10.3389/fgene.2019.00940.

Ivanov, A. *et al.* (2015) 'Analysis of Intron Sequences Reveals Hallmarks of Circular RNA Biogenesis in Animals', *Cell Reports*. Cell Press, 10(2), pp. 170–177. doi: 10.1016/J.CELREP.2014.12.019.

Jackson, J. G. and Pereira-Smith, O. M. (2006) 'Primary and Compensatory Roles for RB Family Members at Cell Cycle Gene Promoters That Are Deacetylated and Downregulated in Doxorubicin-Induced Senescence of Breast Cancer Cells', *Molecular and Cellular Biology*. American Society for Microbiology, 26(7), pp. 2501–2510. doi: 10.1128/mcb.26.7.2501-2510.2006.

Jeck, W. R. *et al.* (2013) 'Circular RNAs are abundant, conserved, and associated with ALU repeats', *RNA*, 19(2), pp. 141–157. doi: 10.1261/rna.035667.112.

Jeck, W. R. and Sharpless, N. E. (2014) 'Detecting and characterizing circular RNAs', *Nature biotechnology*. NIH Public Access, 32(5), p. 453. doi: 10.1038/NBT.2890.

Johnson, R. *et al.* (1992) 'Glomerular epithelial cells secrete a glomerular basement membrane-degrading metalloproteinase.', *Journal of the American Society of Nephrology*, 2(9).

Johnson, R. J. *et al.* (1994) 'Role of oxidants and proteases in glomerular injury.', *Kidney international*, 45(2), pp. 352–9. Available at: http://www.ncbi.nlm.nih.gov/pubmed/8164419 (Accessed: 3 June 2019).

Karasawa, M. *et al.* (1993) 'The human homolog of the glomerulosclerosis gene Mpv17: structure and genomic organization', *Human Molecular Genetics*. Oxford University Press, 2(11), pp. 1829–1834. doi: 10.1093/hmg/2.11.1829.

Karpinski, B. A. *et al.* (1992) 'Molecular cloning of human CREB-2: an ATF/CREB transcription factor that can negatively regulate transcription from the cAMP response element.', *Proceedings of the National Academy of Sciences*, 89(11), pp. 4820–4824. doi: 10.1073/pnas.89.11.4820.

Kasai, S. *et al.* (2019) 'Role of the ISR-ATF4 pathway and its cross talk with Nrf2 in mitochondrial quality control', *Journal of Clinical Biochemistry and Nutrition*. The Society for Free Radical Research Japan, 64(1), pp. 1–12. doi: 10.3164/jcbn.18-37.

Kawaguchi, Y. *et al.* (1996) 'The effects of ultraviolet A and reactive oxygen species on the mRNA expression of 72-kDa type IV collagenase and its tissue inhibitor in cultured human dermal fibroblasts.', *Archives of dermatological research*, 288(1), pp. 39–44. Available at: http://www.ncbi.nlm.nih.gov/pubmed/8750933 (Accessed: 3 June 2019).

Khan, N. A. *et al.* (2017) 'mTORC1 Regulates Mitochondrial Integrated Stress Response and Mitochondrial Myopathy Progression', *Cell Metabolism*. Cell Press, 26(2), pp. 419-428.e5. doi: 10.1016/j.cmet.2017.07.007.

Kim, K. H., Jeong, Y. T., Oh, H., *et al.* (2013) 'Autophagy deficiency leads to protection from obesity and insulin resistance by inducing Fgf21 as a mitokine', *Nature Medicine*, 19(1), pp.

83–92. doi: 10.1038/nm.3014.

Kim, K. H., Jeong, Y. T., Kim, S. H., *et al.* (2013) 'Metformin-induced inhibition of the mitochondrial respiratory chain increases FGF21 expression via ATF4 activation', *Biochemical and Biophysical Research Communications*. Biochem Biophys Res Commun, 440(1), pp. 76–81. doi: 10.1016/j.bbrc.2013.09.026.

Kitsak, M. *et al.* (2016) 'Tissue Specificity of Human Disease Module', *Scientific Reports*. Nature Publishing Group, 6(1), pp. 1–12. doi: 10.1038/srep35241.

Knowlden, J. *et al.* (1995) 'Metalloproteinase generation by human glomerular epithelial cells', *Kidney International*. Nature Publishing Group, 47(6), pp. 1682–1689. doi: 10.1038/ki.1995.233.

Krall, A. S. *et al.* (2016) 'Asparagine promotes cancer cell proliferation through use as an amino acid exchange factor', *Nature Communications*, 7(1), p. 11457. doi: 10.1038/ncomms11457.

Krauss, J. *et al.* (2013) 'transparent, a gene affecting stripe formation in Zebrafish, encodes the mitochondrial protein Mpv17 that is required for iridophore survival.', *Biology open*. Company of Biologists, 2(7), pp. 703–10. doi: 10.1242/bio.20135132.

Lander, E. S. (2011) 'Initial impact of the sequencing of the human genome', *Nature*. Nature Publishing Group, pp. 187–197. doi: 10.1038/nature09792.

Lasda, E. and Parker, R. (2014) 'Circular RNAs: diversity of form and function', *RNA*, 20(12), pp. 1829–1842. doi: 10.1261/rna.047126.114.

Lee, J. S. *et al.* (2014) 'A novel tumor-promoting role for nuclear factor IA in glioblastomas is mediated through negative regulation of p53, p21, and PAI1'. doi: 10.1093/neuonc/not167.

Li, L. *et al.* (2017) 'Comprehensive CircRNA expression profile and selection of key CircRNAs during priming phase of rat liver regeneration', *BMC Genomics*. BioMed Central Ltd., 18(1). doi: 10.1186/s12864-016-3476-6.

Li, R. *et al.* (2018) 'CiRS-7 promotes growth and metastasis of esophageal squamous cell carcinoma via regulation of miR-7/HOXB13', *Cell Death & Disease*. Nature Publishing Group, 9(8), p. 838. doi: 10.1038/s41419-018-0852-y.

Li, X. *et al.* (2018) 'Circular RNA CDR1as regulates osteoblastic differentiation of periodontal ligament stem cells via the miR-7/GDF5/SMAD and p38 MAPK signaling pathway', *Stem Cell Research & Therapy*. BioMed Central Ltd., 9(1), p. 232. doi: 10.1186/s13287-018-0976-0.

Li, Z. *et al.* (2015) 'Exon-intron circular RNAs regulate transcription in the nucleus', *Nature Structural & Molecular Biology*, 22(3), pp. 256–264. doi: 10.1038/nsmb.2959.

Liang, W.-C. *et al.* (2019) 'Translation of the circular RNA circβ-catenin promotes liver cancer cell growth through activation of the Wnt pathway', *Genome Biology*, 20(1), p. 84. doi: 10.1186/s13059-019-1685-4.

Lin, B. F., Huang, R. F. and Shane, B. (1993) 'Regulation of folate and one-carbon metabolism in mammalian cells. III. Role of mitochondrial folylpoly-gamma-glutamate synthetase.', *The Journal of biological chemistry*, 268(29), pp. 21674–9. Available at: http://www.ncbi.nlm.nih.gov/pubmed/8408020 (Accessed: 30 July 2019).

Liu, X. *et al.* (2020) 'Interior circular RNA', *RNA Biology*, 17(1), pp. 87–97. doi: 10.1080/15476286.2019.1669391.

Löllgen, S. and Weiher, H. (2015) 'The role of the Mpv17 protein mutations of which cause mitochondrial DNA depletion syndrome (MDDS): lessons from homologs in different species', *Biological Chemistry*. De Gruyter, 396(1), pp. 13–25. doi: 10.1515/hsz-2014-0198.

LOWRY, O. H. *et al.* (1951) 'Protein measurement with the Folin phenol reagent.', *The Journal of biological chemistry*, 193(1), pp. 265–75. Available at: http://www.ncbi.nlm.nih.gov/pubmed/14907713 (Accessed: 9 January 2019).

Lu, H. *et al.* (2020) 'Circular RNA HIPK3 induces cell proliferation and inhibits apoptosis in non-small cell lung cancer through sponging miR-149', *Cancer Biology and Therapy*. Taylor and Francis Inc., 21(2), pp. 113–121. doi: 10.1080/15384047.2019.1669995.

Lu, S. C. (2013) 'Glutathione synthesis.', *Biochimica et biophysica acta*. NIH Public Access, 1830(5), pp. 3143–53. doi: 10.1016/j.bbagen.2012.09.008.

Malmberg, S. E. and Adams, C. M. (2008) 'Insulin signaling and the general amino acid control response. Two distinct pathways to amino acid synthesis and uptake.', *The Journal of biological chemistry*. American Society for Biochemistry and Molecular Biology, 283(28), pp. 19229–34. doi: 10.1074/jbc.M801331200.

Mandel, H. *et al.* (2001) 'The deoxyguanosine kinase gene is mutated in individuals with depleted hepatocerebral mitochondrial DNA', *Nature Genetics*, 29(3), pp. 337–341. doi: 10.1038/ng746.

Martínez, M. A. (2010) *RNA interference and viruses : current innovations and future trends*. Caister Academic Press.

Martorano, L. *et al.* (2019) 'The zebrafish orthologue of the human hepatocerebral disease gene MPV17 plays pleiotropic roles in mitochondria.', *Disease models & mechanisms*. Company of Biologists, 12(3). doi: 10.1242/dmm.037226.

Mattaini, K. R., Sullivan, M. R. and Vander Heiden, M. G. (2016) 'The importance of serine metabolism in cancer', *The Journal of Cell Biology*, 214(3), pp. 249–257. doi:

10.1083/jcb.201604085.

McBurney, M. W. and Whitmore, G. F. (1974) ‘Isolation and biochemical characterization of folate deficient mutants of Chinese hamster cells.’, *Cell*, 2(3), pp. 173–82. Available at: http://www.ncbi.nlm.nih.gov/pubmed/4547236 (Accessed: 13 June 2019).

Mejia, N. R. and MacKenzie, R. E. (1985) ‘NAD-dependent methylenetetrahydrofolate dehydrogenase is expressed by immortal cells.’, *The Journal of biological chemistry*, 260(27), pp. 14616–20. Available at: http://www.ncbi.nlm.nih.gov/pubmed/3877056 (Accessed: 11 June 2019).

Memczak, S. *et al.* (2013) ‘Circular RNAs are a large class of animal RNAs with regulatory potency’, *Nature*, 495(7441), pp. 333–338. doi: 10.1038/nature11928.

Michel, S. *et al.* (2015) ‘Inhibition of mitochondrial genome expression triggers the activation of CHOP-10 by a cell signaling dependent on the integrated stress response but not the mitochondrial unfolded protein response’, *Mitochondrion*. Elsevier, 21, pp. 58–68. doi: 10.1016/j.mito.2015.01.005.

Mineri, R. *et al.* (2009) ‘How Do Human Cells React to the Absence of Mitochondrial DNA?’, *PLoS ONE*. Edited by T. Preiss. Public Library of Science, 4(5), p. e5713. doi: 10.1371/journal.pone.0005713.

Mosammaparast, N. and Shi, Y. (2010) ‘Reversal of Histone Methylation: Biochemical and Molecular Mechanisms of Histone Demethylases’, *Annual Review of Biochemistry*, 79(1), pp. 155–179. doi: 10.1146/annurev.biochem.78.070907.103946.

Mosmann, T. (1983) ‘Rapid colorimetric assay for cellular growth and survival: Application to proliferation and cytotoxicity assays’, *Journal of Immunological Methods*. Elsevier, 65(1–2), pp. 55–63. doi: 10.1016/0022-1759(83)90303-4.

Moss, C. F. *et al.* (2017) ‘Aberrant ribonucleotide incorporation and multiple deletions in mitochondrial DNA of the murine MPV17 disease model’, *Nucleic Acids Research*, 45(22), pp. 12808–12815. doi: 10.1093/nar/gkx1009.

Mulligan, G. J., Wong, J. and Jacks, T. (1998) ‘p130 Is Dispensable in Peripheral T Lymphocytes: Evidence for Functional Compensation by p107 and pRB’, *Molecular and Cellular Biology*. American Society for Microbiology, 18(1), pp. 206–220. doi: 10.1128/mcb.18.1.206.

Nguyen, H. G. *et al.* (2018) ‘Development of a stress response therapy targeting aggressive prostate cancer’, *Science Translational Medicine*. American Association for the Advancement of Science, 10(439), p. 2036. doi: 10.1126/scitranslmed.aar2036.

Nigro, J. M. *et al.* (1991) ‘Scrambled exons’, *Cell*. Elsevier, 64(3), pp. 607–613. doi:

10.1016/0092-8674(91)90244-S.

Nilsson, R. *et al.* (2014) 'Metabolic enzyme expression highlights a key role for MTHFD2 and the mitochondrial folate pathway in cancer', *Nature Communications*, 5(1), p. 3128. doi: 10.1038/ncomms4128.

O'Leary, M. N. *et al.* (2013) 'The Ribosomal Protein Rpl22 Controls Ribosome Composition by Directly Repressing Expression of Its Own Paralog, Rpl22l1', *PLoS Genetics*. Edited by G. P. Copenhaver. Public Library of Science, 9(8), p. e1003708. doi: 10.1371/journal.pgen.1003708.

Pakos-Zebrucka, K. *et al.* (2016) 'The integrated stress response.', *EMBO reports*. EMBO Press, 17(10), pp. 1374–1395. doi: 10.15252/embr.201642195.

Park, Y. *et al.* (2017) 'mTORC1 Balances Cellular Amino Acid Supply with Demand for Protein Synthesis through Post-transcriptional Control of ATF4', *Cell Reports*. Elsevier B.V., 19(6), pp. 1083–1090. doi: 10.1016/j.celrep.2017.04.042.

Peretz, L. *et al.* (2018) 'Combined shRNA over CRISPR/cas9 as a methodology to detect off-target effects and a potential compensatory mechanism', *Scientific Reports*. Nature Publishing Group, 8(1), p. 93. doi: 10.1038/s41598-017-18551-z.

Pfafenrot, C. and Preußer, C. (2019) 'Establishing essential quality criteria for the validation of circular RNAs as biomarkers', *Biomolecular Detection and Quantification*. Elsevier GmbH, 17, p. 100085. doi: 10.1016/j.bdq.2019.100085.

Politi, N. *et al.* (2014) 'Half-life measurements of chemical inducers for recombinant gene expression', *Journal of Biological Engineering*, 8(1), p. 5. doi: 10.1186/1754-1611-8-5.

Quirós, P. M. *et al.* (2017) 'Multi-omics analysis identifies ATF4 as a key regulator of the mitochondrial stress response in mammals', *Journal of Cell Biology*. Rockefeller University Press, 216(7), pp. 2027–2045. doi: 10.1083/jcb.201702058.

Reinhold, R. *et al.* (2012) 'The Channel-Forming Sym1 Protein Is Transported by the TIM23 Complex in a Presequence-Independent Manner', *Molecular and Cellular Biology*, 32(24), pp. 5009–5021. doi: 10.1128/MCB.00843-12.

Reuter, A. *et al.* (1998) 'Expression of the recessive glomerulosclerosis gene Mpv17 regulates MMP-2 expression in fibroblasts, the kidney, and the inner ear of mice.', *Molecular biology of the cell*, 9(7), pp. 1675–82. Available at: http://www.ncbi.nlm.nih.gov/pubmed/9658163 (Accessed: 27 May 2019).

Rossi, A. *et al.* (2015) 'Genetic compensation induced by deleterious mutations but not gene knockdowns', *Nature*. Nature Publishing Group, 524(7564), pp. 230–233. doi: 10.1038/nature14580.

Rybak-Wolf, A. *et al.* (2015) 'Circular RNAs in the Mammalian Brain Are Highly Abundant, Conserved, and Dynamically Expressed', *Molecular Cell*, 58(5), pp. 870–885. doi: 10.1016/j.molcel.2015.03.027.

Rzymski, T. *et al.* (2009) 'Role of ATF4 in regulation of autophagy and resistance to drugs and hypoxia', *Cell Cycle*, 8(23), pp. 3838–3847. doi: 10.4161/cc.8.23.10086.

Saada, A. (2009) 'Fishing in the (deoxyribonucleotide) pool', *Biochemical Journal*. Portland Press, pp. e3–e6. doi: 10.1042/BJ20091194.

Salzman, J. *et al.* (2012) 'Circular RNAs are the predominant transcript isoform from hundreds of human genes in diverse cell types', *PLoS ONE*, 7(2). doi: 10.1371/journal.pone.0030733.

Salzman, J. *et al.* (2013) 'Cell-Type Specific Features of Circular RNA Expression', *PLoS Genetics*. Edited by J. V. Moran, 9(9), p. e1003777. doi: 10.1371/journal.pgen.1003777.

Schenkel, J. *et al.* (1995) 'Functional rescue of the glomerulosclerosis phenotype in Mpv17 mice by transgenesis with the human Mpv17 homologue.', *Kidney international*, 48(1), pp. 80–4. Available at: http://www.ncbi.nlm.nih.gov/pubmed/7564095 (Accessed: 3 June 2019).

Schneider, T. *et al.* (2018) 'Northern blot analysis of circular RNAs', in *Methods in Molecular Biology*. Humana Press Inc., pp. 119–133. doi: 10.1007/978-1-4939-7562-4_10.

Sekar, S. and Liang, W. S. (2019) 'Circular RNA expression and function in the brain', *Non-coding RNA Research*. KeAi Communications Co., pp. 23–29. doi: 10.1016/j.ncrna.2019.01.001.

Shen, W. *et al.* (2020) 'Homocysteine-methionine cycle is a metabolic sensor system controlling methylation-regulated pathological signaling', *Redox Biology*. Elsevier B.V., 28. doi: 10.1016/j.redox.2019.101322.

Silva, J. M. *et al.* (2009) 'Inhibition of mitochondrial function induces an integrated stress response in oligodendroglia', *Neurobiology of Disease*. Academic Press, 34(2), pp. 357–365. doi: 10.1016/j.nbd.2009.02.005.

De Souza, A. T. *et al.* (2006) 'Transcriptional and phenotypic comparisons of Ppara knockout and siRNA knockdown mice'. doi: 10.1093/nar/gkl609.

Spinazzola, A. *et al.* (2006) 'MPV17 encodes an inner mitochondrial membrane protein and is mutated in infantile hepatic mitochondrial DNA depletion', *Nature Genetics*. Nature Publishing Group, 38(5), pp. 570–575. doi: 10.1038/ng1765.

Starke, S. *et al.* (2015) 'Exon Circularization Requires Canonical Splice Signals', *Cell Reports*, 10(1), pp. 103–111. doi: 10.1016/j.celrep.2014.12.002.

Stover, P. J. and Field, M. S. (2011) 'Trafficking of Intracellular Folates', *Advances in*

Nutrition, 2(4), pp. 325–331. doi: 10.3945/an.111.000596.

Szabo, L. and Salzman, J. (2016) 'Detecting circular RNAs: Bioinformatic and experimental challenges', *Nature Reviews Genetics*. Nature Publishing Group, pp. 679–692. doi: 10.1038/nrg.2016.114.

Tanenbaum, M. E. *et al.* (2009) 'Kif15 Cooperates with Eg5 to Promote Bipolar Spindle Assembly', *Current Biology*. Elsevier, 19(20), pp. 1703–1711. doi: 10.1016/j.cub.2009.08.027.

Taylor, R. T. and Hanna, M. L. (1982) 'Folate-dependent enzymes in cultured Chinese hamster ovary cells: impaired mitochondrial serine hydroxymethyltransferase activity in two additional glycine--auxotroph complementation classes.', *Archives of biochemistry and biophysics*, 217(2), pp. 609–23. Available at: http://www.ncbi.nlm.nih.gov/pubmed/7138028 (Accessed: 13 June 2019).

Tondeleir, D. *et al.* (2012) 'Cells lacking β-actin are genetically reprogrammed and maintain conditional migratory capacity', *Molecular and Cellular Proteomics*. American Society for Biochemistry and Molecular Biology, 11(8), pp. 255–271. doi: 10.1074/mcp.M111.015099.

Tropp, B. E. (2012) *Molecular biology : genes to proteins*. Jones & Bartlett Learning.

Trott, A. and Morano, K. A. (2004) 'SYM1 Is the Stress-Induced Saccharomyces cerevisiae Ortholog of the Mammalian Kidney Disease Gene Mpv17 and Is Required for Ethanol Metabolism and Tolerance during Heat Shock', *Eukaryotic Cell*. American Society for Microbiology (ASM), 3(3), p. 620. doi: 10.1128/EC.3.3.620-631.2004.

Trotter, P. J. *et al.* (2005) 'Mitochondrial transporters involved in oleic acid utilization and glutamate metabolism in yeast', *Archives of Biochemistry and Biophysics*. Academic Press, 442(1), pp. 21–32. doi: 10.1016/J.ABB.2005.07.016.

Tyynismaa, H. *et al.* (2010) 'Mitochondrial myopathy induces a starvation-like response'. doi: 10.1093/hmg/ddq310.

Vallejo, M. *et al.* (1993) 'C/ATF, a member of the activating transcription factor family of DNA-binding proteins, dimerizes with CAAT/enhancer-binding proteins and directs their binding to cAMP response elements.', *Proceedings of the National Academy of Sciences of the United States of America*. National Academy of Sciences, 90(10), pp. 4679–83. doi: 10.1073/pnas.90.10.4679.

Vincent, H. A. and Deutscher, M. P. (2006) 'Substrate recognition and catalysis by the exoribonuclease RNase R', *Journal of Biological Chemistry*. American Society for Biochemistry and Molecular Biology, 281(40), pp. 29769–29775. doi: 10.1074/jbc.M606744200.

Viscomi, C. *et al.* (2009) 'Early-onset liver mtDNA depletion and late-onset proteinuric nephropathy in Mpv17 knockout mice', *Human Molecular Genetics*, 18(1), pp. 12–26. doi: 10.1093/hmg/ddn309.

Wanet, A. *et al.* (2017) 'The Transcription Factor 7-Like 2-Peroxisome Proliferator-Activated Receptor Gamma Coactivator-1 Alpha Axis Connects Mitochondrial Biogenesis and Metabolic Shift with Stem Cell Commitment to Hepatic Differentiation', *STEM CELLS*, 35(10), pp. 2184–2197. doi: 10.1002/stem.2688.

Wang, K. *et al.* (2016) 'A circular RNA protects the heart from pathological hypertrophy and heart failure by targeting miR-223', *European Heart Journal*. Oxford University Press, 37(33), pp. 2602a-2611a. doi: 10.1093/eurheartj/ehv713.

Wang, K. *et al.* (2017) 'Circular RNA mediates cardiomyocyte death via miRNA-dependent upregulation of MTP18 expression', *Cell Death and Differentiation*. Nature Publishing Group, 24(6), pp. 1111–1120. doi: 10.1038/cdd.2017.61.

Wang, L. *et al.* (2019) 'Circular RNA circRHOT1 promotes hepatocellular carcinoma progression by initiation of NR2F6 expression', *Molecular Cancer*, 18(1), p. 119. doi: 10.1186/s12943-019-1046-7.

Wang, P. L. *et al.* (2014) 'Circular RNA Is Expressed across the Eukaryotic Tree of Life', *PLoS ONE*. Edited by T. Preiss, 9(3), p. e90859. doi: 10.1371/journal.pone.0090859.

Wang, Shu *et al.* (2015) 'ATF4 Gene Network Mediates Cellular Response to the Anticancer PAD Inhibitor YW3-56 in Triple-Negative Breast Cancer Cells.', *Molecular cancer therapeutics*. NIH Public Access, 14(4), pp. 877–88. doi: 10.1158/1535-7163.MCT-14-1093-T.

Wang, S. *et al.* (2015) 'ATF4 Gene Network Mediates Cellular Response to the Anticancer PAD Inhibitor YW3-56 in Triple-Negative Breast Cancer Cells', *Molecular Cancer Therapeutics*, 14(4), pp. 877–888. doi: 10.1158/1535-7163.MCT-14-1093-T.

Wang, S. F. *et al.* (2016) 'Mitochondrial dysfunction enhances cisplatin resistance in human gastric cancer cells via the ROS-activated GCN2-eIF2α- ATF4-xCT pathway', *Oncotarget*. Impact Journals LLC, 7(45), pp. 74132–74151. doi: 10.18632/oncotarget.12356.

Wang, X. *et al.* (2019) 'Circular RNA TTN Acts As a miR-432 Sponge to Facilitate Proliferation and Differentiation of Myoblasts via the IGF2/PI3K/AKT Signaling Pathway', *Molecular Therapy - Nucleic Acids*. Cell Press, 18, pp. 966–980. doi: 10.1016/j.omtn.2019.10.019.

Wang, Y. and Wang, Z. (2015) 'Efficient backsplicing produces translatable circular mRNAs.', *RNA (New York, N.Y.)*. Cold Spring Harbor Laboratory Press, 21(2), pp. 172–9.

doi: 10.1261/rna.048272.114.

Wardie, E. N. (1994) ‘Cellular biology of glomerulosclerosis’, *Renal Failure*. Informa Healthcare, pp. 535–545. doi: 10.3109/08860229409044883.

Weiher, H. *et al.* (1990) ‘Transgenic mouse model of kidney disease: insertional inactivation of ubiquitously expressed gene leads to nephrotic syndrome.’, *Cell*, 62(3), pp. 425–34. Available at: http://www.ncbi.nlm.nih.gov/pubmed/1696177 (Accessed: 27 May 2019).

Wi, J., Na, Y., *et al.* (2020) ‘Arabidopsis AtMPV17, a homolog of mice MPV17, enhances osmotic stress tolerance’, *Physiology and Molecular Biology of Plants*. Springer, 26(7), pp. 1341–1348. doi: 10.1007/s12298-020-00834-x.

Wi, J., Park, E. J., *et al.* (2020) ‘PyMPV17, the MPV17 Homolog of Pyropia yezoensis (Rhodophyta), Enhances Osmotic Stress Tolerance in Chlamydomonas’, *Plant Molecular Biology Reporter*. Springer, 38(1), pp. 39–47. doi: 10.1007/s11105-019-01172-3.

Williams, J. A. *et al.* (2015) ‘Chronic deletion and acute knockdown of Parkin have differential responses to acetaminophen-induced mitophagy and liver injury in mice’, *Journal of Biological Chemistry*. American Society for Biochemistry and Molecular Biology Inc., 290(17), pp. 10934–10946. doi: 10.1074/jbc.M114.602284.

Woeller, C. F. *et al.* (2007) ‘Evidence for small ubiquitin-like modifier-dependent nuclear import of the thymidylate biosynthesis pathway’, *Journal of Biological Chemistry*. American Society for Biochemistry and Molecular Biology, 282(24), pp. 17623–17631. doi: 10.1074/jbc.M702526200.

Wolfson, R. L. and Sabatini, D. M. (2017) ‘The Dawn of the Age of Amino Acid Sensors for the mTORC1 Pathway’, *Cell Metabolism*. Cell Press, pp. 301–309. doi: 10.1016/j.cmet.2017.07.001.

Wong, L.-J. C. *et al.* (2007) ‘Mutations in theMPV17 gene are responsible for rapidly progressive liver failure in infancy’, *Hepatology*, 46(4), pp. 1218–1227. doi: 10.1002/hep.21799.

Wortel, I. M. N. *et al.* (2017) ‘Surviving Stress: Modulation of ATF4-Mediated Stress Responses in Normal and Malignant Cells’, *Trends in Endocrinology & Metabolism*, 28(11), pp. 794–806. doi: 10.1016/j.tem.2017.07.003.

Wu, C. S. *et al.* (2014) ‘Integrative transcriptome sequencing identifies trans-splicing events with important roles in human embryonic stem cell pluripotency’, *Genome Research*. Cold Spring Harbor Laboratory Press, 24(1), pp. 25–36. doi: 10.1101/gr.159483.113.

Wu, Y. *et al.* (2018) ‘Elevated g-protein receptor 125 (GPR125) expression predicts good outcomes in colorectal cancer and inhibits wnt/β-catenin signaling pathway’, *Medical Science*

Monitor. International Scientific Information, Inc., 24, pp. 6608–6616. doi: 10.12659/MSM.910105.

Xu, S. *et al.* (2018) 'A comprehensive review of circRNA: from purification and identification to disease marker potential', *PeerJ*. PeerJ Inc., 6, p. e5503. doi: 10.7717/peerj.5503.

Xu, T. *et al.* (2017) 'Circular RNA expression profiles and features in human tissues: a study using RNA-seq data', *BMC Genomics*. BioMed Central Ltd., 18(S6), p. 680. doi: 10.1186/s12864-017-4029-3.

Yang, L. *et al.* (2019) 'Circular RNA circCHFR Facilitates the Proliferation and Migration of Vascular Smooth Muscle via miR-370/FOXO1/Cyclin D1 Pathway', *Molecular Therapy - Nucleic Acids*. Cell Press, 16, pp. 434–441. doi: 10.1016/j.omtn.2019.02.028.

Yang, M. and Vousden, K. H. (2016) 'Serine and one-carbon metabolism in cancer', *Nature Reviews Cancer*. Nature Publishing Group, 16(10), pp. 650–662. doi: 10.1038/nrc.2016.81.

Yang, Q. *et al.* (2017) 'A circular RNA promotes tumorigenesis by inducing c-myc nuclear translocation', *Cell Death and Differentiation*. Nature Publishing Group, 24(9), pp. 1609–1620. doi: 10.1038/cdd.2017.86.

Yang, Y. *et al.* (2018) 'Novel Role of FBXW7 Circular RNA in Repressing Glioma Tumorigenesis', *JNCI: Journal of the National Cancer Institute*, 110(3), pp. 304–315. doi: 10.1093/jnci/djx166.

Yang, Y. *et al.* (2017) 'Extensive translation of circular RNAs driven by N 6 - methyladenosine', *Cell Research*. Nature Publishing Group, 27(5), pp. 626–641. doi: 10.1038/cr.2017.31.

Ye, J. *et al.* (2010) 'The GCN2-ATF4 pathway is critical for tumour cell survival and proliferation in response to nutrient deprivation', *The EMBO Journal*, 29(12), pp. 2082–2096. doi: 10.1038/emboj.2010.81.

Yoon Soon Shin *et al.* (1976) 'Subcellular localization of γ-glutamyl carboxypeptidase and of folates', *Biochimica et Biophysica Acta (BBA) - General Subjects*. Elsevier, 444(3), pp. 794–801. doi: 10.1016/0304-4165(76)90326-3.

You, X. *et al.* (2015) 'Neural circular RNAs are derived from synaptic genes and regulated by development and plasticity', *Nature Neuroscience*. Nature Publishing Group, 18(4), pp. 603–610. doi: 10.1038/nn.3975.

Yu, C. Y. and Kuo, H. C. (2019) 'The emerging roles and functions of circular RNAs and their generation', *Journal of Biomedical Science*. BioMed Central Ltd., pp. 1–12. doi: 10.1186/s12929-019-0523-z.

Zeng, P. *et al.* (2019) 'HER2 Upregulates ATF4 to Promote Cell Migration via Activation of ZEB1 and Downregulation of E-Cadherin', *International Journal of Molecular Sciences*. MDPI AG, 20(9), p. 2223. doi: 10.3390/ijms20092223.

Zeng, Y. *et al.* (2017) 'A Circular RNA Binds To and Activates AKT Phosphorylation and Nuclear Localization Reducing Apoptosis and Enhancing Cardiac Repair.', *Theranostics*. Ivyspring International Publisher, 7(16), pp. 3842–3855. doi: 10.7150/thno.19764.

Zhang, X. O. *et al.* (2014) 'Complementary sequence-mediated exon circularization', *Cell*. Cell Press, 159(1), pp. 134–147. doi: 10.1016/j.cell.2014.09.001.

Zhang, Y. *et al.* (2013) 'Circular Intronic Long Noncoding RNAs', *Molecular Cell*. Cell Press, 51(6), pp. 792–806. doi: 10.1016/J.MOLCEL.2013.08.017.

Zhao, E. *et al.* (2016) 'KDM4C and ATF4 Cooperate in Transcriptional Control of Amino Acid Metabolism', *Cell Reports*, 14(3), pp. 506–519. doi: 10.1016/j.celrep.2015.12.053.

Zhao, X. *et al.* (2019) 'Circular RNA circEZH2 suppresses transmissible gastroenteritis coronavirus-induced opening of mitochondrial permeability transition pore via targeting miR-22 in IPEC-j2', *International Journal of Biological Sciences*. Ivyspring International Publisher, 15(10), pp. 2051–2064. doi: 10.7150/ijbs.36532.

Zwacka, R. M. *et al.* (1994) 'The glomerulosclerosis gene Mpv17 encodes a peroxisomal protein producing reactive oxygen species.', *The EMBO journal*, 13(21), pp. 5129–34. Available at: http://www.ncbi.nlm.nih.gov/pubmed/7957077 (Accessed: 27 May 2019).

ANNEX

MPV17 does not control cancer cell proliferation. PLOS One. 2020.

PLOS ONE

RESEARCH ARTICLE

MPV17 does not control cancer cell proliferation

Morgane Canonne[1], Anaïs Wanet[1], Thuy Truong An Nguyen[1], Alexis Khelfi[1], Sophie Ayama-Canden[1], Martine Van Steenbrugge[1], Antoine Fattaccioli[1], Etienne Sokal[2], Mustapha Najimi[2], Thierry Arnould[1], Patricia Renard[1]*

1 Laboratory of Biochemistry and Cell Biology (URBC), NAmur Research Institute for LIfe Sciences (NARILIS), University of Namur (UNamur), Namur, Belgium, **2** Laboratory of Pediatric Hepatology and Cell Therapy, Institut de Recherche Expérimentale et Clinique (IREC), Université Catholique de Louvain, Brussels, Belgium

* patricia.renard@unamur.be

Check for updates

OPEN ACCESS

Citation: Canonne M, Wanet A, Nguyen TTA, Khelfi A, Ayama-Canden S, Van Steenbrugge M, et al. (2020) MPV17 does not control cancer cell proliferation. PLoS ONE 15(3): e0229834. https://doi.org/10.1371/journal.pone.0229834

Editor: Negin P. Martin, National Institute of Environmental Health Sciences (NIEHS), UNITED STATES

Received: August 1, 2019

Accepted: February 14, 2020

Published: March 10, 2020

Copyright: © 2020 Canonne et al. This is an open access article distributed under the terms of the Creative Commons Attribution License, which permits unrestricted use, distribution, and reproduction in any medium, provided the original author and source are credited.

Data Availability Statement: All RNA sequencing files are available from the Annotare 2.0 database (accession number E-MTAB-8108, https://www.ebi.ac.uk/fg/annotare/).

Funding: The author(s) received no specific funding for this work.

Competing interests: The authors have declared that no competing interests exist.

Abstract

MPV17 is described as a mitochondrial inner membrane channel. Although its function remains elusive, mutations in the *MPV17* gene result in hepato-cerebral mitochondrial DNA depletion syndrome in humans. In this study, we show that *MPV17* silencing does not induce depletion in mitochondrial DNA content in cancer cells. We also show that MPV17 does not control cancer cell proliferation despite the fact that we initially observed a reduced proliferation rate in five MPV17-silenced cancer cell lines with two different shRNAs. However, shRNA-mediated *MPV17* knockdown performed in this work provided misguiding results regarding the resulting proliferation phenotype and only a rescue experiment was able to shed definitive light on the implication of MPV17 in cancer cell proliferation. Our results therefore emphasize the caution that is required when scientific conclusions are drawn from a work based on lentiviral vector-based gene silencing and clearly demonstrate the need to systematically perform a rescue experiment in order to ascertain the specific nature of the experimental results.

Introduction

MPV17 is a functionally elusive protein localized in the inner membrane of mitochondrion and for which the encoding gene is located on chromosome 2p23-21 [1] [2] [3] [4]. MPV17 loss-of-function causes a rare autosomal recessive mitochondrial disorder called Mitochondrial DNA Depletion Syndrome (MDDS) marked by a highly reduced mitochondrial DNA (mtDNA) copy number in affected tissues.

To date, there are 100 known individuals affected by one of the 48 described *MPV17* pathogenic variants (approximately half of which are missense) [5]. The vast majority of these patients (96%) suffer from the hepato-cerebral form of MDDS and exhibit a severe mtDNA depletion in the liver (60–99% reduction). This is correlated with a decreased activity of respiratory chain complexes. The onset of the disease takes place early in life (neonatal period/infancy) and condemn the affected individual to a premature death due to liver dysfunction progressing into liver failure. The remaining 4% of the patients suffer from a late-onset encephalomyopathic disease with mild or no liver involvement [5].

Although the current knowledge about MPV17 and its homologs have been recently reviewed [6], the function of MPV17 is still obscure. There are evidence supporting that MPV17 might be a channel with stress-dependent gating properties [7] [8] involved in nucleotides homeostasis [9] [3] [10] [11] [12].

In a previous work, we found an increased expression of *MPV17* during stem cells hepatogenic differentiation while performing a transcriptomic analysis in order to characterize the mitochondrial biogenesis in this process ([13], data deposited in NCBI's Gene Expression Omnibus through GEO Series accession number GSE75184). Unexpectedly, we observed that while *MPV17* silencing had no impact on hepatogenic differentiation, it significantly reduced the proliferation of expanding Bone Marrow Mesenchymal Stem Cells (MSC) and Umbilical Cord-MSC from different donors, suggesting a role of MPV17 in cell proliferation (unpublished data). This is in accordance with the work of Choi and colleagues who showed that *MPV17* knockdown reduces the proliferation of NSC34 cells, a mouse motor neuronal cell line [14]. As MPV17 has been implicated in stress response [15] [16] and has been described as a channel with stress-dependent gating properties (oxidative and pH stress,. . .) [7], we then wondered whether MPV17 could have a role in the proliferation of cancer cells or not, as they inherently experience oxidative and metabolic stress.

In order to explore the putative role of MPV17 in the control of cancer cell proliferation, we used a loss-of-function approach. Gene silencing and/or overexpression is generally the first approach in order to investigate gene expression/function and lentiviruses are now widely used to deliver transgenes that integrate into the host genome for gene expression tampering. In this study, while demonstrating that MPV17 does not control neither cell proliferation nor mtDNA content in cancer cells, our experimental results illustrate and emphasize the importance of carrying out a rescue experiment when working with shRNA-mediated knockdown.

Results

MPV17 is overexpressed in several tumours

Taking advantage of The Genome Cancer Atlas (TGCA) database, we show that the abundance of *MPV17* transcript is significantly higher in tumours of 10 different tissues, including liver, bile duct, and colon (Fig 1A). This is confirmed at the protein level by immunohistochemistry staining performed on liver tumour biopsies from patients with adenocarcinoma (Fig 1B).

MPV17 silencing is robustly associated with a decreased proliferation rate in different cancer cell lines

In this study, we first assessed the effects of three commercially available shRNAs targeting *MPV17* mRNA: sh129921, sh127649 and sh131038. Using western blot analysis, the efficiency of gene silencing was evaluated by assessing the abundance of MPV17 in Huh7 cells transduced with these three shRNA-encoding lentiviral vectors. Both sh129921 and sh127649 led to an efficient knockdown of the gene while sh131038 did not efficiently induce *MPV17* silencing (Fig 2A).

We then demonstrated that Huh7 cells silenced for *MPV17* with sh129921 and sh127649 displayed a severely decreased proliferation rate, as quantified by three different proliferation assays, namely the doubling time (Fig 2B), the MTT assay (Fig 2C), and the total protein content (Fig 2D). The reduced cell proliferation phenotype was correlated with *MPV17* knockdown efficiency as no decreased proliferation rate was observed in Huh7 cells

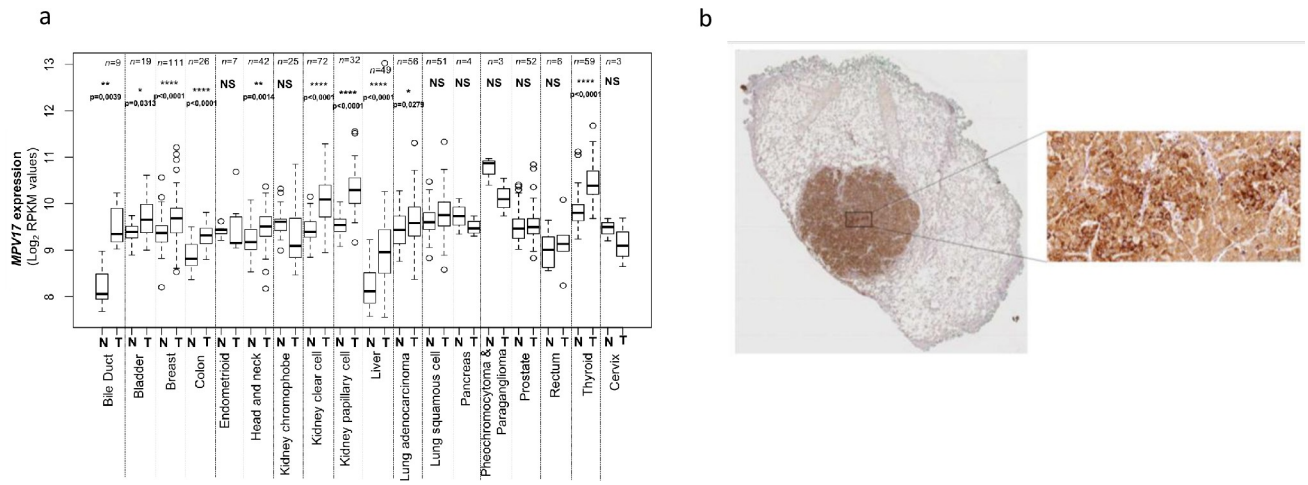

Fig 1. Analysis of MPV17 expression in cancer tissues. The Cancer Genome Atlas (TCGA), a public platform allowing the analysis of gene expression data sets generated by RNA sequencing (http://cancergenome.nih.gov), has been used to determine the expression level of *MPV17* in various tumour tissues (T) *versus* healthy tissues (N). P values were calculated with the two-tailed Wilcoxon signed rank Test ($\alpha = 5\%$; *: $p<0.05$; **: $p<0.01$; ***: $p<0.001$; ****: $p<0.0001$; NS: not significant) (a). Detection of MPV17 by immunohistochemistry in a paraffin-embedded biopsy of a liver adenocarcinoma. A strong signal for MPV17 is associated with the tumour, while the abundance of the protein is low in adjacent normal tissue (b).

https://doi.org/10.1371/journal.pone.0229834.g001

transduced with the vector encoding sh131038, the only shRNA that turned out to be inefficient in the knockdown induction.

To discard the possibility of a putative cell type or cancer type-specific phenotype, we next assessed the impact of sh129921 on the proliferation of two other human hepatoma cell lines, Hep3B and HepG2 cells, and two non-liver cancer cell lines, A549 cells, derived from a human pulmonary adenocarcinoma and SQD9 cells, a human squamous cell carcinoma cell line. Interestingly, Hep3B (Fig 2E), A549 (Fig 2F), SQD9 (Fig 2G) and HepG2 (data not shown) cells transduced with sh129921-encoding vector also displayed a reduced proliferation phenotype.

MPV17 silencing is not associated with mtDNA copy number depletion

As MPV17 deficiency is associated with MDDS, we assessed whether *MPV17* silencing was accompanied by depletion in the mtDNA content or not, possibly accounting for the associated decreased proliferation rate. However, *MPV17* silencing did not lead to a reduction of mtDNA content in any of the tested cancer cell lines (Fig 3). This result is in agreement with the work of Dalla Rosa and collaborators who showed that proliferating fibroblasts from *MPV17*-deficient patients do not display any reduced mtDNA content [9]. It is also in accordance with the recent work of Alonzo and collaborators who did not find any reduction of mtDNA content in *MPV17*-silenced HeLa cells [12].

The decreased proliferation rate in *MPV17*-silenced cells is associated with a decrease in the abundance of ATF4

In order to determine the molecular mechanisms underlying the decreased proliferation rate in *MPV17*-silenced cancer cells, a transcriptomic analysis was performed. The RNA sequencing analysis was performed on Huh7 cells transduced with sh129921 or shNT-encoding vectors. Among the differentially expressed genes, we focused on transcriptional regulators potentially responsible for a reduced proliferation capacity. The activating transcription factor 4 (ATF4) frequently upregulated in cancer cells [17], was

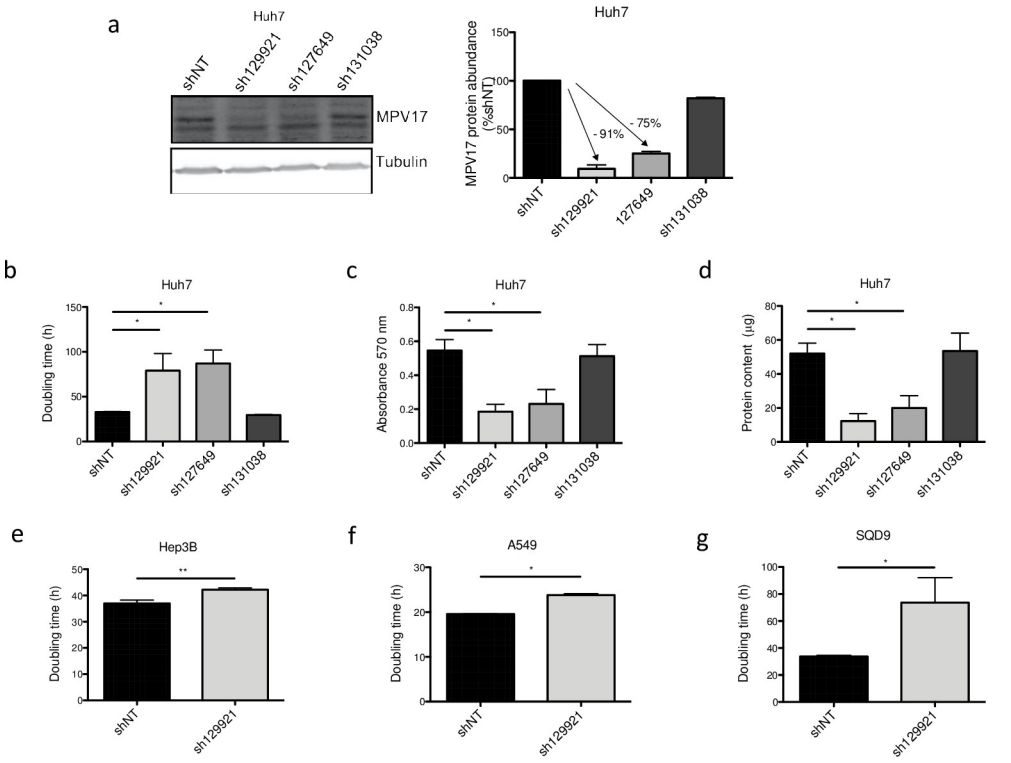

Fig 2. Effect of shRNA-mediated *MPV17* knockdown on the proliferation of cancer cell lines. Huh7 cells were transduced with non-target shRNA lentiviral vectors (shNT) or with shRNA lentiviral vectors targeting *MPV17* expression (sh129921, sh127649, sh131038). Hep3B, A549 and SQD9 cells were transduced with lentiviral shNT-encoding vectors or with sh129921-containing vectors. Cells were selected for 6 days with puromycin (2.5 µg/mL). Cells were seeded at 8×10^3 cells/cm^2 (a, b, c, d, Huh7; g, SQD9), 5×10^3 cells/cm^2 (e, Hep3B) and 2.7×10^3 cells/cm^2 (f, A549) and grown for 4 days. MPV17 protein abundance was assessed by western blot analysis (a, Huh7). A representative western blot of 3 independent biological replicates (2 for sh131038) is shown (left) along with the western blot quantification of all the biological replicates (quantification with Image J software, data expressed as relative protein abundance to cells transduced with shNT-encoding vectors, right). Proliferation was then assessed by manual counting to calculate the doubling time (b, Huh7; e, Hep3B; f, A549; g, SQD9), by MTT assay (c, Huh7) and by the total protein content (d, Huh7). Data are presented as mean ± S.E.M of 3 independent biological replicates (2 for sh131038). P values were calculated with the one-tailed Mann-Whitney Test ($\alpha = 5\%$; *: $p<0.05$; **: $p<0.01$; ***: $p<0.001$). Full blots are presented in S6 Fig.

https://doi.org/10.1371/journal.pone.0229834.g002

downregulated in *MPV17*-silenced cells (Z-score = -2,792; *P* = 1,38E-14). It has been shown that ATF4 not only up-regulates the expression of genes encoding actors implicated in amino acid import and metabolism [18] [19] [20] but also promotes, indirectly, purine synthesis [21], two essential aspects for cell proliferation. Based on this knowledge, ATF4 was an attractive candidate in the attempt to elucidate the molecular mechanisms underlying the reduced cell proliferation. The reduction of *ATF4* transcript abundance was confirmed at the protein level in sh129921 and sh127649-encoding vector transduced Huh7 cells (Fig 4A) as well as in sh129921-encoding vector transduced Hep3B (Fig 4B) and A549 (Fig 4C) cells, when compared with control cells transduced with shNT-containing vector.

Altogether, these results seem to strongly support an involvement of MPV17 in cancer cell proliferation as *MPV17* silencing was consistently accompanied by a reduction of both cell proliferation rate and ATF4 protein abundance.

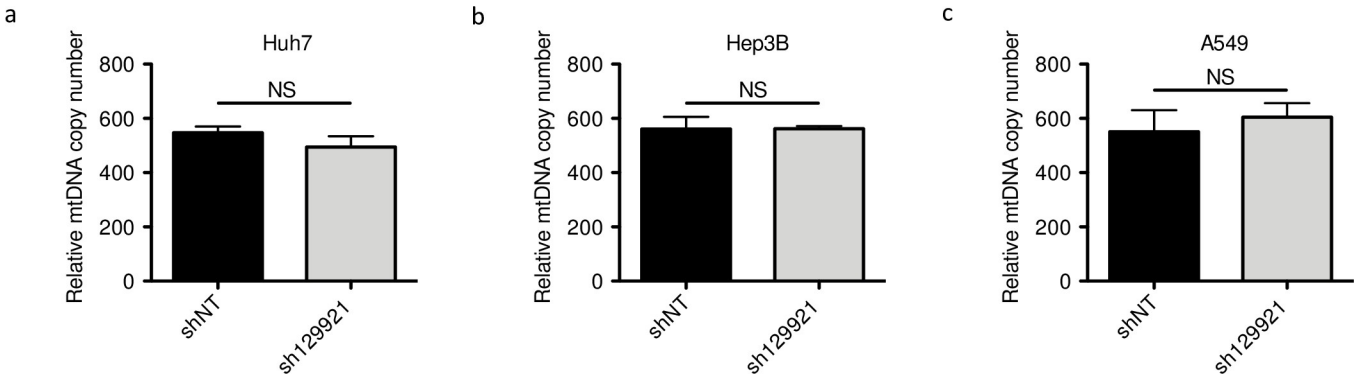

Fig 3. Assessment of mtDNA content in *MPV17*-silenced cancer cell lines. Huh7 (a), Hep3B (b) and A549 (c) cells were transduced with non-target shRNA lentiviral vectors (shNT) or with sh129921-containing vectors. Transduced cells were selected for 6 days with puromycin (2.5 μg/mL). DNA was then extracted and mtDNA content was assessed by qPCR using NADH dehydrogenase 2 as a specific marker of mtDNA content and beclin for normalization with nuclear DNA. Results are presented as means ± S.E.M of 3 independent biological replicates and are expressed in relative copy number to the nuclear DNA. P values were calculated with the one-tailed Mann-Whitney Test (α = 5%; NS; *: p<0.05; **: p<0.01; ***: p<0.001).

https://doi.org/10.1371/journal.pone.0229834.g003

MPV17 silencing is not always associated with a reduced proliferation phenotype

Pursuing our analysis further, we observed that the sh129921-encoding vector transduced Huh7 cells were able to adapt along the passages and progressively restored the proliferation rate (Fig 5A), although MPV17 protein abundance was still strongly reduced (Fig 5B).

As we observed a recovery of the decreased proliferation rate over time, we therefore aimed at generating an IPTG-inducible sh129921 model in Huh7 cells. Strikingly, while we observed a strong *MPV17* knockdown in this inducible expression model, with a silencing efficiency

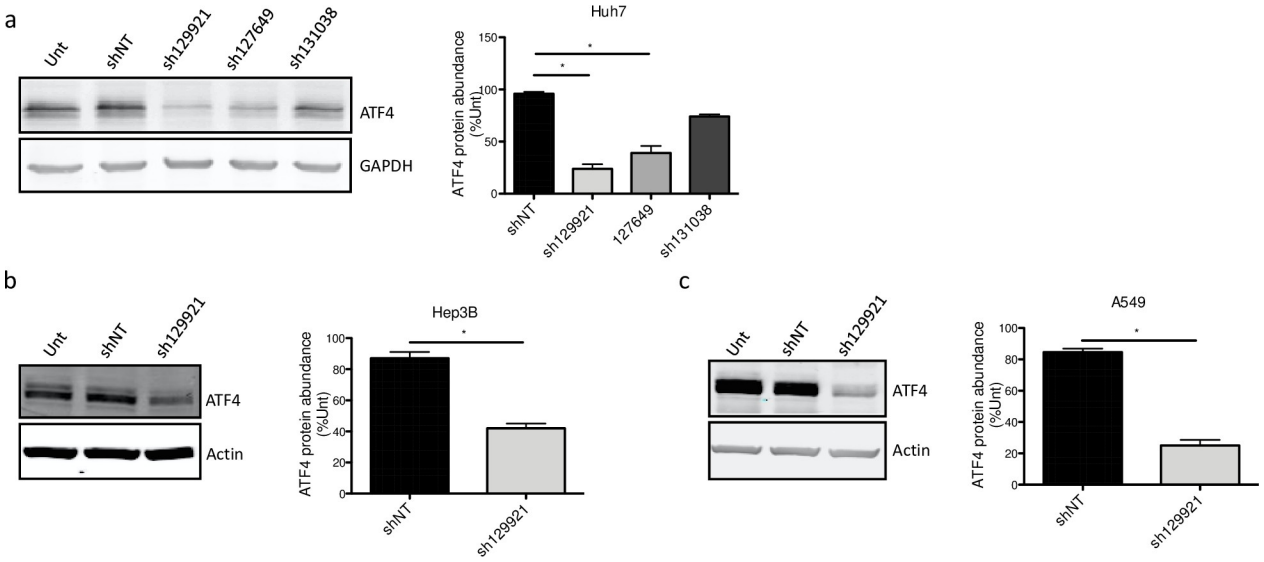

Fig 4. ATF4 protein abundance following *MPV17* knockdown in Huh7, Hep3B and A549 cells. Huh7 cells (a) were transduced with non-target shRNA lentiviral vectors (shNT) or with shRNA lentiviral vectors targeting *MPV17* expression (sh129921, sh127649, sh131038). Hep3B (b) and A549 (c) cells were transduced with lentiviral shNT-encoding vectors or with sh129921-containing vectors. Cells were selected for 6 days with puromycin (2.5 μg/mL) before assessing ATF4 protein abundance by western blot analysis. For each cell line, a representative western blot of 3 (2 for sh131038) independent biological replicates is shown (left) along with the western blot quantification of all the biological replicates (quantification with Image J software, data expressed as relative protein abundance to untranduced (unt) cells, right). P values were calculated with the one-tailed Mann-Whitney Test (α = 5%; *: p<0.05; **: p<0.01; ***: p<0.001). Full blots are presented in S6 Fig.

https://doi.org/10.1371/journal.pone.0229834.g004

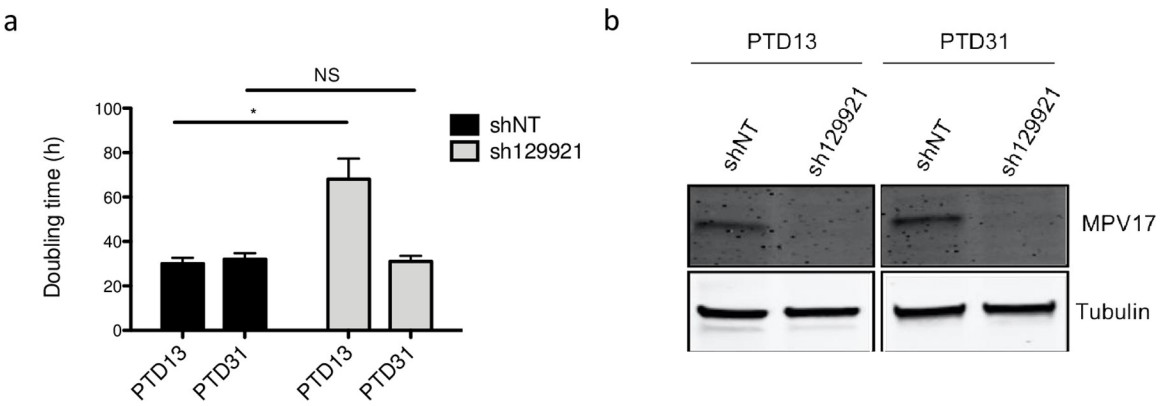

Fig 5. Evolution of Huh7 proliferation rate and MPV17 protein abundance in sh129921-mediated *MPV17* knockdown. Huh7 cells were transduced with non-target shRNA lentiviral vectors (shNT) or with sh129921-containing vectors. Transduced cells were selected for 6 days with puromycin (2.5 μg/mL). At 13 and 31 days after the transduction (PTD: post-transduction day), cells were seeded at 8×10^3 cells/cm^2 and grown for 4 days. Proliferation was then assessed by manual counting to calculate the doubling time (a) and MPV17 protein abundance was analysed by western blot (b). P values were calculated with the one-tailed Mann-Whitney Test (α = 5%; NS; *: $p<0.05$; **: $p<0.01$; ***: $p<0.001$). n = 3. Full blots are presented in S6 Fig.

https://doi.org/10.1371/journal.pone.0229834.g005

comparable to the one observed in the constitutive silencing model (Fig 6A and 6B), the cell proliferation rate was unchanged (Fig 6D). Moreover, ATF4 did not display a decreased protein abundance (Fig 6C).

This absence of effect of *MPV17* silencing on the cell proliferation rate in the inducible expression system could have different origins. First, the IPTG molecule itself could have an unexpected effect on Huh7 cells proliferation, even though IPTG is not known to be metabolized [22]. Second, the reduced proliferation phenotype in the inducible expression system might need more time to settle down. Indeed, in the constitutive system, *MPV17* is silenced for a total of 9 days before assessing the cell proliferation, as opposed to only 5 days in the inducible model (see "Materials and Methods", S1 Fig). A third difference between the two approaches is that in order to ensure a proper knockdown of *MPV17* in the inducible model, the culture medium was changed every day in order to renew the IPTG, as opposed to every two or three days in the constitutive silencing model. One could thus hypothesize that this daily medium renewal could prevent the settling of the reduced proliferation phenotype by discontinuing the putative intercellular communication. These three hypotheses were tested but failed to explain the different phenotypical outcomes observed for the constitutive or inducible expression models (see S2 and S3 Figs).

These considerations led us to evaluate on Huh7 cells the effect of two additional commercially available shRNAs, sh128669 and sh131201, targeting different regions of the *MPV17* transcript (see S4 Fig). Both shRNAs strongly reduce the abundance of MPV17 protein (Fig 7A) but no significant effect on the proliferation rate was observed (Fig 7C, 7D and 7E). Also, the abundance of ATF4 was not affected by *MPV17* knockdown mediated by either sh128669 or sh131201 (Fig 7B). Thus, ATF4 reduced abundance correlates with the proliferation rate but the putative link between the reduced proliferation phenotype (and therefore ATF4) and MPV17 remains to be established.

In conclusion, we found that sh129921, sh127649, sh128669 and sh131201 all led to a strong *MPV17* knockdown while the resulting proliferation rates were highly variable. This lack of consistency led us to suspect a putative involvement of *MPV17* isoforms that would be differentially affected according to the shRNA used.

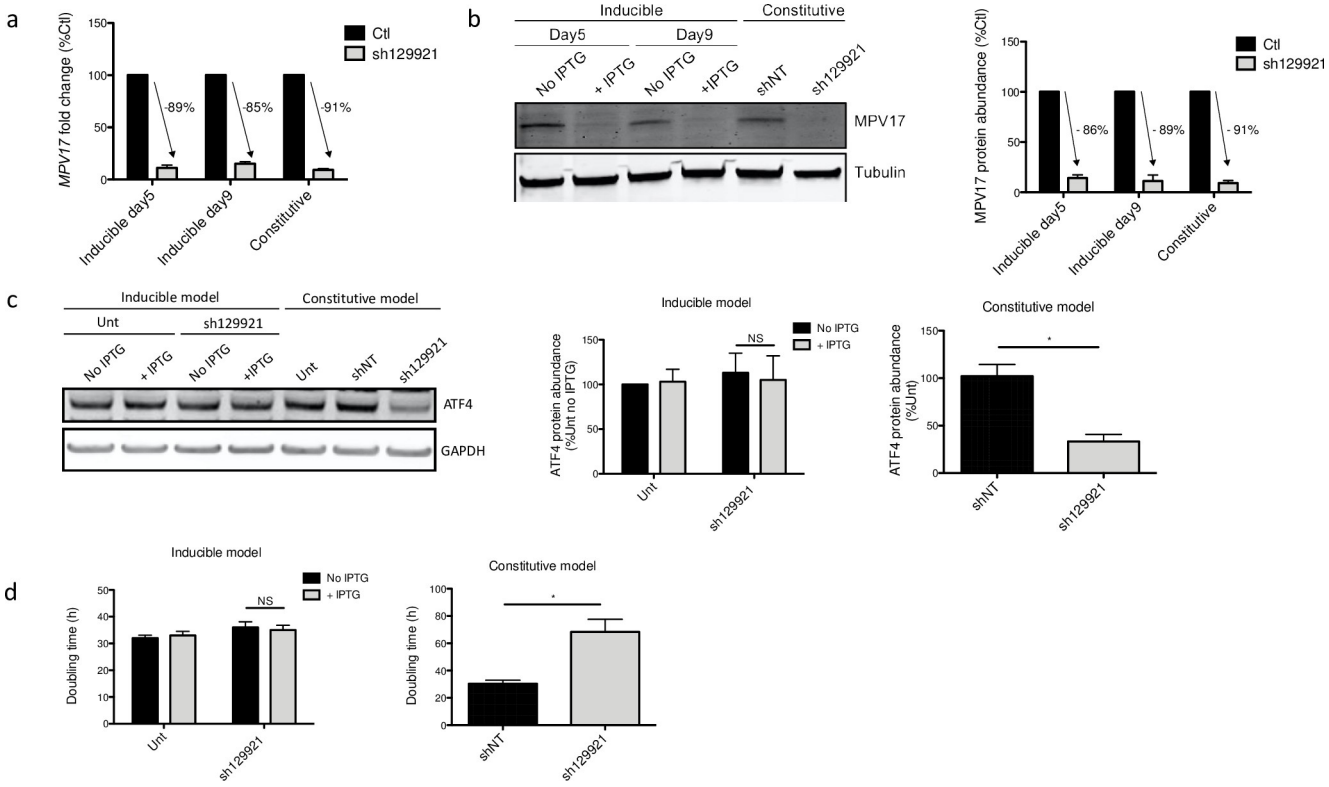

Fig 6. MPV17 and ATF4 abundances and Huh7 cells proliferation rate following inducible sh129921-mediated *MPV17* knockdown. Huh7 cells were transduced, or not (Unt), with inducible sh129921 lentiviral vector. Transduced cells were selected for 6 days with puromycin (2.5 μg/mL). Cells were then incubated for 5 days in the presence of 0.1 mM of IPTG to induce *MPV17* silencing. Cells were seeded at 8×10^3 cells/cm^2 and grown for 4 days in daily renewed medium containing IPTG. RNA was extracted and RT-qPCR was performed to assess *MPV17* transcript level (data expressed relatively to respective control (Ctl), n = 3) (a). MPV17 (b) and ATF4 (c) protein abundances were also assessed by western blot analysis after 5 days (MPV17) and 9 days (MPV17; ATF4) of IPTG induction. For each protein, a representative western blot of 3 independent biological replicates is shown (left) along with the western blot quantification of all the biological replicates (quantification with Image J software, data expressed as relative protein abundance to respective controls (Ctl) for MPV17 and untransduced (unt) cells for ATF4, right). Proliferation was then assessed by manual counting to calculate the doubling time (d). As a comparison, we performed at the same time and on the same cells a similar experiment with the constitutive expression of sh129921 (mediating *MPV17* knockdown) as described in S1 Fig. P values were calculated with the one-tailed Mann-Whitney Test (α = 5%; *: p<0.05; **: p<0.01; ***: p<0.001). Full blots are presented in S6 Fig. n = 3.

https://doi.org/10.1371/journal.pone.0229834.g006

Therefore, we next interrogated the Genotype-Tissue Expression (GTEx) Consortium (2008, NIH) portal, that inventories the impact of genetic variations on gene expression within major tissues in the human body from *post mortem* donors. The GTEx Portal proposes 22 *MPV17* isoforms, including two major ones i.e. a short predominant isoform and a long one (see S5 Fig). This long isoform referenced in RefSeq as NM002437.5 encodes the MPV17 protein that we detected on western blot while the translation of all the other *MPV17* isoforms is not experimentally demonstrated. However, among the 22 isoforms, we observe that all the transcripts targeted by sh129921 (1, 2, 3, 12, 13, 14, 15, 16 and 18) are also targeted by either sh128669 (15, 16) or sh131201 (1, 18) or both (2, 3, 12, 13, 14). The same kind of observation stands for the transcripts targeted by sh127649 (1, 2, 3, 5, 12, 13, 14, 15, 16, 18, 19, 21), providing no clear explanation about the opposite proliferation phenotypes observed for each pair of shRNAs (sh129921/sh127649 versus sh128669/131201) (see S5 Fig).

Altogether, the absence of effect of the inducible sh129921 on the cell proliferation rate, combined with the observation that, at least, two different shRNAs targeting *MPV17* (sh131201 and sh128669) have no effect on the proliferation of Huh7 cells, despite a strong

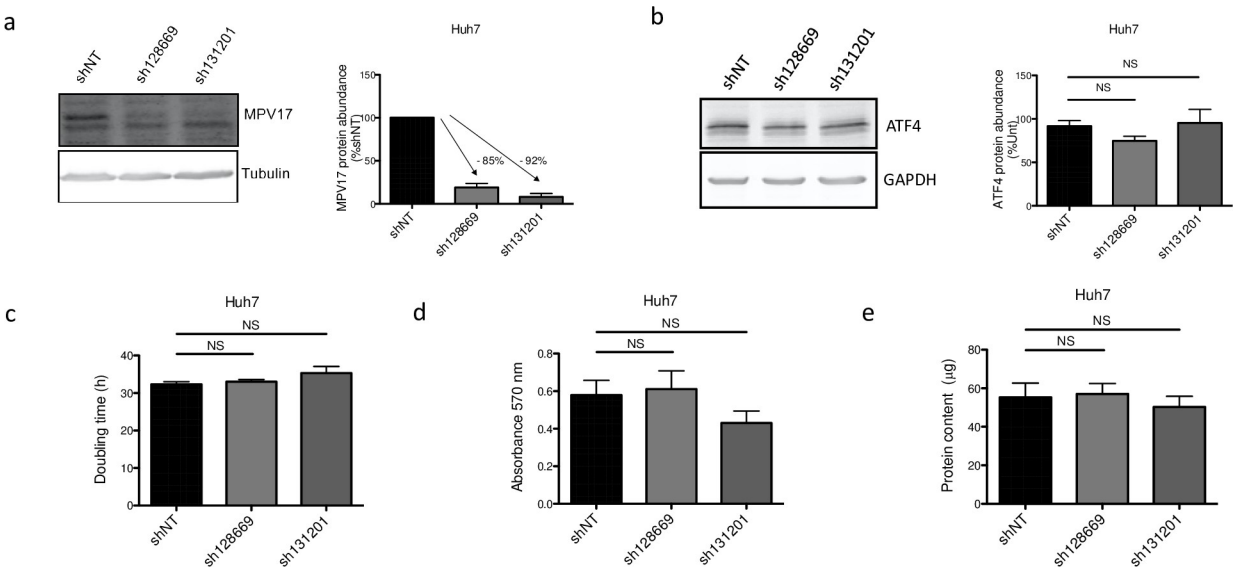

Fig 7. Effect of *MPV17*-targeting sh128669 and sh131201 on Huh7 cells proliferation, MPV17 and ATF4 protein abundances. Cells were transduced with non-target shRNA lentiviral vectors (shNT) or with shRNA lentiviral vectors targeting *MPV17* expression (sh128669 and sh131201). Transduced cells were selected for 6 days with puromycin (2.5 μg/mL). Cells were seeded at 8×10^3 cells/cm^2 and grown for 4 days. The abundance of MPV17 (a) and ATF4 (b) proteins was assessed by western blot analysis. For each protein, a representative western blot analysis of 3 independent biological replicates is shown (left) along with the western blots quantification of all the biological replicates (quantification with Image J software, data expressed as relative protein abundance to cells transduced with shNT-encoding vectors (a, MPV17) or untranduced (unt) cells (b, ATF4), right). Proliferation was then assessed by manual counting to calculate the doubling time (c), by MTT assay (d) and by the total protein content (e) and data are presented as mean ± S.E.M (3 biological replicates). P values were calculated with the one-tailed Mann-Whitney Test ($\alpha = 5\%$; NS; *: $p<0.05$; **: $p<0.01$; ***: $p<0.001$). Full blots are presented in S6 Fig.

https://doi.org/10.1371/journal.pone.0229834.g007

decrease in the MPV17 protein abundance, suggest that the decreased proliferation rate of transduced cells observed for two shRNAs (sh129921 and sh127649) is not related to a reduced MPV17 protein abundance. In an attempt to shed light on this question, we eventually performed a rescue experiment.

Rescuing MPV17 does not restore the proliferation phenotype. As Huh7 cells could neither be efficiently transfected nor transduced with the *MPV17*-expressing vector, HepG2 cells were used for the rescue attempt. Indeed, as mentioned before, we also observed the reduced proliferation rate in this hepatoma cell line silenced for *MPV17*. This cell line turned out to be the most receptive to the lentiviral *MPV17*-expressing vector. Since a rescue experiment consists in re-introducing the shRNA-mediated silenced mRNA, it requires the use of a shRNA targeting the 3′UTR of the targeted mRNA. Thus, the reintroduced transcript that lacks 3′UTR is not affected by the shRNA.

We decided to perform MPV17 overexpression before inducing the constitutive knockdown mediated by sh129921. The justification of this chronology resides in the observation that, on the contrary to shNT-encoding vector transduced cells, sh129921-encoding vector transduced cells were not able to stand a second round of transduction due to cell death. This suggests that *MPV17*-silenced cells are distressed, in accordance with their decreased proliferation rate. This aspect is therefore not compatible with a short-term assessment of cell proliferation.

MPV17 knockdown was properly induced in the overexpression control. Indeed, cells double transduced with pLenti GFP, as a control, and then with pLKO.1 sh129921, displayed a strong reduction of MPV17 abundance accompanied by the decreased proliferation rate (Fig 8A, 8B and 8C). As expected, the reduced proliferation phenotype was absent in pLenti GFP

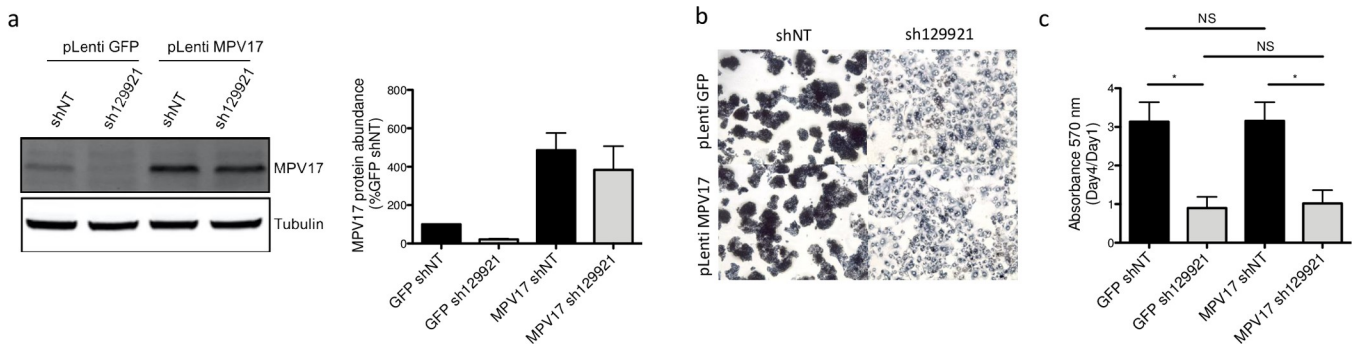

Fig 8. Effect of MPV17 rescue on the proliferation of *MPV17*-silenced HepG2 cells. Cells were first transduced with pLenti GFP or pLenti MPV17 and selected for 6 days with puromycin (2.5 μg/mL). Cells were then transduced with shNT or sh129921-encoding lentiviral vectors and let to recover for 5 days to allow *MPV17* silencing. Cells were then seeded at 1.5×10^4 cells/cm^2 and grown for 4 days before assessing MPV17 protein abundance (a). A representative western blot analysis of 3 independent biological replicates is shown (left) along with the western blots quantification of all the biological replicates (quantification with Image J software, data expressed as relative protein abundance to cells transduced with shNT and GFP-encoding vectors, right). Cell proliferation assessment by MTT assay was also performed at day 1 and day 4. The ratio day 4/day 1 is then calculated in order to correct any putative seeding differences that could mask or mislead to a partial phenotype rescue (c). Micrographies were taken at the phase contrast microscope before adding the lysis buffer for the MTT assay (b). Data are presented as mean ± S.E.M (3 biological replicates). P values were calculated with the one-tailed Mann-Whitney Test (α = 5%; NS; *: $p<0.05$; **: $p<0.01$; ***: $p<0.001$). Full blots are presented in S6 Fig.

https://doi.org/10.1371/journal.pone.0229834.g008

and pLKO.1 shNT double-transduced cells (Fig 8B and 8C). Cells double-transduced with pLenti MPV17 and pLKO.1 shNT suitably overexpressed MPV17 (Fig 8A). It is interesting to emphasize the fact that MPV17 overexpression, on its own, has no significant effect on cell proliferation (Fig 8B and 8C). This observation can be reconciled with the idea that MPV17 is described as a channel. Thus, the qualitative state of MPV17 (open/closed) would be more relevant than its quantitative state. Finally, cells double-transduced with pLenti MPV17 and pLKO.1 sh129921 overexpressed MPV17 but lost the expression of the endogenous protein (Fig 8A). Remarkably, these cells exhibited the reduced proliferation phenotype (Fig 8B and 8C).

Discussion

In this work we studied the putative role of MPV17 in cancer cell proliferation. While *MPV17* silencing did not lead to depletion of mtDNA content in the tested cancer cell lines, in accordance with literature [9] [12], the resulting proliferation phenotypes associated with *MPV17* shRNA-mediated knockdown were unsettling and inconclusive, leading us to perform a rescue experiment that eventually excluded a role of MPV17 in cancer cell proliferation. The intriguing and somewhat misleading results we obtained during this investigation clearly demonstrate the need to systematically perform a rescue experiment in order to ascertain the specific nature of the experimental results.

In this work, we tested five shRNAs targeting *MPV17*. The highly variable phenotypical outcomes in Huh7 cells led us to consider a putative contribution of *MPV17* transcript isoforms or the possible existence of an off-target effect. Despite the fact that we did not find any correlation between the shRNA-targeted *MPV17* transcript isoforms and the proliferation phenotype, it is not sufficient to preclude this hypothesis as there is no guaranty that the *MPV17* transcript isoforms spectrum described in GTEx portal in human healthy liver is conserved in our model.

It is also interesting to note that the predictive alignment (BLAST, ncbi) of sh129921 and sh127649 on the human transcripts did not highlight the putative existence of a shared off-target mRNA. Again, this observation is however not sufficient to exclude a putative off-target effect as it could be taking place through separate effectors for each shRNA.

However, the most intriguing observation in this work was that the same shRNA, expressed either constitutively or induced by IPTG, resulted in different effects on cell proliferation. The emergence of the inducible lentiviral vectors, which enable a reversible and fine tuning of gene knockdown, allows further characterization of gene function, a better ease in studying genes for which knockdown ends up being too deleterious or lethal for the cell, as well as timeframe selection in a developmental process [23]. In this study, we resorted to this tool to overcome an apparent progressive compensation/adjustment of the cells following *MPV17* knockdown. The transient nature of the inducible knockdown would theoretically prevent this compensation to settle. However, we unexpectedly observed that the constitutive and inducible approaches led to different phenotypical outcomes, despite using the same shRNA sequence (sh129921). An explanation to this observation could reside in the fact that the shRNA is expressed at a higher level in the constitutive model. Indeed, it is recommended by Sigma Aldrich to ensure a minimum of 70% knockdown in a constitutive model, before switching to an inducible one. This recommendation reflects the risk of obtaining a less potent gene silencing with an inducible vector when compared to a constitutive one due to a lower shRNA expression. In our experimental conditions, the observation that MPV17 knockdown at the protein level was quite comparable in both expression models does not preclude a higher expression of the shRNA in the constitutive expression system, which could either increase the risk of off-targeting or favour a better targeting of some non coding *MPV17* transcript isoforms.

While most researchers are confident in their interpretation of a particular gene function when a consistent phenotype is observed with at least two different shRNA sequences targeting a transcript, we and others experienced that this is not sufficient and that a rescue experiment is an all-encompassing insurance of the veracity of the scientific conclusions [24]. However, as properly reported by Peretz and collaborators, "Rescue experiments are a good way to ensure specificity and are being added to an increasing number of studies, although, based on a survey of scientific literature, this is probably limited to less than 0.1% of studies" [24]. Our work stresses the imperative necessity to perform a rescue experiment in each study carrying out shRNA-mediated gene knockdown. Nevertheless, the benefit of a rescue experiment often matches its technical complexity. In terms of limitations while performing a rescue experiment, we can mention that the re-expression of the silenced gene, generally at a higher level than the normal endogenous one, might, in itself, lead to undesired effects [24]. In addition, the random integration of the vector can also lead to additional off-target effects. Although the rescue experiment should undeniably be an indispensable control in every experiment based on shRNA-induced knockdown, it is not totally dependable as the absence of rescue of a particular observed phenotype does not necessarily mean that the effect observed with the shRNA was due to off-target effects. Indeed, in ideal circumstances, every splice variant targeted by the shRNA should be restored in the rescue experiment, which might not always be realistic [24]. In this work, the reintroduction of the only known MPV17-coding transcript refuted any role of the protein in cancer cell proliferation.

In conclusion, our work demonstrates that MPV17 does not induce depletion of mtDNA content in cancer cell lines and that MPV17 does not control their cell cycle/proliferation. Importantly, in the future, rescue experiments should be a requirement in any study involving shRNA in order to silence a gene and analyse its subsequent effects on a particular phenotype. While the absence of rescue of the phenotype is not a strict indicator of aspecficity of the results, the restoration of the phenotype surely is a strong argument in favour of the specificity of any shRNA-induced phenotype of interest. Noteworhty, we believe that sh129921 requires further investigation as its robust effect on cell proliferation of different cancer cell lines could bring to light a promising actor that could be exploited in the fight against cancer.

Materials and methods

Cell culture

Cells were grown in Dulbecco′s Modified Eagle′s Medium (DMEM) low glucose (Life technologies, #31885) for human hepatoma cell lines Huh7 and HepG2 or in DMEM high glucose (Life technologies, #41965) for human renal embryonic cell line HEK293T, or in MEM GlutaMAX-1 (Life technologies, #42360) for human pulmonary adenocarcinoma cell line A549 and human squamous cell carcinoma cell line SQD9, or in Roswell Park Memorial Institute medium 1640 (Life technologies, #21875) for human hepatoma cell line Hep3B, supplemented with 10% foetal bovine serum (Life technologies, #10270) in a 5% CO_2 humid atmosphere at 37˚C. SQD9 cells were obtained from UCL (Vanessa Bol, Woluwe, Belgium). Huh7 cells (JCRB0403) were kindly provided by Prof. Sven Diederichs (DKFZ, Heidelberg, Germany). HepG2 (ATCC, HB-8065) were kindly provided by Prof. Luc Bertrand (UCL, Woluwe, Belgium). Hep3B were purchased from ATCC (HB-8064). A549 cells (ATCC, CCL-185) were kindly provided by Dr Jacques Piette (ULg, Liege, Belgium). HEK293T were obtained from ATCC (CRL-11268).

Lentivirus production

HEK293T were seeded at $4x10^6$ cells in 75 cm^2 culture flask (Corning, #430641U). The next day, the DNA mixture and the lipofectamine solution were prepared separately. The DNA mixture was composed of 0.4 μg of the envelope encoding vector pCMV-VSVG (Addgene, #8454), 3.6 μg of the packaging vector psPAX2 (Addgene, #12260) and 4 μg of the expressing plasmid (Table 1), in 240 μL of 5% opti-MEM (Invitrogen, #31985). The lipofectamine

Table 1. List of plasmids used for MPV17 silencing.

Vector	Reference
pLKO.1-puro sh131201	Sigma-Aldrich
	SHCLND-NM_002437
	TRCN0000131201
pLKO.1-puro sh128669	Sigma-Aldrich
	SHCLND-NM_002437
	TRCN0000128669
pLKO.1-puro sh127649	Sigma-Aldrich
	SHCLND-NM_002437
	TRCN0000127649
pLKO.1-puro sh129921	Sigma -Aldrich
	SHCLND-NM_002437
	TRCN0000129921
pLKO.1-puro sh131038	Sigma-Aldrich
	SHCLND-NM_002437
	TRCN0000131038
pLKO.1-puro shNT	Sigma-Aldrich
	SHC016-1EA
pLKO-puro-IPTG-3xLacO sh129921	Sigma-Aldrich
	09301606MN
	TRCN0000129921

The vectors backbone and encoding shRNA are specified along with their references.

https://doi.org/10.1371/journal.pone.0229834.t001

solution was composed of 16 μL of lipofectamine 2000 (Invitrogen, #11669) in 240 μL of 5% opti-MEM. Both preparations were incubated for 5 min at room temperature, combined, incubated for 30 min at room temperature and added in the flask. After 18 h, the medium was renewed and at 48 h and 72 h post-transfection, the medium was collected and filtered on 0.45 μm steriflip (Millipore, SE1M003M00). Lentiviruses were titrated by Reverse Transcription quantitative Polymerase Chain Reaction (RT-qPCR) according to manufacturer′s recommendations (Lentivirus qPCR Titer Kit, Applied Biological Materials, LV900).

MPV17 silencing

Sub-confluent cells were transduced in presence of 60 μg/mL protamine sulphate (Sigma-Aldrich, P4020). The next day, they were selected for 6 days with puromycin (Sigma-Aldrich, P8833) at 2.5 μg/mL. Experimental timelines of *MPV17* silencing with the constitutive and inducible vectors are detailed in S1 Fig. Briefly, for the constitutive silencing of *MPV17*, cells were transduced with different shRNA-encoding vectors (pLKO.1-puro shNT, sh127649, sh128669, sh129921, sh131201, sh131038), selected as described above and let to recover for 2 days without puromycin. They were then seeded and allowed to grow for 4 days before assessing the proliferation.

For the inducible silencing of *MPV17*, cells were transduced or not with pLKO-puro-IPTG-3xLacO encoding sh129921, selected as described above and let to recover for 2 days. *MPV17* silencing was then obtained by incubation of the transduced cells in the presence of 0.1 mM of IsoPropyl ß-D-1-ThioGalactopyranoside (IPTG) (Sigma-Aldrich, I6758), renewed daily for 5 days unless stated otherwise. Cells were then seeded and allowed to grow for 4 days in presence of IPTG renewed daily (unless stated otherwise) before assessing the proliferation.

Proliferation assessment

Cell counting. Cells were seeded in 25 cm^2 culture flask (Corning, #430639) and grown for 4 days. Cells were rinsed with Phosphate Buffered Saline (PBS) pH 7.4, trypsinized with 0.05% trypsin-EDTA (ThermoFisher, 25300) and centrifuged for 5 min at 200 g. The pellet was resuspended in culture medium and cell suspension density was counted in a Neubauer chamber. Doubling time was calculated as follow: time*ln(2) / (ln(number of cells at the end of the experiment)—ln(number of seeded cells)).

MTT assay. Cells were seeded in 24-well culture plates (Corning, #3524), grown for 4 days and incubated for 1 h with 500 μL of tetrazolium dye MTT (Sigma-Aldrich, M2128) (2.5 μg/mL in PBS) at 37˚C. Cells were then lysed for 1 h in lysis buffer (9% sodium dodecyl sulphate, 60% N, N-dimethylformamide, pH 4.7), and absorbance was measured with a spectrophotometer (xMark, Bio-Rad) at 570 nm.

Protein content: Folin protein assay. Cells were seeded in 24-well culture plates (Corning, #3524), grown for 4 days and rinsed twice with PBS. The bovine serum albumin (VWR, 0332) protein standards and samples were incubated 30 min in presence of 200 μL of 0.5 M sodium hydroxide, then 10 min with 750 μL of a solution A (1.96% sodium carbonate, 0.02% sodium and potassium tartrate and 0.01% copper sulphate) and finally 30 min with 75 μL of Folin and Ciocalteu′s phenol reagent (Sigma-Aldrich, F9252) diluted twice in distilled water. Absorbance was measured with a spectrophotometer (xMark, Bio-Rad) at 740 nm [25].

Cell lysates and pierce protein assay

Cells were seeded in 75 cm^2 culture flask (Corning, #430641U), rinsed once with PBS and lysed with radioimmunoprecipitation assay buffer (20 mM tris hydroxymethyl, 150 mM sodium chloride, 1 mM EDTA, 1 mM EGTA, 1% sodium deoxycholate, 10% glycerol, 1%

NP40, pH 7.6) supplemented with protease inhibitor cocktail (Sigma-Aldrich, 11697498001) and phosphatase inhibitor buffer (25 mM sodium orthovanadate, 250 mM 4-nitrophenylphosphate, 250 mM ß-glycerophosphate, 125 mM sodium fluoride). Lysates were sonicated 3 x 10 sec (amplitude 50) and centrifuged (10 min, 15000 g). Cleared cell lysates were assessed for protein content with Pierce 660 Protein Assay Reagent (ThermoFisher, 22660) according to the manufacturer′s recommendations.

Western blotting analysis

Amounts of 20 μg of protein samples were prepared in loading buffer (0.03 M Tris-hydrochloride acid; pH 6.8, 0.04 M sodium dodecyl sulphate, 0.4 M β-mercaptoethanol, 5% glycerol, 0.15 mM bromophenol blue), boiled for 5 min, resolved on polyacrylamide gel and transferred on a nitrocellulose membrane (Bio-Rad). Membrane was blocked for 1 h at room temperature in Odyssey Blocking Buffer (OBB) (LI-COR, P/N 927) diluted twice in PBS and incubated overnight at 4˚C with the primary antibody diluted in OBB with 0.1% Tween-20 (OBB-T). For MPV17 detection, membrane was treated prior to blocking step with Super Signal Western Blot Enhancer (ThermoFisher, 46640) according to the manufacturer′s recommendations. The next day, membrane was rinsed 3 x 5 min in PBS with 0.1% Tween-20 (PBS-T), incubated with secondary antibody diluted in OBB-T 0.1% for 1 h at room temperature, rinsed 3 times in PBS-T 0.1%, dried and scanned with the Odyssey Infrared Imager (LI-COR, 9120). For the description of the antibodies used in this study, see Table 2.

Construct for MPV17 overexpression

MPV17 mRNA was reverse transcribed (Transcriptor First Strand cDNA kit, Roche, 04379012001) using a specific primer (5′-AGGTGGAAACGATGGAGTGA-3′). A PCR was then

Table 2. List of antibodies and their dilutions used for western blotting.

Antibody	Reference	Dilution
Anti-MPV17	Proteintech	1/1000
	10310-1-AP	
Anti-ATF4	Santa Cruz	1/1000
	Sc-390063	
Anti-ATF4	Cell Signaling	1/1000
	#11815 lot 3	
Anti-tubulin	Sigma-Aldrich	1/10000
	T5168	
Anti -actin	Sigma-Aldrich	1/10000
	A5441	
Anti-GAPDH	Abcam	1/10000
	128915	
Anti-rabbit IgG	LI-COR	1/10000
IRDye 800CW Goat	926–32211	
Anti-mouse IgG	LI-COR	1/10000
IRDye 680RD Goat	926–68070	
Anti-rabbit IgG	LI-COR	1/10000
IRDye 680RD Goat	926–68071	
Anti-mouse IgG	LI-COR	1/10000
IRDye 800CW Goat	926–32210	

The antibodies used for the western blot analysis are specified with their reference and working dilutions.

https://doi.org/10.1371/journal.pone.0229834.t002

performed using a forward primer containing a restriction site for BamH1 (F: 5′-AGGATCCA GGAAGCATGGCA-3′) and a reverse primer containing a restriction site for Sal1 (R: 5′-AGT CGACGGCAGGCTTAGA-3′). PCR products were purified using Wizard SV Gel and PCR Clean-Up System (Promega, A9281). An amount of 1 μg of PCR product and pLenti PGK GFP Puro (Addgene, #19070) was digested with BamH1, purified, restricted with Sal1, purified and finally ligated with T DNA ligase (Biolabs, M0202S) to construct the pLenti PGK MPV17 Puro plasmid.

Rescue experiment

HepG2 cells were transduced with pLenti PGK GFP puro or pLenti PGK MPV17 puro-containing lentiviruses and selected for 6 days with puromycin (2.5 μg/mL). Cells were then transduced with PLKO.1-puro vector constitutively encoding sh129921 or shNT (Table 1). Cells were then allowed to recover and generate *MPV17*-targeting shRNA for 5 days, seeded and allowed to grow for 4 days. Cell proliferation was assessed by MTT assay at day 1 and day 4. To overexpress MPV17, we used *MPV17*-silencing and *MPV17*-overexpression vectors that were both bearing the resistance to puromycin. This obviously constitutes an obstacle in the selection of the cells that are double transduced. However, we decided to proceed further based on the knowledge that the sh129921-encoding vector robustly led to a very efficient transduction rate (nearly 100%), therefore allowing to bypass the need for an ensuing antibiotic selection.

mtDNA content determination

DNA was extracted with the Wizard Genomic DNA Purification Kit (Promega, A1120) according to the manufacturer's recommendations. qPCR for mtDNA amplification was performed on the gene encoding ND2 (NADH Dehydrogenase 2) using the forward primer 5′-TGTTGGTTATACCCTTCCCGTACTA-3′ and the reverse primer 5′-CCTGCAAAGATGGTA-GAGTAGATGA-3′. For the normalization with nuclear DNA, the gene encoding Beclin was amplified with the forward primer 5′-CCCTCATCACAGGGCTCTCTCCA-3′ and the reverse primer 5′- GGGACTGTAGGCTGGGAACTATGC-3′. Real time PCR was performed with SYBR Select Master Mix (ThermoFisher, 4472908). mtDNA copy number was calculated according to the following formula: $2^{*}2^{\wedge\text{-}\Delta Ct}$ (where $\Delta Ct = Ctmean_{ND2} - Ctmean_{Beclin}$).

RNA extraction and RT-qPCR

RNA was extracted with RNeasy Mini kit (Qiagen, 74104) according to manufacturer's recommendations and QIAcube (Qiagen). RT was performed with GoScript™ Reverse Transcription Mix (Promega, A2791) according to the manufacturer's recommendations. qPCR was performed with SYBR Select Master Mix (ThermoFisher, 4472908). We used the $2^{-\Delta\Delta Ct}$ method to assess the relative mRNA expression. The *MPV17* primers used in this study are the following: F: GCTCAGGAAGCATGGCACTCT; R: AATGTCACCCAGGCCCATCA.

RNA sequencing

Huh7 cells were transduced with shRNA non-target lentiviral vector (shNT) or with shRNA vector constitutively targeting *MPV17* expression (sh129921). RNA quality was analysed with the Bioanalyzer 2100 (Agilent). RNA samples ($n = 4$) were sent to Genomic Core Leuven (Belgium) for RNA sequencing and data were analysed with Ingenuity Pathway Analysis (QIAGEN Inc., https://www.qiagenbioinformatics.com/products/ingenuitypathway-analysis).

Immunohistochemistry

Slices were incubated 2 x 5 min in xylene (ThermoFisher, X/0200/21), 2 x 3 min in isopropanol (VWR, 20842.330) and 10 min in 1% H_2O_2 (VWR, 23.613.446) / methanol prepared extemporaneously. Slices were washed 3 min in tap water and 3 min in demineralized water. Slices were then incubated 30 min in the 98˚C water bath with the "Target Retrieval Solution 1X" pH 6.1 (Dako, S169984-2) and let to cool down for 15 min at room temperature. Slices were washed 5 min in tap water, 2 x 3 min in PBS and incubated 1 h at room temperature with a solution of PBS-2% Normal Goat Serum (NGS) (ThermoFisher, 16210064). Slices were then incubated with the primary antibody anti-MPV17 (Table 2) diluted 1/100 in a solution of PBS-0.5% NGS, overnight at 4˚C. Slices were washed 3 x 3 min in PBS-T 0.05% baths and 3 min in PBS. Slices were then incubated 30 min at room temperature with the secondary antibody EnVision-HRP anti-rabbit (Dako, K400311). Slices were washed 3 x 3 min in PBS-T 0.05% and 3 min in PBS. Slices were then incubated 4 min at room temperature in the DAB solution (Dako, K346811) and washed 5 min in running tap water. Slices were incubated 5 min in Mayer Hematoxyline and washed 5 min in running tap water. Slices were finally incubated 3x 3 min in isopropanol, 3x 3 min in xylene and mounted on coverslip with Entallan glue.

Statistical analysis

Data are expressed as the mean ± Standard Error of the Mean (S.E.M). Figure plotting was performed with Prism software. Statistical analysis was performed using a one-tailed Mann-Whitney Test or a two-tailed Wilcoxon signed rank Test ($\alpha = 5\%$; *: $p<0.05$; **: $p<0.01$; ***: $p<0.001$; ****: $p<0.0001$).

Supporting information

S1 Fig. Experimental timelines of *MPV17* silencing in the constitutive and inducible models. Cells were transduced and puromycin-selected with a vector allowing a constitutive (a) or an inducible (b) *MPV17* silencing. After 2 days of recovery, cells were either seeded and allowed to grow for 4 days before assessment of proliferation (a) or treated with 0.1 mM of Iso-Propyl ß-D-1-ThioGalactopyranoside (IPTG) for 5 days to induce *MPV17* silencing prior to the seeding (b). The proliferation was then assessed after 4 days of growth in presence of IPTG renewed daily.
(PPTX)

S2 Fig. Effect of IPTG on Huh7 cells proliferation following constitutive sh129921-mediated *MPV17* knockdown. Huh7 cells were transduced with non-target shRNA lentiviral vectors (shNT) or with sh129921-containing vector. Transduced cells were selected for 6 days with puromycin (2.5 μg/mL). Cells were seeded at 8×10^3 cells/cm^2 and grown for 4 days in the presence or in the absence of 0.1 mM of IPTG. To mimic the conditions found in the inducible model of expression, the IPTG-containing medium was renewed daily. We therefore included a control in which no IPTG was present while the medium was also changed every day (Ctl). Data are presented as mean ± S.E.M (3 biological replicates). P values were calculated with the one-tailed Mann-Whitney Test ($\alpha = 5\%$; NS; *: $p<0.05$; **: $p<0.01$; ***: $p<0.001$).
(PPTX)

S3 Fig. Effect of the duration of IPTG pre-treatment and of the medium change frequency on Huh7 cells proliferation in response to inducible sh129921-mediated *MPV17* knockdown. Cells were transduced, or not (Unt), with inducible sh129921 lentiviral vectors and selected for 6 days with puromycin (2.5 μg/mL). Cells were then incubated for 14 days in the presence of 0.1 mM of IPTG to induce *MPV17* silencing and culture medium was changed

daily (a, b, c) or every 2 days (c, d, e). Cells were seeded at 8×10^3 cells/cm^2 and grown for 4 days in presence of IPTG in the same conditions. MPV17 protein abundance was assessed by western blot analysis (a, d) and quantified with Image J software (b, e). Proliferation was then assessed by manual counting to calculate the doubling time (c, f). Full blots are presented in S6 Fig. Data are presented as mean ± S.E.M of 3 independent biological replicates. P values were calculated with the one-tailed Mann-Whitney Test ($\alpha = 5\%$; NS; *: $p<0.05$; **: $p<0.01$; ***: $p<0.001$).
(PPTX)

S4 Fig. Localisation of the shRNA-targeted sites on *MPV17* transcript. The effects of several commercially available shRNAs directed against *MPV17* transcript were assessed in Huh7 cells. Each shRNA Sigma Aldrich reference (sh128669, sh131201, sh131038, sh127649 and sh129921) is indicated above its target site. Each grey box represents an exon of *MPV17* transcript (NM002437.5). A line indicates the 3′UTR and 5′UTR of *MPV17* transcript.
(PPTX)

S5 Fig. Localisation of the shRNA-targeted sites on the *MPV17* transcript isoforms referenced in human liver. The Genotype-Tissue Expression (GTEx) Project was supported by the Common Fund of the Office of the Director of the National Institutes of Health, and by NCI, NHGRI, NHLBI, NIDA, NIMH, and NINDS. The data used for the analysis described in this manuscript and this Fig. were obtained from the GTEx Portal on 02/05/19. We indicated the Sigma Aldrich reference of each shRNA targeting *MPV17* transcripts (sh128669, sh131201, sh131038, sh127649 and sh129921) above its targeted site. Each box represents an exon in *MPV17* transcript isoforms. The darker the purple, the more abundant the transcript (as referred by Log 10 (TPM)). The 3′UTR is located on the left of the image, and the 5′UTR on the right. We added an asterisk (*) that indicates both shRNAs providing the reduced proliferation phenotype, while ø indicates both shRNAs leading to an unchanged proliferation rate.
(PPTX)

S6 Fig. Full-length blots of the cropped blots presented in this work. Protein immunostaining was performed with secondary antibodies coupled to infrared dyes (IRDye; green: 800nm/red: 700 nm). a: Full blot of the one presented in Figs 2A and 7A; b: Full blot of the one presented in Figs 4A and 7B (Anti-ATF4 from Santa Cruz); c: Full blot of the one presented in Fig 8A; d: Full blot of the one presented in Fig 4C (Anti-ATF4 from Cell Signaling); e: Full blot of the one presented in Fig 4B (Anti-ATF4 from Cell Signaling); f: Full blot of the one presented in Fig 5B; g: Full blot of the one presented in Fig 6B; h and i: Full blots of the ones presented in S3 Fig; j: Full blot of the one presented in Fig 6C (Anti-ATF4 from Santa Cruz).
(DOCX)

Acknowledgments

We wish to thank Benjamin LE CALVE for his valuable biological input, the constructive discussions and technical advice. We are grateful to Florian POULAIN for the informative presentation of the GTEx Portal and the help regarding *MPV17* isoforms.

Author Contributions

Conceptualization: Morgane Canonne, Thierry Arnould, Patricia Renard.

Data curation: Sophie Ayama-Canden.

Formal analysis: Morgane Canonne, Anaïs Wanet, Sophie Ayama-Canden.

Funding acquisition: Patricia Renard.

Investigation: Morgane Canonne, Anaïs Wanet, Thuy Truong An Nguyen, Alexis Khelfi, Martine Van Steenbrugge, Antoine Fattaccioli, Mustapha Najimi.

Methodology: Morgane Canonne, Anaïs Wanet, Thierry Arnould, Patricia Renard.

Resources: Etienne Sokal, Thierry Arnould, Patricia Renard.

Supervision: Patricia Renard.

Validation: Morgane Canonne.

Visualization: Morgane Canonne.

Writing – original draft: Morgane Canonne.

Writing – review & editing: Anaïs Wanet, Mustapha Najimi, Thierry Arnould, Patricia Renard.

References

1. Karasawa M, Zwacka RM, Reuter A, Fink T, Hsieh CL, Lichter P, et al. The human homolog of the glomerulosclerosis gene Mpv17: structure and genomic organization. Hum Mol Genet. Oxford University Press; 1993; 2: 1829–1834. https://doi.org/10.1093/hmg/2.11.1829 PMID: 8281143
2. Spinazzola A, Viscomi C, Fernandez-Vizarra E, Carrara F, D'Adamo P, Calvo S, et al. MPV17 encodes an inner mitochondrial membrane protein and is mutated in infantile hepatic mitochondrial DNA depletion. Nat Genet. Nature Publishing Group; 2006; 38: 570–575. https://doi.org/10.1038/ng1765 PMID: 16582910
3. Krauss J, Astrinidis P, Astrinides P, Frohnhöfer HG, Walderich B, Nüsslein-Volhard C. transparent, a gene affecting stripe formation in Zebrafish, encodes the mitochondrial protein Mpv17 that is required for iridophore survival. Biol Open. Company of Biologists; 2013; 2: 703–10. https://doi.org/10.1242/bio.20135132 PMID: 23862018
4. Trott A, Morano KA. SYM1 Is the Stress-Induced Saccharomyces cerevisiae Ortholog of the Mammalian Kidney Disease Gene Mpv17 and Is Required for Ethanol Metabolism and Tolerance during Heat Shock. Eukaryot Cell. American Society for Microbiology (ASM); 2004; 3: 620. https://doi.org/10.1128/EC.3.3.620-631.2004 PMID: 15189984
5. El-Hattab AW, Wang J, Dai H, Almannai M, Staufner C, Alfadhel M, et al. *MPV17*-related mitochondrial DNA maintenance defect: New cases and review of clinical, biochemical, and molecular aspects. Hum Mutat. 2018; 39: 461–470. https://doi.org/10.1002/humu.23387 PMID: 29282788
6. Löllgen S, Weiher H. The role of the Mpv17 protein mutations of which cause mitochondrial DNA depletion syndrome (MDDS): lessons from homologs in different species. Biol Chem. De Gruyter; 2015; 396: 13–25. https://doi.org/10.1515/hsz-2014-0198 PMID: 25205723
7. Antonenkov VD, Isomursu A, Mennerich D, Vapola MH, Weiher H, Kietzmann T, et al. The Human Mitochondrial DNA Depletion Syndrome Gene MPV17 Encodes a Non-selective Channel That Modulates Membrane Potential. J Biol Chem. American Society for Biochemistry and Molecular Biology; 2015; 290: 13840–61. https://doi.org/10.1074/jbc.M114.608083 PMID: 25861990
8. Reinhold R, Kruger V, Meinecke M, Schulz C, Schmidt B, Grunau SD, et al. The Channel-Forming Sym1 Protein Is Transported by the TIM23 Complex in a Presequence-Independent Manner. Mol Cell Biol. 2012; 32: 5009–5021. https://doi.org/10.1128/MCB.00843-12 PMID: 23045398
9. Dalla Rosa I, Cámara Y, Durigon R, Moss CF, Vidoni S, Akman G, et al. MPV17 Loss Causes Deoxynucleotide Insufficiency and Slow DNA Replication in Mitochondria. Larsson N-G, editor. PLOS Genet. Public Library of Science; 2016; 12: e1005779. https://doi.org/10.1371/journal.pgen.1005779 PMID: 26760297
10. Moss CF, Dalla Rosa I, Hunt LE, Yasukawa T, Young R, Jones AWE, et al. Aberrant ribonucleotide incorporation and multiple deletions in mitochondrial DNA of the murine MPV17 disease model. Nucleic Acids Res. 2017; 45: 12808–12815. https://doi.org/10.1093/nar/gkx1009 PMID: 29106596
11. Martorano L, Peron M, Laquatra C, Lidron E, Facchinello N, Meneghetti G, et al. The zebrafish orthologue of the human hepatocerebral disease gene MPV17 plays pleiotropic roles in mitochondria. Dis Model Mech. Company of Biologists; 2019;12. https://doi.org/10.1242/dmm.037226 PMID: 30833296

12. Alonzo JR, Venkataraman C, Field MS, Stover PJ. The mitochondrial inner membrane protein MPV17 prevents uracil accumulation in mitochondrial DNA. J Biol Chem. 2018; 293: 20285–20294. https://doi.org/10.1074/jbc.RA118.004788 PMID: 30385507

13. Wanet A, Caruso M, Domelevo Entfellner J-B, Najar M, Fattaccioli A, Demazy C, et al. The Transcription Factor 7-Like 2-Peroxisome Proliferator-Activated Receptor Gamma Coactivator-1 Alpha Axis Connects Mitochondrial Biogenesis and Metabolic Shift with Stem Cell Commitment to Hepatic Differentiation. Stem Cells. 2017; 35: 2184–2197. https://doi.org/10.1002/stem.2688 PMID: 28795454

14. Choi Y-R, Hong Y Bin, Jung S-C, Lee JH, Kim YJ, Park HJ, et al. A novel homozygous MPV17 mutation in two families with axonal sensorimotor polyneuropathy. BMC Neurol. BioMed Central; 2015; 15: 179. https://doi.org/10.1186/s12883-015-0430-1 PMID: 26437932

15. Dallabona C, Marsano RM, Arzuffi P, Ghezzi D, Mancini P, Zeviani M, et al. Sym1, the yeast ortholog of the MPV17 human disease protein, is a stress-induced bioenergetic and morphogenetic mitochondrial modulator. Hum Mol Genet. Narnia; 2010; 19: 1098–1107. https://doi.org/10.1093/hmg/ddp581 PMID: 20042463

16. Bottani E, Giordano C, Civiletto G, Di Meo I, Auricchio A, Ciusani E, et al. AAV-mediated liver-specific MPV17 expression restores mtDNA levels and prevents diet-induced liver failure. Mol Ther. American Society of Gene & Cell Therapy; 2014; 22: 10–7. https://doi.org/10.1038/mt.2013.230 PMID: 24247928

17. Wortel IMN, van der Meer LT, Kilberg MS, van Leeuwen FN. Surviving Stress: Modulation of ATF4-Mediated Stress Responses in Normal and Malignant Cells. Trends Endocrinol Metab. 2017; 28: 794–806. https://doi.org/10.1016/j.tem.2017.07.003 PMID: 28797581

18. Harding HP, Zhang Y, Zeng H, Novoa I, Lu PD, Calfon M, et al. An Integrated Stress Response Regulates Amino Acid Metabolism and Resistance to Oxidative Stress. Mol Cell. Cell Press; 2003; 11: 619–633. https://doi.org/10.1016/s1097-2765(03)00105-9 PMID: 12667446

19. Malmberg SE, Adams CM. Insulin signaling and the general amino acid control response. Two distinct pathways to amino acid synthesis and uptake. J Biol Chem. American Society for Biochemistry and Molecular Biology; 2008; 283: 19229–34. https://doi.org/10.1074/jbc.M801331200 PMID: 18480057

20. Wang S, Chen XA, Hu J, Jiang J-K, Li Y, Chan-Salis KY, et al. ATF4 Gene Network Mediates Cellular Response to the Anticancer PAD Inhibitor YW3-56 in Triple-Negative Breast Cancer Cells. Mol Cancer Ther. NIH Public Access; 2015; 14: 877–88. https://doi.org/10.1158/1535-7163.MCT-14-1093-T PMID: 25612620

21. Ben-Sahra I, Hoxhaj G, Ricoult SJH, Asara JM, Manning BD. mTORC1 induces purine synthesis through control of the mitochondrial tetrahydrofolate cycle. Science. NIH Public Access; 2016; 351: 728–733. https://doi.org/10.1126/science.aad0489 PMID: 26912861

22. Politi N, Pasotti L, Zucca S, Casanova M, Micoli G, Cusella De Angelis M, et al. Half-life measurements of chemical inducers for recombinant gene expression. J Biol Eng. 2014; 8: 5. https://doi.org/10.1186/1754-1611-8-5 PMID: 24485151

23. RNA Interference and Viruses: Current Innovations and Future Trends—Google Books [Internet]. [cited 27 Feb 2019]. Available: https://books.google.be/books?id=C5TY8W74scIC&pg=PA204&lpg=PA204&dq=inducible+vector+reversible+fine+tuning&source=bl&ots=j8lvhrcKPL&sig=ACfU3U0knMfwhxsLArPPpV4QXORxuiAuHQ&hl=en&sa=X&ved=2ahUKEwjakOO159vgAhWTQhUIHa0OA4IQ6AEwEHoECAAQAQ#v=onepage&q=inducibl

24. Peretz L, Besser E, Hajbi R, Casden N, Ziv D, Kronenberg N, et al. Combined shRNA over CRISPR/cas9 as a methodology to detect off-target effects and a potential compensatory mechanism. Sci Rep. Nature Publishing Group; 2018; 8: 93. https://doi.org/10.1038/s41598-017-18551-z PMID: 29311693

25. LOWRY OH, ROSEBROUGH NJ, FARR AL, RANDALL RJ. Protein measurement with the Folin phenol reagent. J Biol Chem. 1951; 193: 265–75. Available: http://www.ncbi.nlm.nih.gov/pubmed/14907713 PMID: 14907713